STRUCTURE AND DYNAMICS OF BACTERIAL S-LAYER PROTEINS

DISSERTATION

ZUR ERLANGUNG DES DOKTORGRADES DER NATURWISSENSCHAFTEN

AN DER FAKULTÄT FÜR MATHEMATIK, INFORMATIK UND NATURWISSENSCHAFTEN

DER UNIVERSITÄT HAMBURG

VORGELEGT VON

JUN LIU

AUS LESHAN, CHINA

HAMBURG, 2014

Die vorliegende Arbeit wurde im Zeitraum von Januar 2011 bis April 2014 in der Arbeitsgruppe von Prof. Dr. Ch. Betzel im Laboratorium für Strukturbiologie von Infektion und Entzündung am Institut für Biochemie und Molekularbiologie des Fachbereichs Chemie der Universität Hamburg durchgeführt.

1. Gutachter **Prof. Dr. Ch. Betzel**
2. Gutachter **Prof. Dr. R. Bredehorst**

Tag der Disputation: 11. April 2014

To my wife and daughter

TABLE OF CONTENTS

LIST OF ABBREVIATIONS I

SYMBOLS FOR AMINO ACIDS V

SYMBOLS FOR NUCLEOTIDES V

ABBREVIATION OF ORGANISMS VI

1 INTRODUCTION 1

1.1 Location, Morphogenesis and Structure of S-layers 1

1.2 Isolation and Biochemical Characteristics of S-layers 4

1.3 Assembly and Function of S-layers 6

1.4 Research History of S-layers 8

1.4.1 Bacillus anthracis *9*

1.4.2 Clostridium difficile *9*

1.4.3 Lactobacillus sp. *10*

1.4.4 Geobacillus stearothermophilus *11*

1.4.5 Lysinibacillus sphaericus *12*

1.4.6 Several other Gram-negative organisms carrying S-layers *12*

1.5 Nanobiotechnological Applications of S-layers 13

1.6 Biosorption and Nanocluster Formation 16

1.7 S-layer Proteins Analysed 18

2 AIM OF THIS WORK 19

3 MATERIALS AND METHODS 20

3.1 Brief Preparation Process of Biomass 20

3.1.1 Basic procedures of the S-layer proteins preparation *20*

3.1.2 Analysis of S-layer proteins *21*

3.1.3 Preparation of buffer and sample solutions in respective experiments *22*

3.2 Circular Dichroism (CD) Spectroscopy 29

3.2.1 Circular Dichroism *29*

3.2.2 Study of biological molecules 31

3.3 Atomic Force Microscopy (AFM) Technology 33

3.3.1 Probe 34

3.3.2 AFM cantilever deflection measurement 35

3.3.3 Imaging modes 35

3.3.4 Identification of individual surface atoms 36

3.4 Dynamic Light Scattering (DLS) Technology 36

3.4.1 Dynamic light scattering 36

3.4.2 Applications of DLS 39

3.5 Small Angle X-ray Scattering (SAXS) Technology 39

3.5.1 Small angle X-ray scattering (SAXS) from proteins 39

3.5.2 Computational techniques for modeling protein flexibility 42

3.6 Protein Crystallization 43

3.6.1 Crystallization screening and optimization of slfB 44

3.6.2 Crystallization screening of slp-B53 44

4 RESULTS 49

4.1 Secondary Structure Analysis 49

4.1.1 Flexible regions prediction 49

4.1.2 Secondary structure determination by CD measurements 52

4.2 S-layer Protein Processing Prior to Investigation 55

4.3 Formation of S-layers Observed by AFM 55

4.3.1 AFM of slfB 56

4.3.2 AFM of slp-B53 57

4.4 DLS Measurements 58

4.4.1 DLS experiments of slfB 59

4.4.2 DLS experiments of slp-B53 59

4.5 SAXS Measurements 60

4.5.1 SAXS measurements of slfB 60

4.5.2 SAXS measurements of slp-B53 63

4.6 Crystallization Experiments of S-layer Proteins 65
4.6.1 Crystallization screening of slfB 65
4.6.2 Crystallization optimization of slfB 66
4.6.3 Crystallization screening of slp-B53 67
5 DISCUSSION 70
5.1 Basic Symmetry of Target Proteins 70
5.1.1 Secondary structure analysis 70
5.1.2 Analysis of S-layer formation 70
5.2 Dynamics and Structure of S-layer Proteins 72
5.2.1 Monodispersity as analyzed by DLS measurements 72
5.2.2 Analysis of SAXS experiments 74
5.3 Analysis of crystallization experiments 75
5.4 General Discussion and Outlook 76
6 SUMMARY - ZUSAMMENFASSUNG 77
6.1 Summary 77
6.2 Zusammenfassung 78
7 REFERENCES 80
8 APPENDIX 96
8.1 Self-Designed Screens 96
8.2 Self designed screen – *pPEG7 series* 96
8.3 Self designed screen – *PACT series* 96
9 INSTRUMENTATION AND CHEMICALS 105
9.1 Instrumentation 105
9.2 Formulations and Chemicals 106
9.2.1 Formulations 106
9.2.2 Chemicals 109
10 ACKNOWLEDGEMENTS 114

11 CURRICULUM VITAE 116

12 EIDESSTATTLICHE ERKLÄRUNG 118

List of abbreviations

2D	Two dimensional
3D	Three dimensional
AA	Amino acid
ACF	Auto correlation function
AFM	Atomic force microscopy
Am	Ammonium-
ANSI	American National Standards Institute
APD	Avalanche photo diode
APS	Advanced Photon Source
AS	Ammonium sulfate
ATCC	American Type Culture Collection
B_{22}	Second virial coefficient
BLAST	Basic Local Alignment Search Tool
BSSB	Blast Server for Structural Biology
c	Concentration
$CaCl_2$	Calcium chloride
CCM	Czech Collection of Microorganisms
CD	Circular dichroism
CLP	Cubic lipid phase
Cm	Curium
cryoEM	Cryo electron microscopy
D_0	Diffusion coefficient
DDLS	Depolarized Dynamic Light Scattering
DDM	n-Dodecyl β-D-maltoside
DESY	Deutsches Elektronen Synchrotron (German electron synchrotron)
DFT	Density Functional Theory
DLS	Dynamic Light Scattering
DNA	Deoxyribonucleic acid

D_0	Diffusion coefficient at infinite dilution
DPI	Dual Polarization Interferometry
DTT	Dithiothreitol
ED	Essential Dynamics
EM	Electronic Microscopy
EMBL	European Molecular Biology Laboratory
EQ	Equation
EU	European Union
EU(III)	Europium(Trivalent)
Fe(II)	Iron(Divalent)
Fe(III)	Iron(Trivalent)
GCB	Granada Crystallization Box
GCB-D	Granada Crystallization Box Domino
HEPES	4-(2-Hydroxyethyl)-1-piperazineethanesulfonic acid
HOAc	Acetic acid
HTS	High throughput screening
HZDR	Helmholtz Zentrum Dresden-Rossendorf
I_0	Intensity at $q=0$
Iq	Function of moment transfer, $\boldsymbol{q=(4\pi sin\Theta)/\lambda}$
JGA12	Johanngeorgenstadt strain A12
JGB53	Johanngeorgenstadt strain B53
k	Boltzmann constant
kD	Interaction factor
kDa	Kilo Dalton (1 kDa = 1000 g/mol)
kHz	Kilo Hertz
LMW	Low Molecular Weight
LPS	Lipopolysacchraride
L-CPL	Left-handed circularly polarized light
M	Molar

MC	Monte Carlo
MD	Molecular Dynamics
$MgCl_2$	Magnesium chloride
MME	Monomethyl ether
MO	Monoolein (1-Oleoyl-rac-glycerol)
MOPS	3-(N-morpholino)propanesulfonic acid
MPD	2-Methyl-2,4-pentanediol
MW	Molecular weight (1 g/mol or 1 Da)
NA	Avogadro's constant
NaCl	Sodium chloride
NaOAc	Sodium acetate
NCTC	National Collection of Type Cultures
NMA	Normal models analysis
NMR	Nuclear Magnetic Resonance
OAc	Acetate-
PAGE	Polyacrylamide gel electrophoresis
PCR	Polymerase chain reaction
PCT	Pre-crystallization test
PDB	Protein data bank
PEG	Polyethylene glycol
PEL	Polyelectrolyte layers
P(r)	Pair-distribution function
PMT	Photo multiplier tube
q	Wave vector
R-CPL	Right-handed circularly polarized light
R_g	Radius of gyration
R_H	Hydrodynamic radius
R_s	Stokes' radius
RNA	Ribonucleic acid

SANS	Small angle neutron scattering
Sap	Surface array protein
SAXS	Small angle X-ray scattering
SBS	Society for Biomolecular Screening
SCWP	Secondary cell wall polysaccharides
SEC	Size exclusion chromatography
SDS	Sodium dodecyl sulfate
SEM	Scanning Electronic Microscopy
SLAC	Stanford Linear Accelerator Center
S-layer	Surface Layer
SLH	Surface layer homology domain
SLP	Surface layer Protein
SLS	Static Light Scattering
t	Time (in seconds)
T	Temperature (in Kelvin)
Tar	-Tartrate
TEM	Transmission Electronic Microscopy
TEMED	Tetramethylethylenediamine
Triton 100	4-(1,1,3,3-Tetramethylbutyl)phenyl-polyethylene glycol
Tris	Tris(hydroxymethyl)aminomethane
U(IV)	Uranium(Tetravalent)
UV	Ultra violet
U(VI)	Uranium(Hexavalent)
v/v	Volume to volume (for concentrations)
VIS	Visible
w/v	Weight to volume (for concentrations)
w/w	Weight to weight
XFEL	European X-ray Free Electron Laser
xg	Relative centrifugal force (rcf) as multiples of the gravitational acceleration on earth (g)

Symbols for amino acids

Amino acids	IUPAC-Code（3-Let.）	Short-Code
alanine	Ala	A
arginine	Arg	R
asparagine	Asn	N
aspartic acid	Asp	D
cysteine	Cys	C
glutamine	Gln	Q
glutamic acid	Glu	E
glycine	Gly	G
histidine	His	H
isoleucine	Ile	I
leucine	Leu	L
lysine	Lys	K
methionine	Met	M
phenylalanine	Phe	F
proline	Pro	P
serine	Ser	S
threonine	Thr	T
tryptophan	Trp	W
tyrosine	Tyr	Y
valine	Val	V

Symbols for nucleotides

A Adenine

T Thymine

C Cytosine

G Guanine

Abbreviation of organisms

A. thermophilus	*Aneurinibacillus thermophilus*
B. anthracis	*Bacillus anthracis*
B. pseudofirmus	*Bacillus pseudofirmus*
B. sphaericus	*Bacillus sphaericus*
Bd. bacteriovorous	*Bdellovibrio bacteriovorous*
C. fetus	*Campylobacter fetus*
Ca. vibrioides	*Caulobacter vibrioides*
Cl. difficile	*Clostridium difficile*
E. coli	*Escherichia coli*
G. stearothermophilus,	*Geobacillus stearothermophilus*
H. influenzae	*Haemophilus influenzae*
Lac. acidophilus	*Lactobacillus acidophilus*
Lac. amylovorus	*Lactobacillus amylovorus*
Lac. brevis	*Lactobacillus brevis*
Lac. buchneri	*Lactobacillus buchneri*
Lac. bulgaricus	*Lactobacillus bulgaricus*
Lac. casei	*Lactobacillus casei*
Lac. crispatus	*Lactobacillus crispatus*
Lac. fermentum	*Lactobacillus fermentum*
Lac. gallinarum	*Lactobacillus gallinarum*
Lac. gasseri	*Lactobacillus gasseri*
Lac. helveticus	*Lactobacillus helveticus*
Lac. johnsoni	*Lactobacillus johnsoni*
Lac. plantarum	*Lactobacillus plantarum*
Lac. suntoryeus	*Lactobacillus suntoryeus*
L. sphaericus	*Lysinibacillus sphaericus*
P. gingivalis	*Porphyromonas gingivalis*
T. forsythia	*Tannerella forsythia*

1 Introduction

1.1 Location, Morphogenesis and Structure of S-layers

S-layers, as the most outer membrane of the cell wall, are being studied with respect to synthesis, structure, assembly and function. They present superb models for investigating the proteinaceous cell wall component [1-4]. Almost all archaeal cell envelopes and nearly every other bacterial phylogenetic group possess this universal feature- "monosurfacelayer" [5-8].

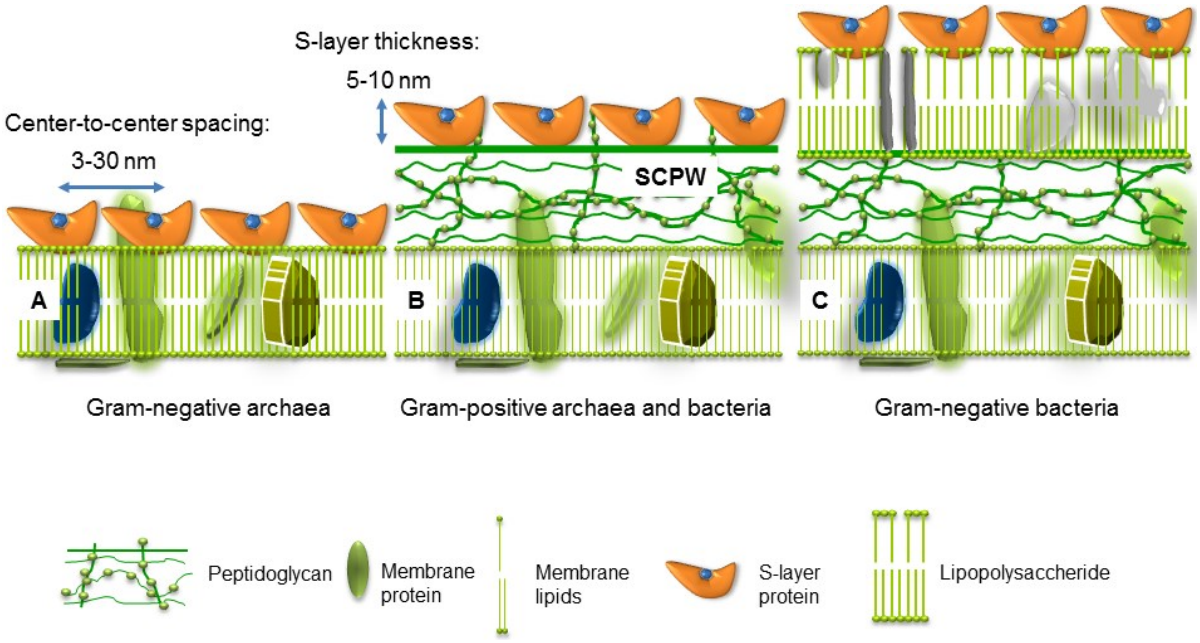

Figure 1.1.1 Schematic illustration showing major classes of prokaryotic cell envelopes containing crystalline cell surface layers (S-layer (glyco) proteins). Gram-negative archaea (A): Cell-envelope structure with S-layers is the only cell-wall component on the external cytoplasmic membrane. Gram-positive archaea and bacteria (B): In bacteria, the rigid wall component is primarily composed of peptidoglycan. SCWPs (secondary cell wall polymers) are only present in bacteria. In archaea, other wall polymers (e.g. pseudomurein or methanochondroitin) are generally detected. Gram-negative bacteria (C): The cell envelope profile is constituted of a flimsy peptidoglycan layer and of an outer membrane. If present, the S-layer is closely related with the lipopolysaccharide of the outer membrane (modified from Sleytr and Beveridge, 1999).

Despite the structures and the chemical properties of prokaryotic envelopes have substantial variations due to the course of evolution (Figure 1.1.1), structural co-evolution has obviously happened on S-layers. Generally, S-layers are inserted or attached to the plasma membrane in most archaea (see Figure 1.1.1A). In Gram-negative bacteria although, the S-layer

assembles on the outer membrane associated with the here existing lipopolysaccharide layer (LPS) (see Figure 1.1.1C). Both in Gram-positive archaea and in bacteria, the S-layer covers the rigid wall matrix, which primarily consists of pesudomurein and peptidoglycan, respectively, as shown in Figure 1.1.1B.

In some organisms, different S-layer proteins can also form superimposed S-layer lattices. For instance, S-layer-like monomelcular lattices could be observed on the surface of eukaryotic algae [9] bacterial sheaths [10] and spore cotes [11] envelopes. Electron-microscopy (EM), combined with freeze-etching techniques [12-15] and atomic force microscopy (AFM), have been applied to investigate the presence of S-layers on intact cells. Around the 1990s, the two- and three-dimensional image analysis, as well as the computer-image reconstruction of structural information, provided insight with an approximal resolution of 1 nm [16-21]. More recently, some higher-resolution studies describing the mass distribution of S-layers could be obtained by the improvement of AFM techniques on the one hand [21, 22] and by tertiary structure prediction based on amino acids sequence on the other hand [23].

Smooth outer and more corrugated inner surfaces have been found in the S-layer of bacteria and could be observed as their common features. Also, pillar-like domains have been described to occur frequently on the inner surface of archaeal S-layers. An S-layer is composed of so called surface layer proteins (S-layer proteins) that are self-assembled to two dimensional crystal lattices (2D crystals). This provides the primary protective barrier for the cells of prokaryotic organisms [3, 22, 24-26]. Regarding the 2D structure of these S-layer lattices, three types of space group symmetry have been found so far: oblique (p1, p2), square (p4), and hexagonal (p3, p6) (see Figure 1.1.2), whereas the morphological units are corresponding to one or two, four, and to three or six identical (glyco)protein subunits, respectively [27]. They are involved in the cell shape protection of bacteria and in the interaction of the bacteria with its host and outer environment. In addition, they act as molecular sieves, mediating the exchange of nutrients and metabolites [28]. In some pathogenic bacteria, S-layer proteins are key virulence factors [29-33]. Surface layers may have valuable applications in nanomedicine technologies [14, 24, 34-38], as they could act as biosorption catalysts for radioactive materials, such as promoting the adsorption of uranium and other heavy metal molecules. It is expected that they could be applied in the cleanup of

nuclear leak pollution [14, 39-44].

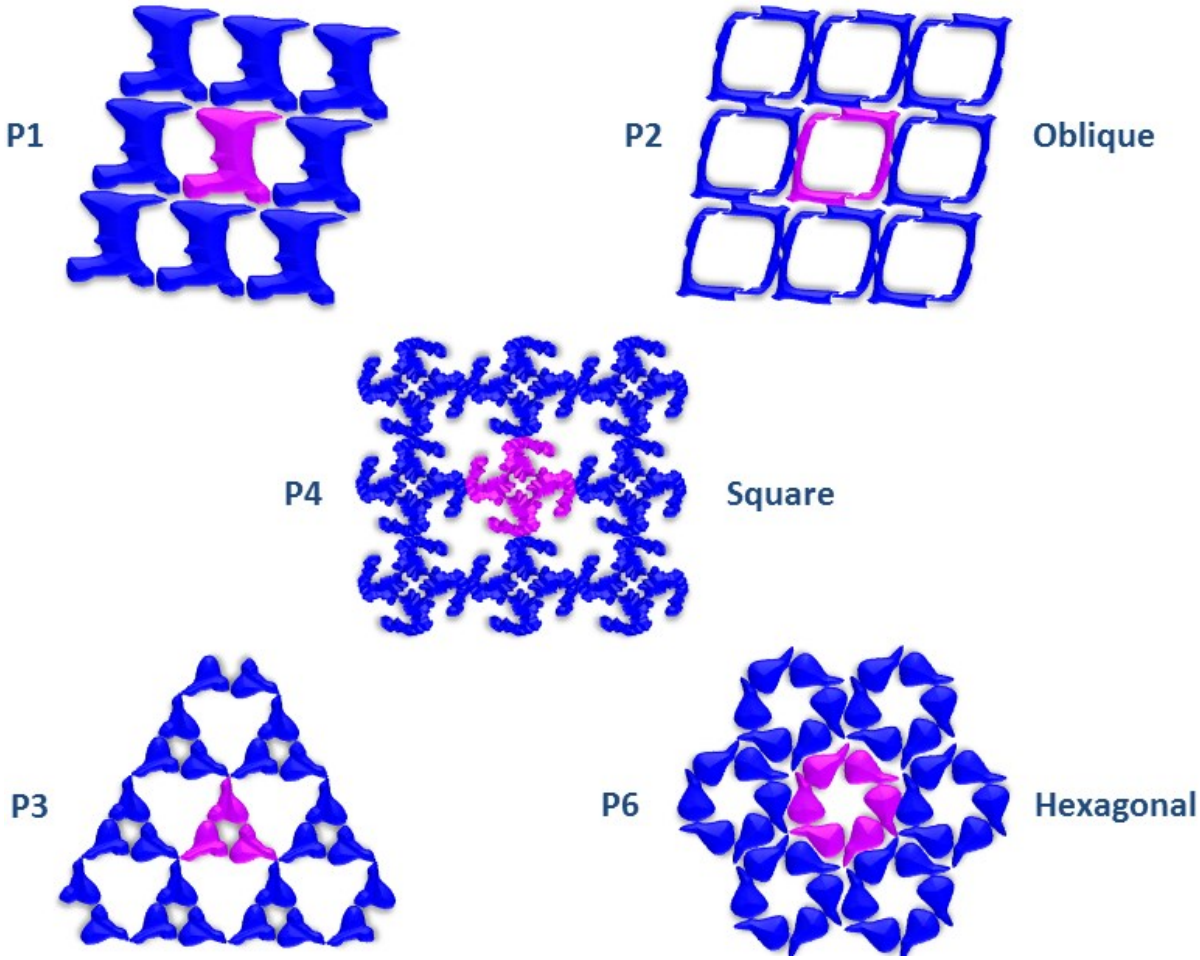

Figure 1.1.2 Schematic drawing of different S-lattice types (modified from U. B. Slytr *et al.,* 1999).

Up to date, not much is known concerning the detailed atomic structure of full length S-layer proteins, as only the most basic elements of S-layers are described. So far, only the 3D structure of the surface layer protein SbsB from G. stearothermophilus PV72/p2 is known, as has been published recently [45] with the PDB-coordinates: 4aq1. However, in order to investigate possible applications, detailed structural information of S-layer proteins as well as better knowledge of their assembly is required [28]. There are two main reasons for the lack of 3D structural information of S-layer proteins so far.

1) The fundamental building block of S-layers consists of high molecular weight proteins, with molecular weights ranging from 40 to 200 kDa [14]. Additionally, they are either usually glycosylated or they possess other post-translational modifications. This, in

principle, excludes the structure analysis by NMR methods, which typically allow the investigation of molecules not exceeding 30 kDa [36].

2) S-layers form functional 2D lattices directed by self-assembly forces, as the S-layer proteins are evolutionary optimized to form two dimensional instead of three dimensional crystals. However, the growth of 3D crystals is required for X-ray structure analysis. Thus, almost all attempts for successful screening appropiate conditions to obtain nucleation of 3D crystals are constantly disturbed by the self-assembly of 2D-crystals. The first full length structure of an S-layer protein could be obtained by Baranova et al. [45] by using specific nanobodies to stabilize the S-layer protein SbsB. By this, X-ray suitable crystals could be obtained and finally its 3D crystal structure could be calculated and described to atomic resolution.

1.2 Isolation and Biochemical Characteristics of S-layers

Regarding the diversity in the macromolecular structure of prokaryotic cell envelopes, many methods have been developed to facilitate the preparation of S-layer proteins. Different lysis and isolation procedures of bacterial cell walls that govern the S-layers or S-layer proteins relying on the different characteristic of individual bacteria have been developed. Generally, they are isolated from purified cell wall fragments by the addition of detergents or hydrogen-bond breaking agents (e.g. guanidine hydrochloride or urea) [46, 47] or by using cation replacement (e.g. Na^+ or Li^+ shifting Ca^{2+}) [48]. Many attempts in isolation trials of S-layers demonstrated that the bond energy between the subunits and the envelope is much weaker than those of inter-subuints bonds [49]. Certainly, as S-layers are attached to the plasma membrane, special isolation procedures are required [50] (see Chap. 9). Characteristic biochemical analysis on many S-layers indicated that they usually consist of one single or several protein or glycoprotein molecules with masses ranging from 40 to 170 kDa [6-8, 22, 51-54]. The pIs of S-layer proteins significantly differ between bacteria, lactobacilli and some archaea. In bacteria, S-layers are typically weak acidic proteins containing 40-60% hydrophobic amino acids and they possess few or no sulphur-containing amino acids, with pIs ranging from 4 to 6. However, the pIs of S-layer proteins from

lactobacilli and some archaea comprise values from 8 to 10 (e.g. *M. fervidus*).

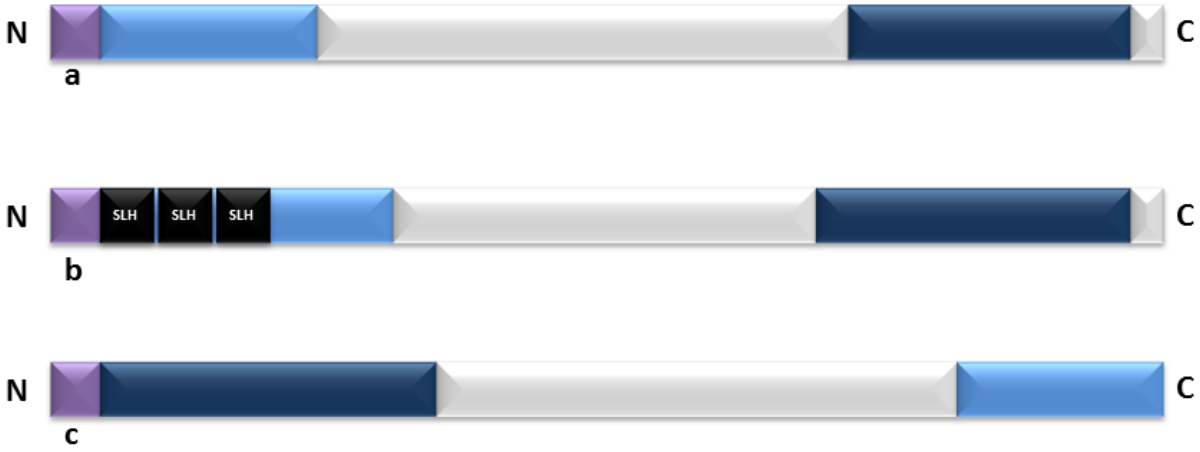

Figure 1.2 Schematic drawing showing the primary organization of S-layer protein domains. (a) S-layer protein without SLH domains and N-terminal cell wall anchoring (e.g., *G. stearothermophilus* wild-type strains ATTC 12980 and NRS 2004/a); (b) S-layer protein with SLH domains at N-terminus and N-terminal cell wall anchoring (e.g., *G. stearothermophilus* wild-type strains PV72/p2 and *L. sphaericus* CCM 2177); (c) S-layer protein without SLH domains and C-terminal cell wall anchoring (e.g., *A. thermoaerophilus* L420-91 and *Lac. acidophilus* ATCC4356). The signal peptide (purple square), the S-layer cell wall binding domain (white rectangle) and the crystallization domain (light blue and darkblue) are displayed, respectively. The highlighted domains are not in scale to the S-layer protein. N, N-terminus; C, C-terminus.

Based on comparative studies investigating the biological genes, it is known that the homologies of S-layers from different, unrelated taxonomic organisms are very low, even if their amino acids compositions possess highly dominant similarity. High compositional homology can be commonly explained by evolutionary relationships. Nevertheless, other factors may also be considerable for the structural homologies of S-layer genes, such as growth conditions and environmental stress. One typical example is that high sequence identities are found at the N-terminus, if present, in Bacillaceae. Also, in some strains, S-layer homology (SLH) domains [55] are related with the attachment to polysaccharides, which are part of secondary cell wall polymers [56-58]. However, investigations of S-layer proteins from *G. stearothermophilus* strain PV72/p2 showed that three SLH domains are linked to the cell wall attachment of S-layer proteins (compare with section below *G. stearothermophilus* and Figure 1.2a). The interaction of the S-layer protein SbsC of *G. stearothermophilus* ATCC12980^{T}

is highly specific, as described in section *G. stearothermophilus* [59]. Usually, in the S-layer proteins without SLH motives, positively charged amino acids are enriched at either the conserved N-terminal region (Figure 1.2b), or at the C-terminal region (Figure 1.2c). They interact with a peptidoglycan-associated secondary cell wall polymer *via* direct hydrogen bonds or electrostatic interactions thereby mediating the attachment to the cell wall [56, 60, 61].

Various EM techniques (e.g. TEM and AFM) have been used to study the ultrastructure of S-layers so far. As a result, their molecular-level ultrastructure is well investigated. However, not much is known regarding the atomic-level structures or even S-layer protein structure-function relationships, allthough some advance methods have been employed during the past decades, such as deletion analysis, cloning of domains, linker mutagenesis and cysteine scanning mutagenesis [62-65]. Due to the development of recombinant DNA technologies, the improvement of EM techniques, the widespread application of SAXS and diversification of crystallization methods, valuable new structure information could be obtained within the recent years. This progress continues to attract many scientists to focus on the funcational relationship and application potential of S-layers or S-layer proteins [1, 45].

1.3 Assembly and Function of S-layers

The biosynthesis of S-layer proteins almost comprises 20% of the total protein biosynthesis. As the most abundant cellular proteins (if present), S-layer proteins are completely spread over the entire cell, accompanied with a closed S-layer lattice formation during all stages of the bacterial growth cycle. This proves that S-layer proteins not only have strong S-layer gene promoters, but also possess high mRNA stability. Several years ago, scientists have studied the biosynthesis of prokaryotic glycoproteins and thereby gained increased knowledge on the diverse glycan structures of bacterial S-layer glycoproteins in detail [66, 67]. Due to the highly environmental dependence for the gene expression of S-layer proteins, some S-layer proteins can synthesize different alternative counterparts, which are able to evade the host's immune response, e.g. the regular S-layer gene biosynthesis of the pathogen *C. fetus* [68].

Table 1.3 Functions of S-layers (according to U.B. Sleytr et al. 2002).

General functions	Description
Cell shape determination and maintence	Determination of cell shape and cell division in archaea that possess S-layers as exclusive wall components
Isoporous membrane structure	Molecular sieve in the ultrafiltration range; Delineating a compartment (periplasm) in Gram-positive bacteria; prevention of non-specific adsorption of macromolecules; hindrance of molecules to reach the cell wall proper (e.g. lytic enzymes)
Protective coat	Prevention of predation of Gram-negative bacteria by bacterial viruses (*Bd. bacteriovorous*)
Surface recognition and cell adhesion to substrates	Physicochemically and morphologically well defined matrices; masking of net-negative charges of peptidoglycan-containing layer in *Bacillaceae*
Adhesion zone for exoenzymes	High-molecular-weight amylase of *G. stearothermophilus* wild-type strains; pullulanase and glycosyl hydrolases of *T. thermosulfurigenes*
Pathogenicity and cell adhesion	Virulence factor of pathogenic organisms; important role in invasion and survival within the host; specific binding of host molecules; Protective coat against complement killing; ability to associate with macrophages and to resist the effect of proteases; production of immunologically non-crossreactive S-layers (S-layer variation)
Template for fine grain mineralization	Induction of precipitation of gypsum and calcite in *Synechococcus* strains and shedding of mineralized S-layers
Biomineration	Complexation of U(IV) and Eu(III)

So far, S-layers served as valuable models for studying self-assembly mechanisms of macromolecular structures [69, 70]. Morphogenesis investigations of S-layers *in vivo* indicated that, at highgrowth, its synthesis rates comprise approximately 500 subunits per second. Hereafter, they will soon cover the entire cell surface and participate in the pre-existing S-layer lattice with proper orientation [6].

Many assumed biological functions of S-layers are still on hypothetic level and, up to now, could not be confirmed by detailed experimental data (for complication see Table 1.3) [3, 6, 24, 71, 72]. It is worth to note that S-layers can be lost when the organisms are no longer restricted to natural environment selection pressures. This indicates that nearby all considerable biosynthesis work of S-layer (proteins) is only required in natural habitats.

1.4 Research History of S-layers

The overlying cell wall, the cytoplasmic membrane plus the outer membrane (if one exists), constitute the bacterial cell envelope. Most bacteria are divided into two categories, differentiated by their Gram staining characteristics: “Gram-negative and Gram-positive”. The cell surfaces of Gram-negative bacteria are composed of thin peptidoglycan layers covered by the outer membranes, while those of Gram-positive bacteria are characterized by a very thick peptidoglycan layer and specific abundant Gram-positive cell wall carbohydrates, missing any outer membrane. The traditional classic model favors the mesh-like structure to lie horizontally to the peptidoglycan layer and that the cytoplasmic membrane layer is interconnected in a vertical orientation. The very strong three-dimensional network of the cell wall assures its basic function, which is to provide protection and to maintaine the cell shape. The basic layers are accompanied by other cell wall components, including proteins, teichoic and lipoteichoic acids, lipoglycan, teichuronic and other adidic or neutral polysaccharides (see Figure 1.1.1) [73-76]. S-layers are the monolayer, which consists of many equal (glyco)proteins possessing a regularly arrayed crystalline form, being a most universal feature of almost all archaebacteria [77]. The very interesting phenomenon of biological molecules organizing themselves into a variety of ordered large-scale structures has attracted the attention of scientists nearly half a century. S-layers have been found in

more than 300 organisms, so far [78]. The summery of S-layer-carrying organisms was reviewed several times by Sleytr and Messner *et al.* (1992, 1996 and 2010), respectively [27]. A number of specific S-layer carring organisms, which are preferred by many scientists as their primary research targets, are briefly described in the following subsections.

1.4.1 Bacillus anthracis

B. anthracis is the pathogenic form of anthrax with the feature of Gram-positive, endospore-forming, rod-shaped bacteria related to toxemia and septicemia. There are two S-layer proteins, Sap and EA1, which both have the same modular organization. They possess an anchoring domain containing three SLH motifs at its N-terminal responsible for fixation on the cell wall, followed by a putative crystallization domain at its C-terminus [79, 80]. With the innovation of biochemical technology and the improvement of physical optics observation techniques, many scientific attempts are constantly advancing. Unfortunately though, almost all trials have failed to score a breakthrough achievement with respect to three dimensional structural analyses. For EA1, it could be also demonstrated, that is not a spore component but a persistent contaminant in spore preparation [81, 82]. More recently, *J. Kern et al.* [3] have successfully solved the three-dimensional structure of SLH, which can be regarded as a remarkable progress.

1.4.2 Clostridium difficile

Cl. difficile, the pathogen type of antibiotic-associated diarrhea and pseudo-membraneous colitis in humans, can cause significant morbidity in hospitalized patients and belongs to Gram-positive, spore-forming anaerobic bacteria [83]. The pathogenic factors are two effective issue-damaging enzymes, named A and B, which both can destroy the colonic mucosa of human beings [84]. For two expressional products of S-layer proteins, known as HMW (high molecular weight) and LMW (low molecular weight) peptides, the encoding genes *slpA* could be obtained [85-87]. Most studies have focused on the basic mechanism of these two proteins, like its strong transcription as a bicistronic transcript [88], or the relationship between the designated serogroup and the sequence of slpA [89], the function as an adhesion protein [90, 91] and further more. Concerning the structure analysis of *slpA*

from *Cl. difficile*, only few studies have been reported.

1.4.3 Lactobacillus sp.

Until now, the utilization of *Lactobacilli* has become increasingly attractive, because they can act as *in vivo* delivery vectors for biologically active molecules, due to their survivability and harmlessness for the gastrointestinal tract. They can be referred to Gram-positive, non-sporulating rod-shaped bacteria including the S-layer carrying strains *Lac. acidophilus, Lac. crispatus, Lac. casei, Lac. plantarum, Lac. brevis, Lac. buchneri, Lac. fermentum, Lac. bulgaricus, Lac. amylovorus, Lac. gallinarum* [5] and *Lac. suntoryeus* [92, 93] as well as in addition several strains of enteric *lactobacilli* [94]. TEM (Transmission electron microscopy) and SDS-PAGE techniques have been also applied to investigate two surface proteins with compositional characteristics similar to S-layer proteins that function as aggregation promoting factors in *Lac. johnsonii* and *Lac. gasseri* cells [95]. Up to date, many structural genes of S-layer have been sequenced. Regarding the primary structure prediction of the encoded S-layers proteins, the basic isoelectric points (pI) possess values more than 9 due to the lysine-rich terminal regions. For *Lac. brevis* ATCC14869 it was proved, that different expressional products can be obtained in different environmental conditions. In this organism, three *slp* genes (*slpB, slpC* and *slpD*) were identified [96] and its S-layer gene is known to possess variability [97].

Self-assembly is a very important characteristic of *Lactobacillus* S-layer proteins. Interestingly, all S-layer arrays of this organism exhibit very similar, oblique (p2) lattice structures [5], [50] (Chap. 2 p55). S-layer proteins from *Lac. helveticus* and *Lac. crispatus* encode two domains. The first one builds two thirds of the high conserved N-terminal, which is responsible for either intra- or intermolecular subunit interaction and hence, is very important for domain structure–function. The second domain comprises the last third of the protein, which is the C-terminal (SAC) part. This is the cell wall binding domain of slpA and acts as a binding mediator, as it possesses an acid-labile, peptidoglycan-associated compound [98, 99]. Although the SAC repeat size is very similar to SLH domain, there is no sequence similarity between these two motifs. Another S-layer protein self-assembly was studied, the folding of CbsA from *Lac. crispatus* has been investigated by molecular force driving using AFM

techniques [100]. Interestingly, it could be reported that S-layer-carrying *Lactobacillus* strains do not adhere better hydrophobic substrates than strains without S-layers, even if Lactobacillus is known for its hydrophobicity of S-layers [101-103]. After a series of similar studies, a summary was drawn by Paul Messner et al. [50] (Chap. 2 p76, see Figure 5.1.2 in the discussion of this work), which reports that *Lactobacillus* S-layer proteins comprise two structurally and functionally independent domains. Also, reports on corresponding vaccines to treat this bacillus have been successively published [99, 104, 105].

1.4.4 Geobacillus stearothermophilus

As a strictly aerobic species of endospore-forming bacteria, *G. stearothermophilus* represents a Gram-positive staining and can be covered with crystalline S-layers of different lattice geometries [6, 13, 106]. Most frequent studies on the *G. stearothermophilus* NRS 2004/3a strains mainly focused on the observation and elucidation of S-layer proteins with regard to post-translational modifications [53, 66, 67, 106-116]. Its structural gene sgsE encodes four S-layer proteins, named SbsA-D. The N-terminal signal peptide sequences of SbsA, SbsC, SbsD and SbsB consist of 30 amino acids, respectively. All four proteins present a weakly acidic isoelectric point and have an identical signal peptide cleavage Ala-Ala motif [110, 112, 117]. Interestingly, SbsB does not only have a different homology as compared to the other three proteins, but also possesses the unique SLH domain [55, 118]. More recently, the general glycosylation process of S-layer proteins was also studied within the *in vivo* biosynthesis in WbaP-deficient strains of *E. coli* and *S. enterica serovar Typhimurium* [115].

Two other important species are the strains *G. stearothermophilus* ATCC 12980^T and PV72. The first S-layer gene *sbs*A was cloned and sequenced from the wild-type *G. stearothermophilus* PV72/p6, exhibiting a p6 lattice symmetry [119, 120]. Upon cultivation under high oxygen concentrations in harsh environments, the hexagonal symmetry of the PV72/p6 formed by SbsA was rearranged to an oblique lattice type known for the S-layer protein SbsB of the variant designated PV72/p2 [120]. Actually, the square (p4) symmetry of PV72/p2 is most stable in this species, as this symmetry is even kept after removing 237 C-terminal amino acids. The deletion of 350 C-terminal amino acids, although, results in a change from the square (p4) to the oblique (p1) lattice structure [58]. The SLH domains of

SbsB are located in N-terminal region, and the comprising alpha helixes are responsible for SCWP binding, as has been studied by circular dichroism spectroscopy (CD). The C-terminal parts of SbsB could be characterized as a beta sheet protein in charge of self-assembly [121]. The successful three dimensional structure determination of SbsB, which has been published recently (PDB ID:4aq1) [45], highlighted the S-layer research to a great extent.

1.4.5 *Lysinibacillus sphaericus*

L. sphaericus, formerly also called *B. sphaericus,* represents a strictly aerobic group of mesophilic endospore-forming bacteria. Most studies of S-layer proteins from *L. Sphaericus* comprise the basic research, such as feature estimation and molecular dynamics motions, the sequencing, cloning and expressing of *L. sphaericus* CCM 2177 [122], as well as the calculation of the electric point (4.69), the molecular weight estimation (129 kDa) and the research of abnormal insertion elements in different strains [38]. Furthermore, the secondary structure prediction by CD spectroscopy revealed that alpha helices are enriched in the N-terminus and loops and beta strands dominate in the middle and in the C-terminal parts of the protein [58]. It was also demonstrated that the deletion of the C-teminus did not affect the capability of self assembly within the *L. sphaericus* protein [122]. A research with remarkable application potential was the successful complexation of uranium with S-layers, enabled by the *L. Sphaericus* S-layer protein carrying the phosphate groups [123].

1.4.6 *Several other Gram-negative organisms carrying S-layers*

Several other S-layer-carrying organisms have also been reported in recent years. For example, functional tests of *T. forsythia* demonstrate that the S-layer is highly in charge of adherence/invasion to human gingival epithelial. It causes hemagglutination and is associated to coaggregation with *P. gingivalis*, which is another crucial oral pathogen [30, 124]. Another example is *Ca. vibrioides*, which is covered by a hexagonal S-layer lattice. The most interesting finding is that the assembly of this hexagonal array always needs the presence of calcium and that the S-layer anchoring motifs have not been identified, in contrast to Gram-positive organisms [125-127]. Sap type genes of *C. fetus* encode a series of sap proteins, some of them function as a human pathogen, like for instance sapA and sapB

[128, 129]; some other S-layer proteins can induce protective immune responses, which may promote the synthesis of vaccine candidates for *C. fetus ssp. fetus-associated* ovine abortion [130].

In summary, S-layers can now be considered as one of the most universally observed prokaryotic cell envelope structures, regarding the increasing knowledge on the genetics, the assembly, the structure and chemistry over the recent decades. However, up to date, the investigation of 3 dimensional structures based on crystallization and X-ray diffraction analysis is still difficult and the structure-function relationship for the vast majority of S-layers is still not completely understood. Nevertheless, regarding the increasing data describing S-layers, applications are certainly forthcoming in life and in non-life sciences.

1.5 Nanobiotechnological Applications of S-layers

The self-assembly capability of single subunits, reconstructing monomolecular lattices with defined orientation in suspension or on suitable surfaces or interfaces, promotes potential applications of S-layers.

Up to now, most results regarding the morphological studies of S-layers could be achieved by investigating the formation of the self-assembly system. Generally, the intersubunit bonds in the S-layer lattices are much stronger than those binding to the supporting envelope layer, as discussed previously [49]. Different environmental parameters like temperature, pH, ion composition, and/or ionic strength, can form different shape and size self-assembly products, such as flat sheets, open-ended cylinders, or closed vesicles [6, 13, 51, 60, 70, 131].

In view of many recrystallization studies of S-layer lattices from *L. sphaericus* and *G. stearothermophilus* strains, highly anisotropic structures with regard to their inner and outer surfaces have been revealed. Based on the research of many intermolecular effects like protein-protein or protein-metal ions interaction, it could be described that S-layer matrices immobilize the corresponding macromolecules and that the nanoparticles function as a string rope [132-136].

The recombination of functional S-layer fusion proteins has also attracted many scientists since the nanotechnological applications of self-assembly system are of high interest.

Table 1.5 Properties of S-layer fusion proteins (modified from U.B. Slytr, Eva-Maria Eglseer)

S-layer fusion protein	Length of function (aa)	Functionality	Reference
rSbsB1-889/core streptavidin rSbpA31-1068/core streptavidin	118 aa	Binding of biotinylated molecules	Ref. [152, 153]
rSbpA31-1068/Bet v 1 rSbsC31-920/Bet v 1	116aa	Birch pollen allergen for immunomodulation	Ref. [122, 154]
rSbpA31-1268/Strep-tag rSbpA31-1068/Strep-tag	9aa	Affinity tag for streptavidin	Ref. [122]
rSbpA31-1068/ZZ	116aa	Binding of IgG	Ref. [137]
rSbpA31-1068/EGFP	238aa	Intrinsic fluorencence	Ref. [122]
rSbpA31-1068/cAb	117aa	Heavy chain camel antibody recognizing lysozyme and PSA	Ref. [155, 156]
rSbpA31-1068/AG4/AGP35/CO2P2	12aa	Binding of ciliver and cobalt	Ref. [157]
rSbpA31-1068/Lam A	263aa	(Hyper)thermophilic enzyme activity	Ref. [141]
rSgsE331-903/RmlA	299aa	Enzyme activity (biocatalyst)	Ref. [140]
SbsA/Omp 26	200aa	Vaccine against H. influenza infection	Ref. [145]
rSbpA31-1068/F1 rSbpB1-889/F1	20aa	Antibody binding for EBV diagnostics	Ref. [142]

Table 1.5 lists almost all S-layer fusion proteins, which have been cloned and expressed in *E. coli* so far. Due to the successful re-crystallization of rSbpA/ZZ (from *L. sphaericus*) on microbeads, a microsphere-based detoxification matrix with highly biocompatibility used for extracorporeal blood purification of patients suffering from autoimmune disease, could be obtained [137]. Benefiting from the immunomodulating capacity of two chimeric S-layer proteins (rSbpA31–1068/Bet v 1 and rSbsC31–920/Bet v 1), this chimeric effect provides a promising way to treat related allergic diseases [138]. These S-layer fusion proteins can be used for label-free detection systems, as layers that finally result from the specific binding event, become detectable by the increase in mass [139]. Two types of self-assembly biocatalysts, not only in solution but also on diverse support substrates, could be generated due to the intrinsic self assembly property of the chimeric S-layer monomers into an oblique (SgsE) or square (SbpA) 2D crystalline array with a periodicity in the nanometer scale [140, 141].

In combination with the diagnostic studies on the peptide mimotope F1, it is indicated that these S-layer fusion proteins have great potential to play the role of a matrix, which can immobilize small ligands into solid-phase immunoassays by site-direction [142].

S-layers can be used as an antibacterial vaccine carrier or adjuvant, like the S-layer protein of the fish-pathogenic bacteria itself is essential for virulence [143]. Some basic researches also proposed that it is a good vaccine candidate of immunotherapy, cancer and anti-allergy [6, 144]. Possible vaccines against *Haemophilus influenzae* (NTHi) infection, in combination with the investigation of both S-layer fusion proteins and bacterial ghosts systems, show that the latter can induce Omp26-specific anti-body response in mice and can play a role of intrinsic adjuvant in vaccine delivery system [145]. Some potential applications of S-layers, such as whole-cell vaccines, tumor suppressors, cellular adsorbents and peptide display libraries have also been studied [146-149]. The self-assembly products of S-layer fusion proteins comprising the antigen mpt64 have also been reported recently, which serve as carriers and adjuvants of a vaccine against tuberculosis [142]. Current studies on S-layer fusion proteins mainly concentrate in the recombinational production from *G. stearothermophilus* PV72/p2 and *L. sphaericus* CCM 2177.A further important application is the function as an isoporous molecular sieve, as the S-layer from *Bacillaceae* serves as a natural bio-ultrafiltration

membrane [150, 151]. Furthermore, the synthesis of different membranes with different charges or hydrophilic or hydrophobic components is possible by chemical modification of reactive groups, which are located on each constituent subunit at an identical position and identical orientation [5, 158, 159].

The relationship between the adjacent lipid monolayer and the attached S-layer protein has been studied by microscopic and light scattering techniques [160, 161]. As semifluid lipid membranes, S-layer-supported lipid membranes posses nanopatterned properties that function as stabilizing fences for liposomes and lipid membranes, consequently S-layers-coated liposomes resemble the role of archaeal cell or virus envelopes[162, 163].

Currently, the research hotspots in nanobiotechnology mainly concentrate on the design and on the creation of novel materials in the nanoscale, exploiting self-assembly systems with building blocks at the molecular level. In the future, S-layers stabilizing lipid membranes may mimic the supramolecular assembly of archaeal cell envelopes. In the present work, the S-layer proteins self-assembling capability of forming monomolecular arrays, not only in suspension but also on surfaces and interfaces, were investigated and discussed.

1.6 Biosorption and Nanocluster Formation

In the turn of the century, it was demonstrated that prokaryotic organisms were involved in precipitation and biosorption of inorganic compounds, based on the analysis of microfossils [164-167].

The main metal-binding groups of Gram-positive and Gram-negative bacteria are the carboxylic and phosphate groups that possess various biopolymer characteristics. They are locating on cell walls of bacteria or archaea, where the primary accumulation of metals occurs. With increasing metal ion concentrations near the metal-binding sites of organisms, the bio-mineral interaction forming the complexes reaches saturation, which finally leads to precipitation and nucleation and mineral building.

In the case of Gram-negative bacteria, the cell wall comprises lipopolysacharides, which build a complex mosaic bilayered structure containing phospholipids and proteins (see Figure 1.1.1). The carboxylic and phosphate groups of the rather thin (about 3 nm)

peptidoglycan layer of Gram-negative bacteria, which are located in the periplasm between SCWP and the lipid membranes, mainly contribute to the metal binding, but the extent is significantly higher than that in Gram-positive bacteria [167]. Due to the lack of lipopolysaccharide layer, the metal-binding relies on the negative charge of the attached secondary polymers, which contains peptidoglycan phosphate groups [167, 168].

Most archaea and a large number of bacteria possess S-layers, which are in some cases glycosylated and phosphorylated, this strongly indicates that S-layers contain thriving carboxylic and phosphate groups. As a result, they possess a high affinity to metal cations [5, 38, 169, 170]. Some S-layers of photosynthetic bacteria and others, such as capsules, slimes and shealths as the outermost membrane, all can activate the process of biominerization due to the high enrichment in the two groups mentioned above [164, 167, 171].

During the past 30 years, the accumulation and biosorption of iron (Fe) and uranium (U) in S-layers has been reported in a variety of literature, including natural and laboratory simulated environments. Generally, there are two types of uranium in the natural environment, one is soluble in liquid wastes, U(VI), another one is immobilized in sediments, insoluble U(IV) [172-174]. Despite the reduction of the soluble U(VI) to insoluble U(IV) is easily occurred upon addition of electron donors such as lactate, pyruvate, acetate, or ethanol [172-174], the immobilized uranium (U(IV)) will be reoxidized and returned back to the treated habitat (U(VI)) when electron donors complete depletion [175-177]. Five years ago, *Geissler et al.* have confirmed that the addition of uranyl nitrate leads to immobilization of the added U(VI) in mixed inorganic and organic phosphate compounds in model microcosm experiments. These were performed under oligotrophic and anaerobic conditions, with the samples being close to the natural condition. Collecting occurred from depleted and lightly contaminated uranium mining wastes near the city of Johanngeorgenstadt (Germany) [178]. The reductive driving force is precisely promoted by the activity of organic phosphate compounds. The principle of reduction from Fe(III) to Fe(II) is very similar to the uranium experiment. One representative bacterium is *L. sphaericus*, more precisely the two isolated strains JG-7B and JG-A12. Uranium was able to bind exclusively to the components of the cell wall. Most of it was accumulated in the inner side of the S-layer and onto the outer side of the cross-linked peptidoglycan layers and no

intracellular precipitates of uranium was found in these two strains [123, 179]. Utilizing the capability of U(VI), which is known to selectively and reversibly accumulate great amounts in mill tailing waters [180], the strain JG-A12 was successfully applied into construction of biological ceramics for bioremediation [181]. The S-layer from JG-A12 is also related in interactions with other radionuclides, for example, the accumulation of the chemical analog of Cm(III), namely Eu(III), onto the surface of the strain. Similarly, studies on the localization of metallic palladium nanoparticles have been reported, with only one exception of metal-binding ligands changing to the carboxylic groups of the S-layer [169, 182].

Under simulated natural uranium mining waste conditions, bacteria accumulate the soluble U(VI) mainly *via* phosphate groups on their cell walls forming meta-autunite mineral phases. Particularly, both archaea and bacteria are able to facilitate uranyl phosphate mineral phases due to the secretion of orthophosphate groups into their extracellular surface polymers.

1.7 S-layer Proteins Analysed

In order to define the binding behavior of S-layer proteins and to specify the nanoparticles at the amino acid level, it is required to obtain detailed structural information concerning S-layer proteins [28]. To address this challenge, three-dimensional structures of two S-layer proteins resulting from different strains of the same species were characterized and compared in this work. Both strains were isolated from the uranium mining waste pile Haberland near Johanngeorgenstadt, Germany. SlfB (surface layer protein function B), from *L. sphaericus* JGA12 (*L. Sphaericus, Johanngeorgenstadt strain A12*), consists of 1238 amino acids (with 32 N-terminal amino acids serving as the signal peptide) and a corresponding molecular weight of 129 kDa with a pI value of 5.2 [181]. Thermal and chemical unfolding studies revealed a complex unfolding behavior leading to the assumption of a multi-domain protein [38]. Slp-B53 is one of 8 putative S-layer protein genes with distinct differences. It consists of 1104 amino acids (with 31 N-terminal amino acids comprising the signal peptide), possesses a pI value of 5.5 and a molecular weight of 116 kDa [183]. These two proteins have a high affinity for metal binding and show outstanding re-crystallization properties.

2 Aim of This Work

Numorous striking functional information of S-layer protein on the one hand, but rare reports about their structures on the other hand, focussed the interest of biologists towards detailed structure investigations.

In terms of this thesis, the difficulties why only few suitable S-layer protein crystals could be obtained during the past should be rationally analysed. The objective of this work was firstly to overcome the self-assembly of target proteins slfB and slp-B53 due to long distance transportation or long-term storage. Consequently, the secondary structure of both purified S-layer proteins should be analyzed on the basis of their sequence property and by CD spectroscopy. Particularly, the influence of bivalent cations on the flexibility of S-layer proteins should be addressed. Also the monodispersity and radius distribution of slfB and slp-B53 in the presence and absence of bivalent cations, such as Ca^{2+} and Mg^{2+}, should be determined by DLS. The phenomena of S-layer proteins self-assembly should be elaborated on the basis of CD and AFM experiments [184, 185]. What's more, the effect of different cations on the protein-protein interaction should be discussed, followed by investigations concerning the S-layer proteins self-assembly mechanism.

The shape and 3D assembly of S-layer proteins in solution, as well as pre-(post-)self-assembly processes should be analysed by SAXS. Specifically, the data concerning the 3D-structural shape, the mechanism, the dynamics of self-assembly and the ion-binding for both S-layer protein slfB and slp-B53 should be investigated using SAXS.

Futher more, the possibility to carry out crystallization experiments using slfB and slp-B53 with and without bivalent cations should be questioned, including the possibility of crystallizing slp-B53 with bound Mg^{2+}.

3 Materials and Methods

Both sIfB and slp-B53 were provided by Dr. J. Raff and his colleagues from the institute of resource ecology at HZDR (Helmholtz-Zentrum, Dresden-Rossendorf). To characterize these two proteins, especially the effect of cation binding and its 2D self-assembly, four techniques have been employed: Circular Dichroism (CD) Spectroscopy, Atomic Force Microscopy (AFM), Dynamic Light Scattering (DLS) and Small Angle X-ray Scattering (SAXS). Additionally, secondary structure predictions have been performed on the basis of sequence analysis.

3.1 Brief Preparation Process of Biomass

As described before [181, 183], the preparation procedure of biomass (sIfB and slp-B53) was briefly summarized as following.

3.1.1 Basic procedures of the S-layer proteins preparation

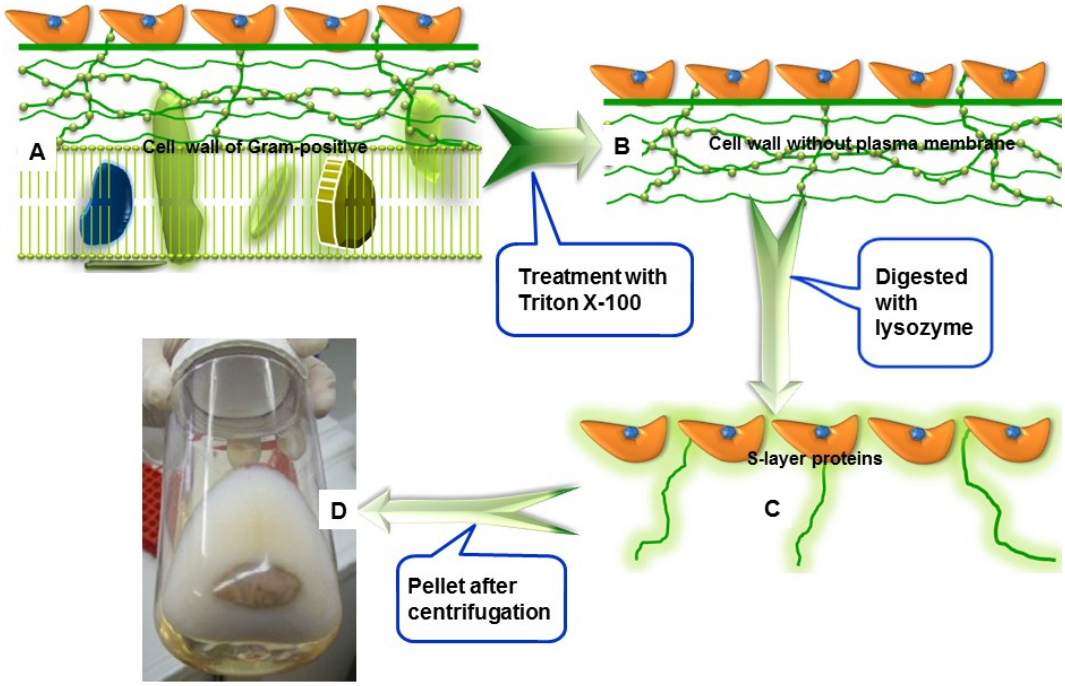

Figure 3.1.1 A) Cell wall of a Gram-positive bacterium, comprising S-layer proteins, secondary cell wall polymers, peptidoglycan and plasma membrane, B) Cell wall of Gram-positive bacteria after treatment with Triton X-100, the plasma membrane has been withdrawn. C) Digestion of S-layer proteins with lysozyme, the peptidoglycan was completely removed, D) After centrifugation of digested S-layer proteins, the two-layer pellet is clearly visible.

Figure 3.1.1 shows the basic procedures of the S-layer proteins preparation. The cell walls consist of S-layer proteins, peptidoglycans, secondary cell wall polymers and the plasma membrane (Figure 3.1.1A). The plasma membrane is chemically removed with Triton X-100, as shown in Figure 3.1.1B. Then, the peptidoglycan is digested enzymatically with lysozyme (Figure 3.1.1C). By means of centrifugation (Figure 3.1.1D) and dialysis, small proteins can be recovered by simultaneous removing the cell wall components. In detail, the pellet was resuspended with buffer (1:1 (w/v)), containing lysozyme and the right amount of DNase and RNase. This mixture was incubated under shaking for 6 hours in a water bath. The solution was then centrifuged for at least 90 minutes at 20,000 g. The supernatant was collected, which is a mixture of the proteins polymer / monomer / oligomer equilibrium (Polymer pellet; monomer solution). The monomers were obtained by using the characteristic of S-layer proteins to aggregate or disaggregate in correlation to the pH value, as shown in Table 3.1.1.

Table 3.1.1 S-layer suspension of strains JG-A12 at different pH values (pH 2 to pH 8). The table shows the polymer content of the suspensions (%) by (modified from the presentation communication of J. Raff et al, 2012).

Polymer content of the suspensions (%)	pH 2	pH 3	pH 4	pH 4.5	pH 5	pH 6	pH 7	pH 8
JG-A12 (1 g/L)	0	40	83	-	84	91	91	75

At lower pH values, the polymer content of the suspensions is reduced. For JG-A12, the polymer content tends towards zero at pH 2.0. Nevertheless, the biochemical properties of the protein are maintained, when the pH is restored to normal, physiological values. The result of this procedure is highly purified S-layer protein.

3.1.2 Analysis of S-layer proteins

The respective protein concentration was determined by NanoDrop measurements. SDS-PAGE was applied to determine the molecular weight of the S-layer proteins. Gel filtration was used to re-purify proteins that were kept by long-term storage or were retrieved by long-distance transports.

3.1.3 Preparation of buffer and sample solutions in respective experiments

Unless stated else, the protein buffer used in protein investigations consisted of 75 mM NaCl, 25mM Tris at a pH of 7.4. Protein concentration was estimated prior to every experiment by analysis of the absorption at a wavelength of 280 nm applying a Nanodrop 2000c (Fisher Scientific, Peqlab, Germany).

In order to avoid negative influence on the monodispersity of proteins, all long-distance transport and long-term cryopreservation proteins were applied to a superdex 200 (S-200) (GE-Healthcare) gel filtration column. The FPLC (Fast protein liquid chromatography), i.e. by using the ÄKTA purifier system (GE Healthcare, UK), was performed to repurify the proteins. The run was initiated by the software and an A_{280} detection unit was turned on to monitor the elution of proteins. Peak fractions, showing high A_{280} signals were collected and analyzed on SDS gels. The protein size was determined by size exclusion chromatography (SEC) with a calibration run according to the manufacturer´s protocol. The calibration curve was used to estimate the molecular weight of the proteins.

For AFM measurements, polyelectrolyte capsules were used (Substrate, silica wafer SiO_2 + polyelectrolyte layer). PEL coating with S-layer proteins was produced as described before [186-188]. Both final protein concentrations were in approx. of 0.2 mg/mL

For each measurements of CD, DLS and SAXS, the corresponding conditions used for the slfB and slp-B53 examinations are listed in Table 3.1.3 a and b, respectively.

Table 3.1.3a Corresponding concentrations of slfB and bivalent cations additives for different measurements.

CD		DLS		SAXS		
				1	**2**	**3**
1	0.05 mg/mL **slfB**	**1**	10.2 mg/mL **slfB**	**slfB**	**slfB + 100 mM Ca^{2+}**	**slfB + 100 mM Mg^{2+}**
2	0.05 mg/mL **slfB + 5 mM Ca^{2+}**	**2**	10.2 mg/mL **slfB + 100 mM Ca^{2+}**	0.49 mg/mL	0.46 mg/mL	0.64 mg/mL
				1.0 mg/mL	1.34 mg/mL	1.33 mg/mL
3	0.05 mg/mL **slfB + 50 mM Mg^{2+}**	**3**	10.2 mg/mL **slfB + 100 mM Mg^{2+}**	1.67 mg/mL	1.74 mg/mL	1.63 mg/mL
				2.70 mg/mL	2.48 mg/mL	2.81 mg/mL

Table 3.1.3b Corresponding concentrations of slp-B53 and bivalent cations additives for different measurements.

CD		DLS		SAXS		
				1	**2**	**3**
1	0.05 mg/mL **slp-B53**	**1**	9.7 mg/mL **slp-B53**	**slp-B53**	**slp-B53 + 100 mM Ca^{2+}**	**slp-B53 + 100 mM Mg^{2+}**
2	0.05 mg/mL **slp-B53 + 5 mM Ca^{2+}**	**2**	9.7 mg/mL **slp-B53 + 100 mM Ca^{2+}**	0.41 mg/mL	0.55 mg/mL	0.58 mg/mL
				0.83 mg/mL	1.10 mg/mL	1.13 mg/mL
3	0.05 mg/mL **slp-B53 + 50 mM Mg^{2+}**	**3**	9.7 mg/mL **slp-B53 + 100 mM Mg^{2+}**	1.29 mg/mL	1.51 mg/mL	1.74 mg/mL
				2.15 mg/mL	2.21 mg/mL	2.30 mg/mL

3.2 Circular Dichroism (CD) Spectroscopy

3.2.1 Circular Dichroism

Circular Dichroism (CD) characterizes the difference in the absorption of left-handed circularly polarized light (L-CPL) and right-handed circularly polarized light (R-CPL) when a molecule possesses one or more light-absorbing groups. These so called chiral chromophores can arouse CD signals. Thus, the CD signal in term of absorbance can be expressed as following equation: CD =$\mathbf{\Delta A(\lambda) = A(\lambda)_{LCPL} - A(\lambda)_{RCPL}}$, where λ is the wavelength. Figure 3.2.1a reveals the respective principle of circularly polarized and linear polarized light. Obviously, circularly polarized is more complex as compared to the linear polarization. The difference in absorbance of left-hand and right-hand circularly polarized light is the basis of circular dichroism. A molecule that absorbs LCP and RCP differently is optically active, or chiral, like for instance bio-macromolecules or some chiral inorganic molecules.

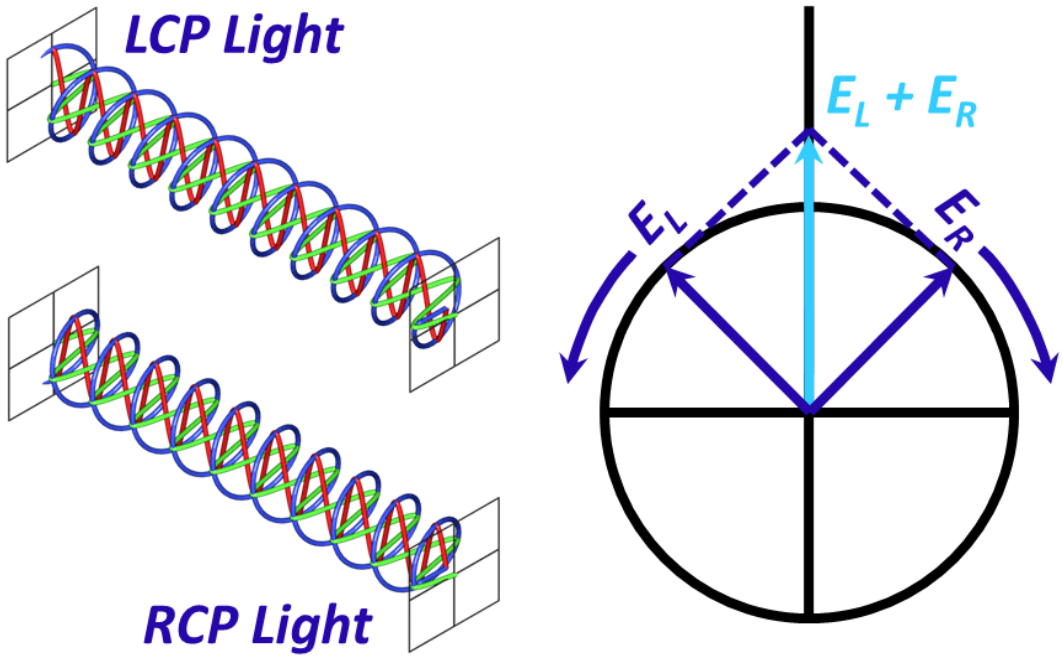

Figure 3.2.1a Upper circularly polarized is the (LCP) Light, lower circularly polarised is the (RCP) Light. The red line is vertically polarized light and the green line is horizontally polarized light, as shown in the left part of the figure. The right part of the picture presents a linear polarized light, which can be viewed as a superposition of opposite circular polarized light with equal amplitude and phase.

Figure 3.2.1b gives insight into the principle of circular dichroism polarization when the light hits on the bio-macromolecules. Circular dichroism measured as a function of wavelength is termed circular dichroism (CD) spectroscopy. Particularly, wavelengths with left-and right-circular polarized light will be absorbed to different extents. For instance, a chiral chromophore may absorb 90% of R-CPL and 88% of L-CPL. As a consequence, CD data can be defined in terms of ellipticity: The mean residue ellipticity at a wavelength λ, $[\Theta]_{mrw,}\lambda$, in units of $deg.cm^2.dmol^{-1}$. Where mrw is the mean residue weight, with usual values around 110, the accurate value can be obtained by dividing the molecular mass by *N-1* (*N* is the number of amino acids). The classic formula function is $[\Theta]_{mrw,}\lambda$ [189], with λ given by: $[\Theta]_{mrw,}\lambda = MRW\ \Theta/10dc$.

Where Θ is the observed ellipticity (degrees), *d* and *c* are the pathlength (cm) and concentration (g/mL), respectively.

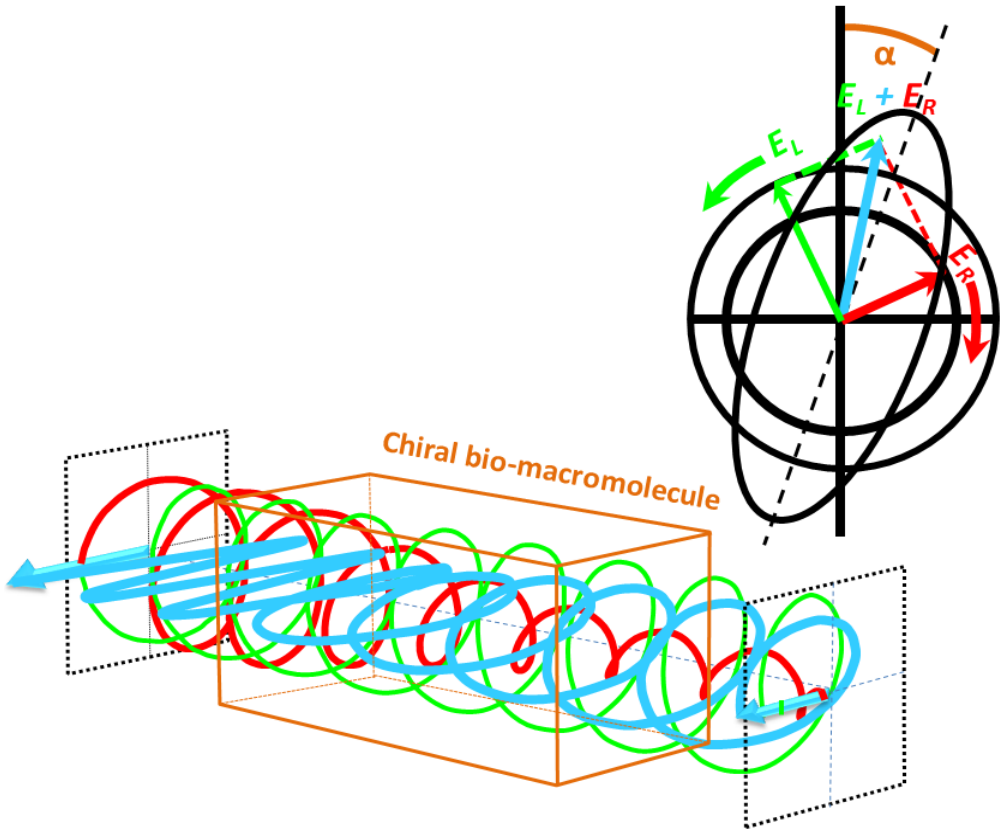

Figure 3.2.1b Circular Dichroism occurs at wavelengths of light, which can be absorbed by a chiral molecule (the orange cuboid represents the sample).

3.2.2 Study of biological molecules

Based on the analysis of a CD spectrum in the far UV region (240-180 nm), which corresponds to the peptide bond absorption, the content of regular secondary structural features such as α-helices and β-sheets can be provided. Some of the common protein secondary structural elements with their associated CD spectra are shown in Figure 3.2.2a. Obviously, the primary role of CD spectroscopy is the analysis of the secondary conformation of proteins [190-194], which is one of the most successful applications of this method (see Figure 3.2.2b). Particularly, regarding that the secondary structural component of a protein is sensitive to its environment, variations in temperature or pH can also be applied to observe how a secondary structure changes, as monitored by CD spectroscopy.

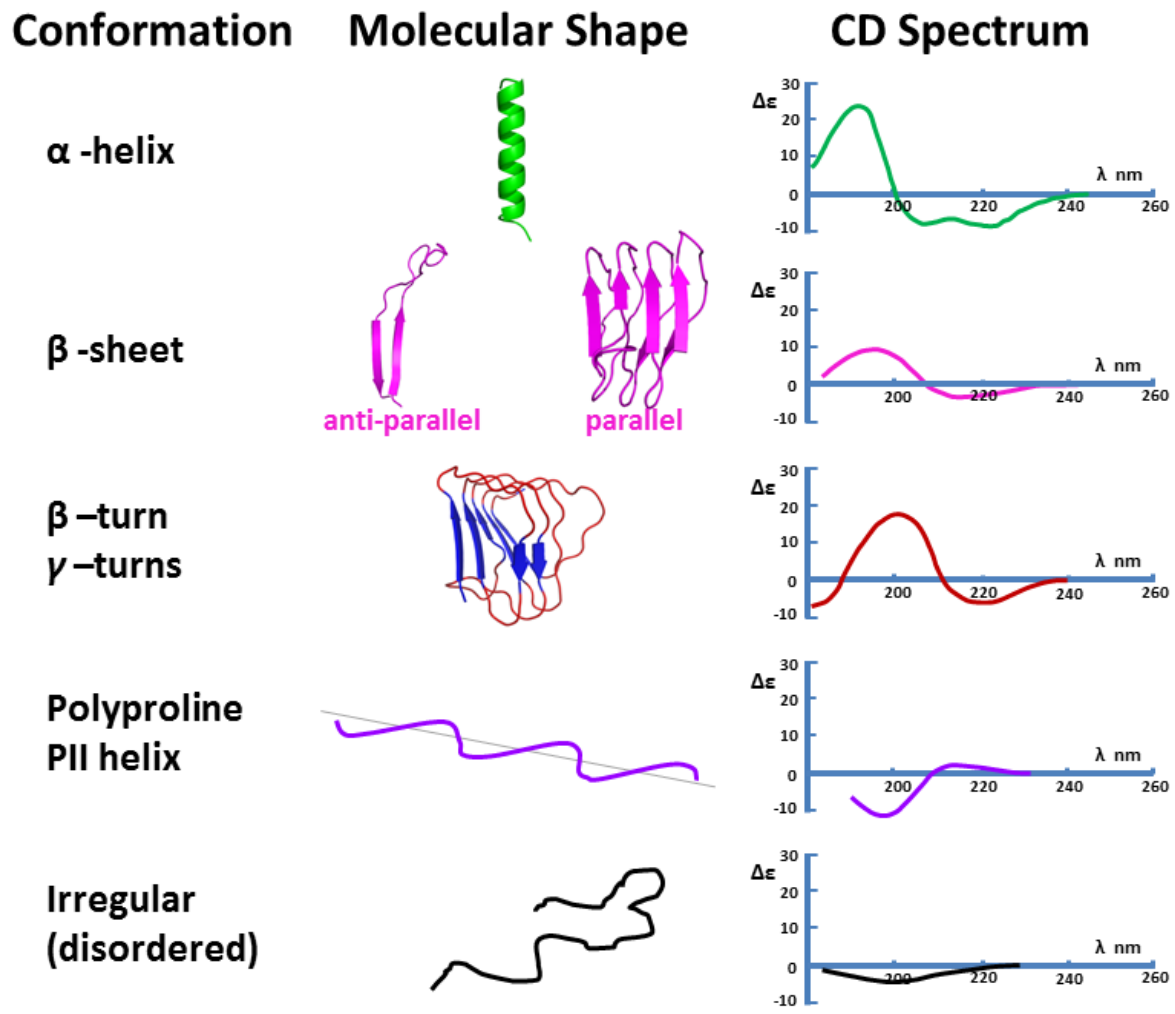

Figure 3.2.2a Circular Dichroism signatures of secondary structural elements.

Each structure has a specific circular dichroism signature, and this can be used to identify structural elements and to follow changes in the structure of chiral macromolecules. Figure 3.2.2a shows circular dichroism signatures of corresponding secondary structural elements. Every secondary structural conformation was followed by its corresponding molecular shape and the associated CD spectrum. It is worth to note that the CD spectrum of a protein or DNA molecule is not a simple sum of the CD spectra of the individual residues or bases, but is greatly influenced by the 3-dimensional structure of the macromolecule itself.

Another powerful application of circular dichroism is to compare the structure of two macromolecules, or to analyze the same molecule under different conditions and thereby to determine whether they have a similar structure. This can be used simply to ascertain if a newly purified protein is correctly folded, to determine if a mutant protein has folded correctly in comparison to the wild-type, or for the analysis of biopharmaceutical products to confirm that they are still in a correctly folded active conformation.

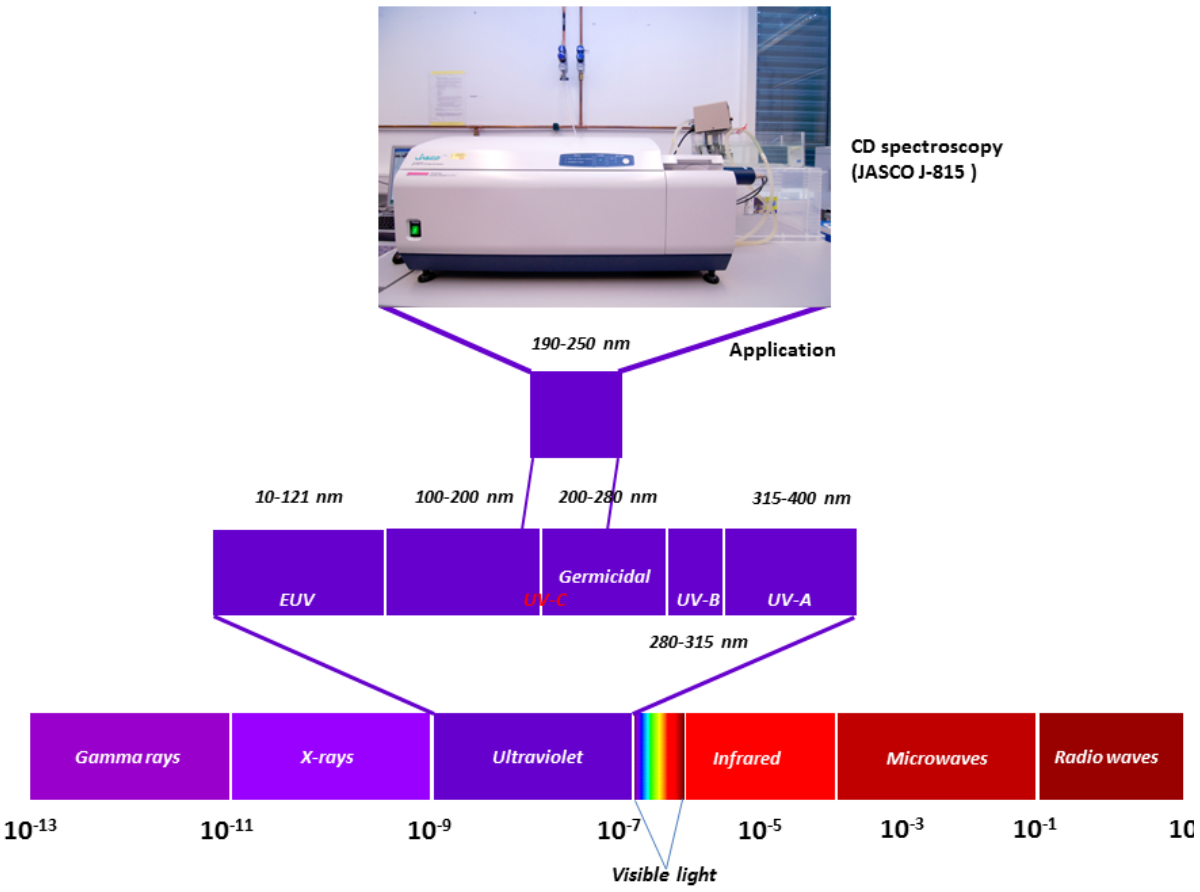

Figure 3.2.2b CD spectroscopy: A most successful application of UV polarized light.

So far, several algorithms can be applied for fitting the circular dichroism spectra of proteins to assess the secondary structure content, such as Selcon3 [195]/CDSSTR [196]/ContinII [197]. In this work, both the web server and the CD spectroscopy were used to study the secondary structures contents on the one hand and to investigate the domain distribution regions on the other hand, in order to understand the properties and characteristics of S-layer proteins.

3.3 Atomic Force Microscopy (AFM) Technology

AFM is composed by a cantilever with a sharp tip (probe) at its end that is used to scan the specimen surface. The cantilever is typically silicon or silicon nitride with a tip radius at the curvature on the order of nanometers. When the tip is brought into proximity of a sample surface, forces between the tip and the sample lead to a deflection of the cantilever according to Hooke's law. Basically, AFM has the advantage of imaging almost any type of surface, including polymers, ceramics, composites, glass and biological samples. Especially within the last few decades, the application of AFM in biology has become very popular, which greatly broadened structural science in the examination of 3-dimensional structures and deepened insight in the particle shape of bio-macromolecules [34, 184, 198]. Additionally, sample requirements without any special treatments (such as metal/carbon coatings) which would irreversibly change or damage the sample are greatly facilitated to the operability of such experiments. Most AFM modes can work perfectly well in the ambient air. Particularly the way of operation in liquid environment enhances the simplicity of sample preparation. It avoids the distortion of the images *i.e.* sample shrinkage and shape changes in the morphology of the cell due to the evaporation of the sample in the requested ultra-high vacuum in a normal electron microscope. This advantage enables the investigation of biological macromolecules and even living organisms. In principle, AFM can provide higher resolution than SEM [34]. Certainly, there are also some disadvantages as compared to other types of electron microscopy. For example, its scanning speed is very slow [199-201] and it cannot detect the undercuts of whole sample, only the top-down way [198]. Other disadvantages of AFM, such as the scan image size, the possible imaging with only a

maximum height in the range of 10-20 micrometers and a maximum scanning area of about 150×150 micrometers also have to be further improved. Also, images of AFM influenced by nonlinearity, hysteresis [202] and creep of the piezoelectric material, as well as cross-talk between the x, y, z axes that may require software enhancement and filtering, need to be further developed.

Since the invention of AFM by Binnig *et al.* in the year 1986, this method emerges to one of the foremost tools for imaging, measuring and manipulating samples at the nanoscale region [203], promoted by the increasing development of corresponding elements, such as piezoelectric scanners [204, 205] (Chap. 1) and probe tips [206].

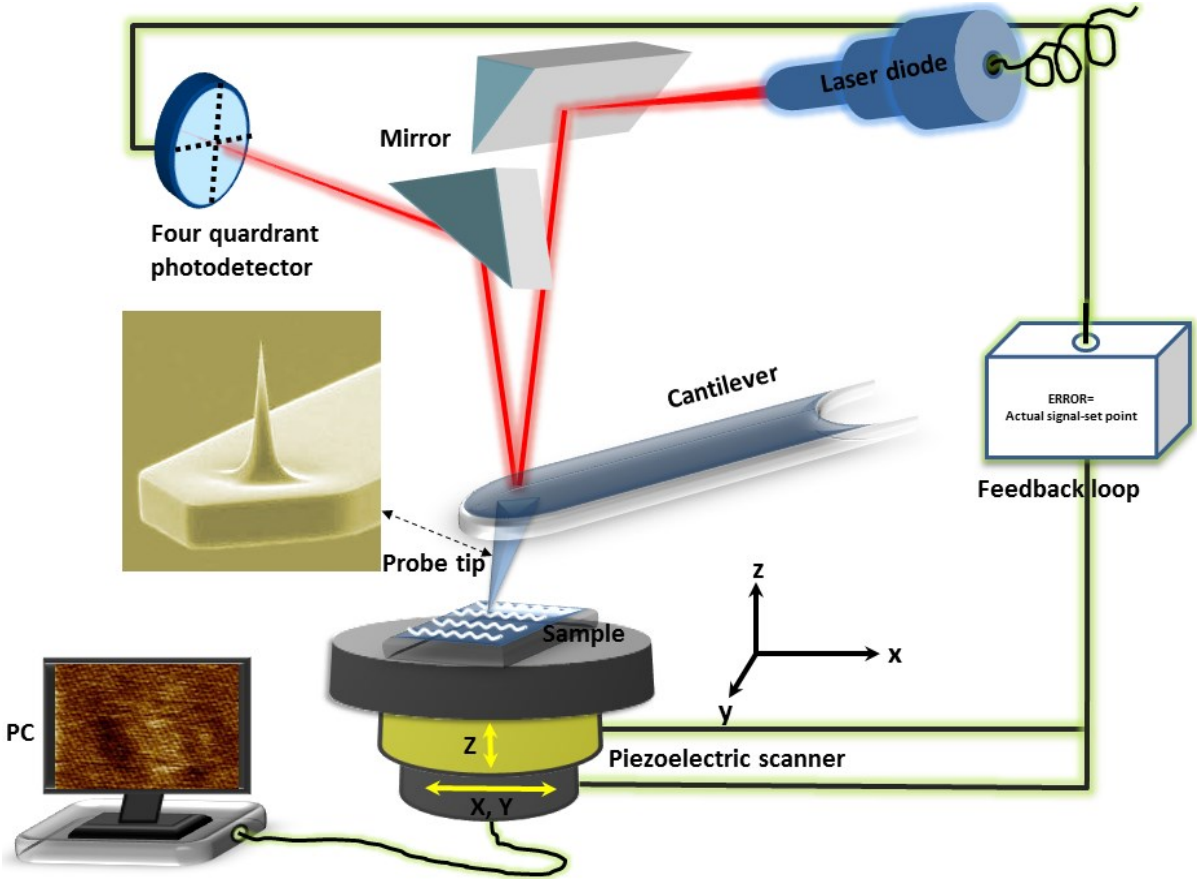

Figure 3.3 Atomic Force Microscopy setup.

3.3.1 Probe

AFM can be operated in a number of modes depending on the application, the consistence of the tip and the cantilever. In general, possible imaging modes are divided into static (also

called contact) modes and a variety of dynamic (non-contact or "tapping") modes where the cantilever is vibrated [203]. An AFM probe is a consumable and measuring device with a sharp tip on the free swinging end of a cantilever, which protrudes on the holder plate used in AFM [207]. Most AFM probes used are made from silicon (Si) or silicon nitride. Depending on the interaction of sample investigated, the surface of the AFM probe tip needs to be modified with some special coating substrates [208-210]. Today, a variety of commercial probes can be provided for users, such as PFTUNA from the Bruker Company, USA and the SiNi (Si_3N_4) probe from Innovative Solutions Bulgaria Ltd.

3.3.2 AFM cantilever deflection measurement

The beam deflection method is the most common technique for cantilever deflection measurements. In this method, laser light from a solid state diode is reflected from the back of the cantilever and is subsequent collected by a position sensitive detector (PSD) consisting of two closely spaced photodiodes whose output signal is collected by a differential amplifier, as shown in Figure 3.3. Positional shifting of the cantilever leads to one photodiode collecting more light as compared to the other photodiode, generating an output normalized signal which is related to the deflection of the cantilever. The detected cantilever deflection is less than 10 nm due to the limitation of thermal noise. Many Other deflection measurement methods were also exploited, such as Piezoelectric detection [211], Laser Doppler vibrometry [212], STM [203], Optical Interfermoetry [213], Capacitive detection [214] and Piezoresistive [215].

3.3.3 Imaging modes

The primary modes of operation for an AFM are the static mode and the dynamic mode. In the static mode, the cantilever is "dragged" across the surface of the sample and the contours of the surface are measured directly using the deflection of the cantilever including the contact mode and the non-contact mode [216, 217]. In the dynamic mode, the cantilever is externally oscillated at or close to its fundamental resonance frequency or a harmonic one. The dynamic contact mode (also called intermittent contact, AC mode or tapping mode) was developed to bypass the problem, as in ambient conditions most samples develop a liquid

meniscus layer. Because of this, the probe tip has to be kept close enough to the sample for short-range forces to become detectable while preventing the tip from sticking to the surface. This presents a major problem for the non-contact dynamic mode in ambient conditions [34, 218, 219].

3.3.4 Identification of individual surface atoms

AFM is used not only to image but also to manipulate atoms and structures on a variety of surfaces. The atom at the head of the tip can sense individual atoms on the corresponding surface when it forms initial chemical bonds with each atom. Due to these chemical interactions that change the vibration frequency of tip, these can be recorded and then mapped even for that very slight frequency alteration. This principle was utilized to differentiate the atoms of silicon, those of tin, as well as those of lead within an alloy surface, by contrasting different vibration frequency values obtained from large-scale density functional theory (DFT) simulations [220]. The results revealed that the tip interacted most strongly with silicon atoms. The potency of tin and lead atoms is 23% and 41% of the silicon atoms interaction strength, respectively. Therefore, diverse type of atoms can be identified in the matrix when the tip is moved across the surface. Here, AFM is allowed to investigate the shape of the target bio-macromolecules as well as its surface characteristics.

3.4 Dynamic Light Scattering (DLS) Technology

The dynamic light scattering technique (also termed photon correlation spectroscopy or quasi-elastic light scattering) is applied to monitor the behavior of complex fluids such as concentrated polymer solutions in real time. It can also be used to determine the size distribution profile of small particles in suspension or polymers in solution [221].

3.4.1 Dynamic light scattering

When a laser strikes small particles, the light scatters in all directions as long as the laser wavelength (250 nm) is bigger than the particle sizes. Therefore, a time-dependent fluctuation in the scattering intensity can be observed and calculated. The driving force of this fluctuation is generated by the so called Brownian motion of small molecules in solution.

Consequently the distance between the scatterers is varying constantly depending on the time they persist in the solution. This scattered light then suffers either constructive or destructive interference by the surrounding particles, and within this intensity fluctuation, the scatterers record the time scale of movement and can be analyzed. In order to minimize the influence of dust and artifacts from the sample preparation in solution, in general, filtration or centrifugation is applied as a very common and critical method. The scheme of instrumentation for DLS is shown in Figure 3.4.1.

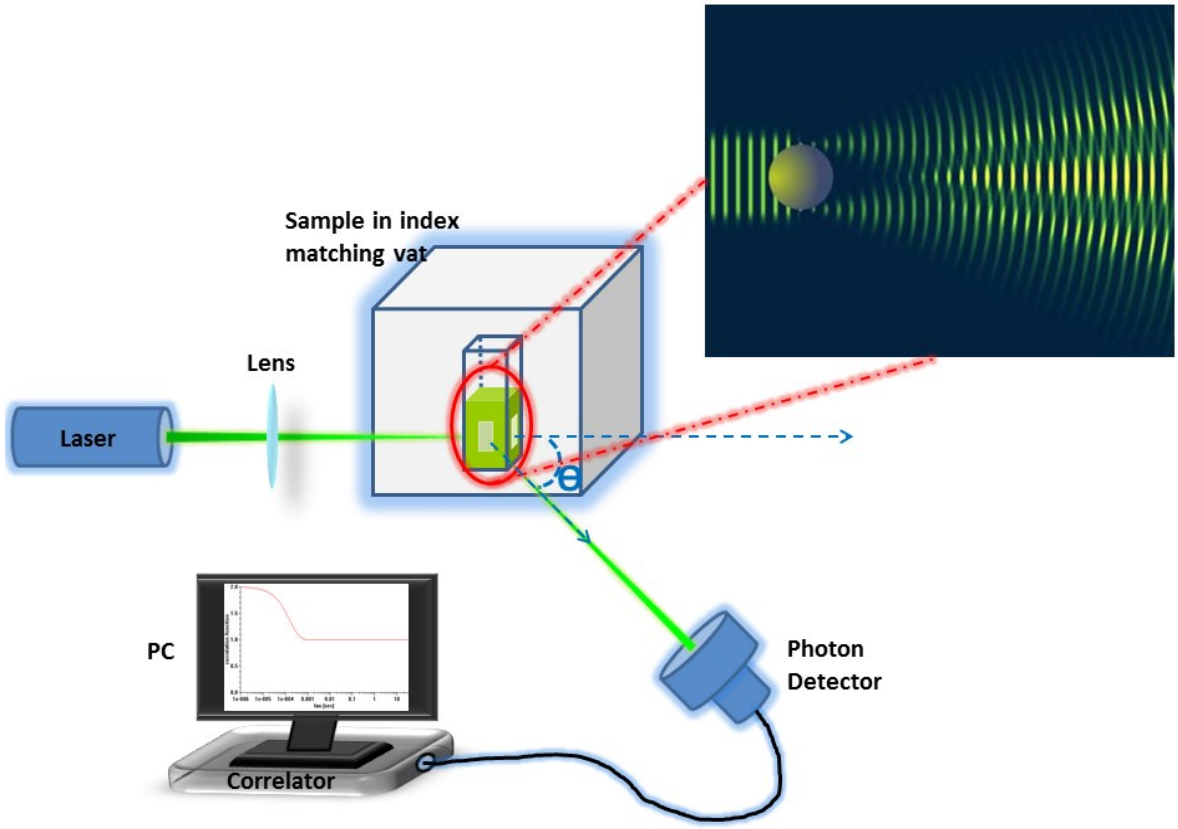

Figure 3.4.1 Dynamic Light Scattering setup.

The dynamic data of the particles are calculated from an autocorrelation of the intensity trace recorded during the experiment. The second order autocorrelation curve is created from the intensity trace as follows:

$$g^2(q;\tau) = \frac{\langle I(t)I(t+\tau)\rangle}{\langle I(t)\rangle^2}$$

In this equation, $g^2(q;\tau)$ denotes the autocorrelation function at a particular wave vector,

q, and delay time, τ ; and I is the intensity. The correlation is proportional to τ because the particles have no chance to shift to a great extent at short time delays. The two signals are thus essentially unchanged when compared after only a very short time interval. As the time delays become longer, the correlation decays exponentially, indicating that no correlation exists between the scattered intensity of the initial and final states after a long time period elapsed. This exponential decay is associated with the motion of the particles, especially to the diffusion coefficient. To match the decay (i.e., the autocorrelation function), numerical methods based on calculations of assumed distributions are usually used. The decay of monodisperse sample is simply a single exponential. The Siegert equation concerns the second-order autocorrelation function and the first-order autocorrelation function $g^1(q;\tau)$ as follows:

$$g^2(q;\Gamma) = 1 + \beta\left[g^1(q;\tau)\right]$$

The correction factor that depends on the geometry and alignment of the laser beam in the light scattering setup is represented by symbol β. It is roughly equal to the inverse of the number of speckle from which light is collected. The most significant usage of the autocorrelation function is its application in size determination.

Treating the first order autocorrelation function as a single exponential decay is the simplest strategy. This is applicable to a monodisperse population.

$$g^1(q;\tau) = \exp(-\Gamma\tau)$$

Here, Γ is the decay rate. The translational diffusion coefficient D_t can be established at a single angle or at a range of angles relying on the wave vector q.

$$\Gamma = q^2 D_t$$

with

$$q = \frac{4\pi n_0}{\lambda}\sin\left(\frac{\theta}{2}\right)$$

λ represents the incident laser wavelength, n_0 denotes the refractive index of the sample and ϑ is the angle at which the detector is located with respect to the sample cell, as shown in Figure 3.4.

3.4.2 Applications of DLS

The essential application of DLS is the size characterization of various particles like proteins, polymers, micelles, carbohydrates and nanoparticles. Since DLS mainly measures fluctuations in scattered light intensity caused by diffusing particles, the diffusion coefficient of the particles can be determined. Stability studies can be determined conveniently using DLS. Periodical DLS measurements of a sample can indicate whether the particles aggregate upon a certain time period by observing whether the hydrodynamic radius of the particle increases. If particles aggregate, there will be a larger population of particles with increasing radius. Additionally, in certain DLS machines, stability depending on temperature can be analyzed by controlling the temperature [222]. Due to continuous efforts of engineers and scientists, a derivative technique of DLS - DDLS (deplorized dynamic light scattering) [223] can be even used to estimate the shape of the protein without any invasive so far. In the present study, DLS was used to determine the monodispersity and radius distribution of target proteins with and without bivalent cations.

3.5 Small Angle X-ray Scattering (SAXS) Technology

3.5.1 Small angle X-ray scattering (SAXS) from proteins

Small angle x-ray scattering (SAXS) is inherently used to compare the scattering signal difference of the average electron density, $\Delta\rho(r)$. It can be expressed as: $\Delta\rho(r) = \rho(r) - \rho s$, where $\rho(r)$ represents the electron density of solute molecules of interest, and ρs is the electron density of the solvent (~ 33 $e^-/Å^3$ for pure water). However, proteins possess an average electron density of ~ 44 $e^-/ Å^3$. Larger $\Delta\rho(r)$ values arouse larger signals, which is important for the maximization of scattering differences and the contrast variation techniques from dilute solutions. SAXS data collected include the scattering signals from the buffer blank and from the samples. Thus, scattering signals of the blank from the sample must be subtracted as precisely as possible to accurately determine over three orders of magnitude differences. Considering the sample as homogeneous, monodisperse and lacking long-range interactions in solution [224], the relationships relevant to structure reconstruction that are most usually used are summarized in Table 3.5.1 [39, 225].

The two most important parameters, the Guinier approximation or the so called radially symmetric (isotropic) *I(q)* [226] and Pair distribution function *P(R)*, are used to reconstruct the SAXS structure. Here, *q* is the momentum transfer function, as the scattering angle 2Θ and expressed as $q=(4\pi \sin\Theta)/\lambda$, λ is the wavelength of incident X-ray beam (see the advance X-ray beam of EMBL in Figure 3.5.1); the pair-distribution function *P*(*R*) is the SAXS function corresponding to the Patterson function, which is a autocorrelation function that can be directly calculated through a Fourier transform of the scattering curve (see Table 3.5.1). The result provides direct information about the distances between electrons in the scattering particles in the sample, in a manner similar to the Patterson function. Typically, in practical balancing the smoothness of the trial *P*(*R*) functions with the goodness of fit to the data, a regularizing multiplier is usually used, for example in the GNOM program [227]. In this work, SAXS was applied to analyze the shape variation of S-layer proteins.

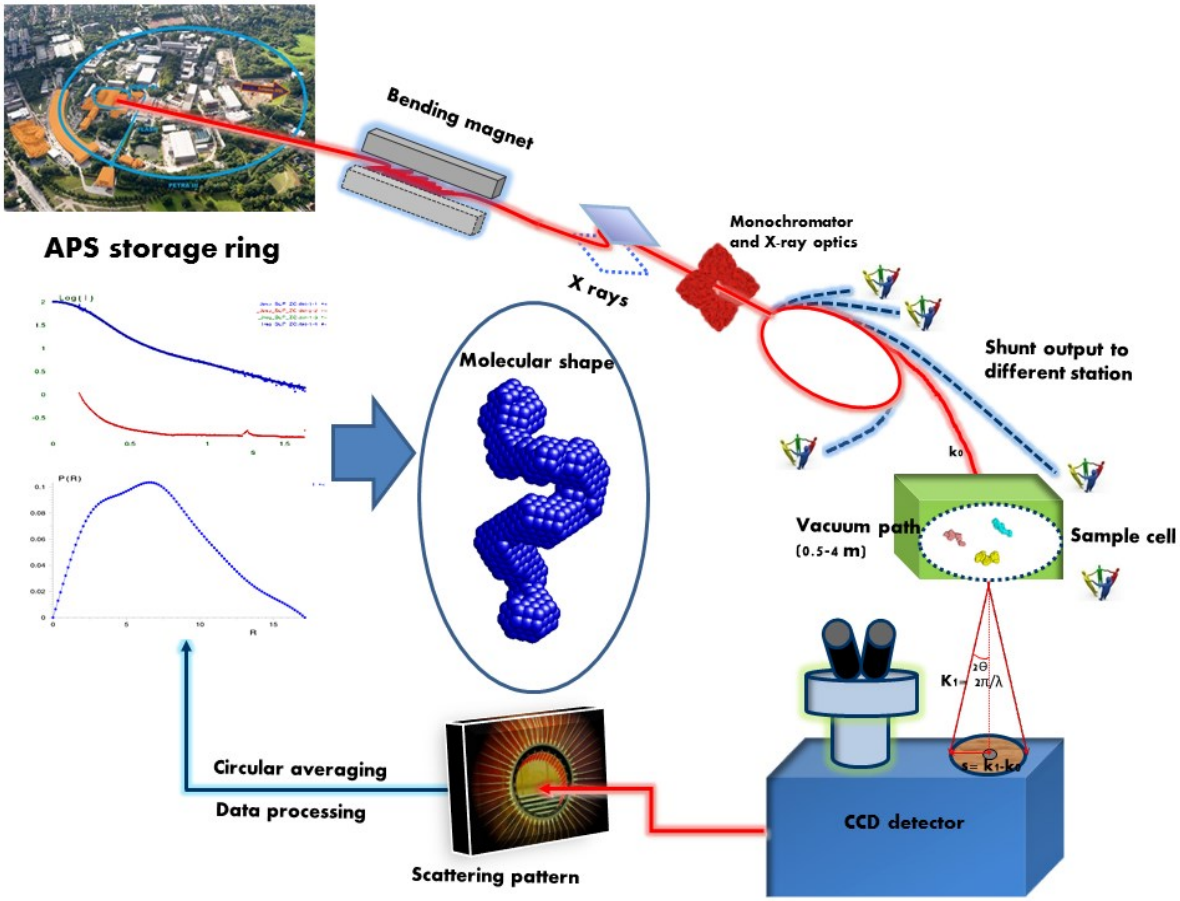

Figure 3.5.1 Work flow chart of the advanced EMBL SAXS beamline (DESY).

Table 3.5.1 Common parameters defined by SAXS for monodisperse and homologenous scatters (modified from C.D. Putnam *et al.*, 2007).

Parameter	Formula	Range of data used and variable definitions	comments
Radius of gyration (R_G) Guinier approximation	$\ln[I(q)] = \ln[I(0)] - \frac{q^2 R_G^2}{3}$	qR_G<1.3 globular, qR_G<0.8 elongated. $I(0)$: Intensity of the scattering profile extrapolated to q=0	Most common method of estimating R_G Measured via the slope of the plot ln[$I(q)$] vs. q^2
Radius of gyration (R_G) Debye approximation	$I(q) = \frac{2I(0)}{q^4 R_G^4}\left(q^2 R_G^2 - 1 + e^{-q^2 R_G^2}\right)$	qR_G <1.4 for elongated macromolecules	Particularly useful for elongated proteins where the Guinier approximation is valid over narrower range
Radius of gyration (R_G) Debye approximation	$R_G^2 = \int_0^{D_{\max}} r^2 P(r)dr \Big/ \int_0^{D_{\max}} P(r)dr$	Entire q-range. D_{max} : Maximum dimension of particle	Good consistency check for R_G, D_{max}, and $P(r)$
Pair distribution function ($P(r)$)	$P(r) = \frac{r}{2\pi^2}\int_0^{\infty} I(q) q \sin(qr) dq$	Entire q-range	Indirect Fourier transform methods have been developed for calculating $P(r)$
Maximum dimension (D_{max})	$D_{\max}$ *is the value of r at* $P(r) = 0$ *for larger*	Requires data q<=π/D_{max}	Assignment of D_{max} may be complicated by flexibility or multimerization
Partical volume (V): defined by Porod Invariant	$V = 2\pi^2 I_{\exp}^2(0) \Big/ \left(\int_0^{\infty} I(q) q^2 dq\right)$	Entire q-range. $I_{exp}(0)$ is the experimental intensity at q=0 and does not require an absolute scale	The integral portion of this equation is known as the Porod invariant. Accuracy varies for shape and size; however absolute scale and concentration information are unnecessary
$I(0)$: Intensity at q=0 which is also proportional to mass and volume	$I(0) = 4\pi\left(\int_0^{D_{\max}} P(r)dr\right)$	Entire q-range	Calculation of M and V using this version of $I(0)$ is less susceptible to aggregation and inter-particle correlations than extrapolation of low q data
Mass (M)	$M = \frac{I(0)\mu^2}{N_A\left(1 - (\rho_s / \rho_p)\right)^2}$	μ: Average mass per number of electrons.ρ_S : Solvent electron density ρ_p : Particle electron density N_A: Avagadro's number	$I(0)$ must be on an absolute scale and normalized by mass/volume and not molar concentration
Radius of gyration of cross-section (R_{XC})	$\ln[qI(q)] = \ln[qI(0)] - \frac{q^2 R_{XC}^2}{2}$	Intermediate q values	The slope of the linear portion of a plot of ln[qI(q)] vs. q^2 is R_{XC}^2 ; however, R_{XC}^2 goes to 0 as q goes to 0 in regimes where scattering is dominated by R_G
Length (L)	$L = \left(12\left(R_G^2 - R_{XC}^2\right)\right)^{\frac{1}{2}}$	See R_G and R_{XC}	The co-axial length rather than the hypotenuse (D_{max})

3.5.2 Computational techniques for modeling protein flexibility

With the application of SAXS for studying the 3D structure of proteins, also macromolecular motion processes can be derived. These can be experimentally observed at high resolution or can be derived from computational techniques such as normal modes analysis (NMA), molecular dynamics (MD) and Monte Carlo-based techniques. All these techniques were required not only to substantially improve SAXS interpretation tools, but also to provide experimental feedback for improving the accuracy of modeling. Certainly, many other factors should also be considered in flexible protein modeling, such as time scales [228] and the application of essential dynamics (ED) methods [229, 230].

3.5.2.1 Normal modes analysis

NMA is a valid computational tool to study the slow, large-scale motions of macromolecules [231, 232]. Those calculations which are used to measure the distance observed in the static or equilibrium structures can be carried out using Cartesian or Torsion angle space [233]. NMA calculation costs much less than MD, and has the advantage of long time scales running [234]. NMA calculation focuses more on the geometry of the adjacent atoms instead of the details of the force field used [235-237]. Normal modes have been used for molecular replacement and refinement in protein crystallography due to the ability of handling systematically deformed molecules in agreement with the corresponding experimental data [238, 239]. These are real useful to calculate atomic models to fit EM and SAXS data.

3.5.2.2 Molecular dynamics simulations

MD is most commonly applied in many areas of structural biology [240]. MD simulates the influence of bonding, electrostatics and van der Waals interactions between adjacent atoms for calculating the energies and dynamics of molecules. A great advantage of MD simulations is that the force fields used are far exceeding the sizes as compared to the treatment by quantum mechanical methods. Thus, force fields are effective to determine chemical parameters, including bond lengths, bond angles, torsion angles, planarity restraints and

non-bonded distances [241]. In combination with SAXS data, the calculation of large conformational changes becomes possible to mold [14, 39-44].

3.5.2.3 Monte Carlo simulations

Monte Carlo simulations have been proved quite useful for modeling of SAXS data [14, 39-44] and have also been used for the sample pattern spacing in proteins [242]. This simulation can directly investigate their final states without requiring physically relevant trajectories as compared to MD simulations, such as the user-defined energetic force-field description for evaluating the conformation at each step. Monte Carlo algorithms have been widely used not only to study the protein folding [243], but also for modeling large rearrangements between protein domains [244].

3.6 Protein Crystallization

In principle, protein crystallization is the ultimate purpose and expected consequence of trial and error method, with which the protein is gradually precipitated from its solution. Generally, the crystallization of protein includes four vital steps: Determination of purity, searching of suitable solvent conditions, achievement of supersaturation and formation of nuclei.

To obtain high quality crystals, supersaturation must be maintained at a lower level to avoid the formation of too many nuclei and therefore too many small crystals. In practice, however, many factors can affect the saturation of proteins, such as salt effects (salting-out and salting-in) or the addition of PEG, or increasing the effective concentration of proteins. Other methods are to diminish the repulsive forces or to increase the attractive forces between the protein molecules by varying the temperature, adding organic solvent to change electrostatic forces or a change in pH, regarding the proteins as ionic compounds [245] (2^{nd} edition, Chap.1).

Many crystallization techniques were employed in this work such as liquid-liquid diffusion, vapor diffusion, counter diffusion and many more. Additional crystallization strategies were used to obtain suitable crystals and to further optimize their quality, for example, the

application of the flexible spare matrix screen for screening and seeding for crystallization optimization.

In summary, obtaining three-dimensional structure information of proteins is very complex. This work can be divided into several detailed parts, including samples treatment prior to structure analysis (SDS and gelfiltration), monodispersity analysis (DLS and SAXS, buffer optimization by adding additives or ions), pre-test crystallization (PCT, estimating protein concentration for crystallization), crystallization screening procedures and following optimization, data collection as well as data processing and data analysis.

3.6.1 Crystallization screening and optimization of slfB

SlfB was screened with the Honeybee 961 robot against common commercial screens (Nextal Classic suite, JCSG suite, PACT suite, Morpheus suite, Ammonium Sulfate suite, Stura Footprint and Macrosol suite and Compass suite) and *self-designed screen-pPEG series*. Several screen matrixes, which are aimed to optimize crystals quality, have been designed. They were based on the crystallization screening results from the pPEG7 suite that was used for slfB crystallization, as shown in the appendix- *self designed screen -pPEG series*. Table 3.6.1 shows the formulation of the pPEG7 screen.

3.6.2 Crystallization screening of slp-B53

For slp-B53, Honeybee 961 robot was also used to pipette the samples and reservoir solution against the same commercial screens: Nextal Classic suite, JCSG suite, PACT suite, Morpheus suite, Ammonium Sulfate suite, Stura Footprint and Macrosol suite and Compass suite. On the basis of these conditions, some screen matrixes have also been designed to obtain crystals, as shown in the appendix-*self-designed screen-PACT series*. Table 3.6.2 shows the components ratio of the PACT premier ™ Cacodylate free.

Table 3.6.1 pPEG7 Screen Conditions1-48

Source	1	2	3, 24	4	5, 12	6	7	8	9	10	11	13	14	15	16	17	18	19	20	21	22	23
Stock	PEG3350	PEG8000	PEG10000	AS	NaOAc pH4.75	NaCitrat pH4	Anion-Mix1	Anion-Mix2	Anion-Mix3	Wasser	Wasser2	AmNO3	NaI	NaBr	AnioMix5	AnioMix6	AmCl	AmBr	AmI	AmAc	AmFor	AmTar
Cstock	50	35	35	3	0,25	1	100	100	100			5	1	1	100	100	1	1	1	1	2	1
Vges	500																					

Number (Destiny)	Well	Prec	Cprec	Vprec	Source	Salt	Csalt	Vsalt	Source	Buffer	Cbuffer	Vbuffer	Source	Additive	Cadditive	Vadditive		Vsum	Vwater	Source
1	A1	PEG10000	15	214,2857143	3	AS	0,2	33,33333333	4	NaCitrat pH4	0,1	50	6	Anion Mix 2	10	50	8	347,6190476	152,3809524	10
2	A2	PEG10000	15	214,2857143	3	AS	0,2	33,33333333	4	NaCitrat pH4	0,1	50	6	Anion Mix 2	10	50	8	347,6190476	152,3809524	10
3	A3	PEG10000	15	214,2857143	3	AS	0,18	30	4	NaCitrat pH4	0,1	50	6	Anion Mix 2	10	50	8	344,2857143	155,7142857	10
4	A4	PEG10000	15	214,2857143	3	AS	0,18	30	4	NaCitrat pH4	0,1	50	6	Anion Mix 2	10	50	8	344,2857143	155,7142857	10
5	A5	PEG10000	15	214,2857143	3	AS	0,2	33,33333333	4	NaCitrat pH4	0,1	50	6	NaI	0,1	50	14	347,6190476	152,3809524	10
6	A6	PEG10000	15	214,2857143	3	AS	0,2	33,33333333	4	NaCitrat pH4	0,1	50	6	NaI	0,1	50	14	347,6190476	152,3809524	10
7	A7	PEG10000	15	214,2857143	3	AS	0,18	30	4	NaCitrat pH4	0,1	50	6	NaI	0,1	50	14	344,2857143	155,7142857	10
8	A8	PEG10000	15	214,2857143	3	AS	0,18	30	4	NaCitrat pH4	0,1	50	6	NaI	0,1	50	14	344,2857143	155,7142857	10
9	A9	PEG10000	15	214,2857143	3	AS	0,2	33,33333333	4	NaCitrat pH4	0,1	50	6	NaBr	0,1	50	15	347,6190476	152,3809524	10
10	A10	PEG10000	15	214,2857143	3	AS	0,2	33,33333333	4	NaCitrat pH4	0,1	50	6	NaBr	0,1	50	15	347,6190476	152,3809524	10
11	A11	PEG10000	15	214,2857143	3	AS	0,18	30	4	NaCitrat pH4	0,1	50	6	NaBr	0,1	50	15	344,2857143	155,7142857	10
12	A12	PEG10000	15	214,2857143	3	AS	0,18	30	4	NaCitrat pH4	0,1	50	6	NaBr	0,1	50	15	344,2857143	155,7142857	10
13	B1	PEG10000	15	214,2857143	3	AS	0,2	33,33333333	4	NaCitrat pH4	0,1	50	6	AnioMix5	10	50	16	347,6190476	152,3809524	10
14	B2	PEG10000	15	214,2857143	3	AS	0,2	33,33333333	4	NaCitrat pH4	0,1	50	6	AnioMix5	10	50	16	347,6190476	152,3809524	10
15	B3	PEG10000	15	214,2857143	3	AS	0,18	30	4	NaCitrat pH4	0,1	50	6	AnioMix5	10	50	16	344,2857143	155,7142857	10
16	B4	PEG10000	15	214,2857143	3	AS	0,18	30	4	NaCitrat pH4	0,1	50	6	AnioMix5	10	50	16	344,2857143	155,7142857	10
17	B5	PEG10000	15	214,2857143	3	AS	0,2	33,33333333	4	NaCitrat pH4	0,1	50	6	AnioMix6	10	50	17	347,6190476	152,3809524	10
18	B6	PEG10000	15	214,2857143	3	AS	0,2	33,33333333	4	NaCitrat pH4	0,1	50	6	AnioMix6	10	50	17	347,6190476	152,3809524	10
19	B7	PEG10000	15	214,2857143	3	AS	0,18	30	4	NaCitrat pH4	0,1	50	6	AnioMix6	10	50	17	344,2857143	155,7142857	10
20	B8	PEG10000	15	214,2857143	3	AS	0,18	30	4	NaCitrat pH4	0,1	50	6	AnioMix6	10	50	17	344,2857143	155,7142857	10
21	B9	PEG10000	15	214,2857143	3	AS	0,2	33,33333333	4	NaCitrat pH4	0,1	50	6	AmCl	0,1	50	18	347,6190476	152,3809524	10
22	B10	PEG10000	15	214,2857143	3	AS	0,2	33,33333333	4	NaCitrat pH4	0,1	50	6	AmCl	0,1	50	18	347,6190476	152,3809524	10
23	B11	PEG10000	15	214,2857143	3	AS	0,18	30	4	NaCitrat pH4	0,1	50	6	AmCl	0,1	50	18	344,2857143	155,7142857	10
24	B12	PEG10000	15	214,2857143	3	AS	0,18	30	4	NaCitrat pH4	0,1	50	6	AmCl	0,1	50	18	344,2857143	155,7142857	10
25	C1	PEG10000	15	214,2857143	3	AS	0,2	33,33333333	4	NaCitrat pH4	0,1	50	6	AmBr	0,1	50	19	347,6190476	152,3809524	10
26	C2	PEG10000	15	214,2857143	3	AS	0,2	33,33333333	4	NaCitrat pH4	0,1	50	6	AmBr	0,1	50	19	347,6190476	152,3809524	10
27	C3	PEG10000	15	214,2857143	3	AS	0,18	30	4	NaCitrat pH4	0,1	50	6	AmBr	0,1	50	19	344,2857143	155,7142857	10
28	C4	PEG10000	15	214,2857143	3	AS	0,18	30	4	NaCitrat pH4	0,1	50	6	AmBr	0,1	50	19	344,2857143	155,7142857	10
29	C5	PEG10000	15	214,2857143	3	AS	0,2	33,33333333	4	NaCitrat pH4	0,1	50	6	AmI	0,1	50	20	347,6190476	152,3809524	10
30	C6	PEG10000	15	214,2857143	3	AS	0,2	33,33333333	4	NaCitrat pH4	0,1	50	6	AmI	0,1	50	20	347,6190476	152,3809524	10
31	C7	PEG10000	15	214,2857143	3	AS	0,18	30	4	NaCitrat pH4	0,1	50	6	AmI	0,1	50	20	344,2857143	155,7142857	10
32	C8	PEG10000	15	214,2857143	3	AS	0,18	30	4	NaCitrat pH4	0,1	50	6	AmI	0,1	50	20	344,2857143	155,7142857	10
33	C9	PEG10000	15	214,2857143	3	AS	0,2	33,33333333	4	NaCitrat pH4	0,1	50	6	AmNO3	0,1	10	13	307,6190476	192,3809524	10
34	C10	PEG10000	15	214,2857143	3	AS	0,2	33,33333333	4	NaCitrat pH4	0,1	50	6	AmNO3	0,1	10	13	307,6190476	192,3809524	10
35	C11	PEG10000	15	214,2857143	3	AS	0,18	30	4	NaCitrat pH4	0,1	50	6	AmNO3	0,1	10	13	304,2857143	195,7142857	10
36	C12	PEG10000	15	214,2857143	3	AS	0,18	30	4	NaCitrat pH4	0,1	50	6	AmNO3	0,1	10	13	304,2857143	195,7142857	10
37	D1	PEG10000	15	214,2857143	3	AS	0,2	33,33333333	4	NaCitrat pH4	0,1	50	6	AmAc	0,1	50	21	347,6190476	152,3809524	10
38	D2	PEG10000	15	214,2857143	3	AS	0,2	33,33333333	4	NaCitrat pH4	0,1	50	6	AmAc	0,1	50	21	347,6190476	152,3809524	10
39	D3	PEG10000	15	214,2857143	3	AS	0,18	30	4	NaCitrat pH4	0,1	50	6	AmAc	0,1	50	21	344,2857143	155,7142857	10
40	D4	PEG10000	15	214,2857143	3	AS	0,18	30	4	NaCitrat pH4	0,1	50	6	AmAc	0,1	50	21	344,2857143	155,7142857	10
41	D5	PEG10000	15	214,2857143	3	AS	0,2	33,33333333	4	NaCitrat pH4	0,1	50	6	AmFor	0,1	25	22	322,6190476	177,3809524	10
42	D6	PEG10000	15	214,2857143	3	AS	0,2	33,33333333	4	NaCitrat pH4	0,1	50	6	AmFor	0,1	25	22	322,6190476	177,3809524	10
43	D7	PEG10000	15	214,2857143	3	AS	0,18	30	4	NaCitrat pH4	0,1	50	6	AmFor	0,1	25	22	319,2857143	180,7142857	10
44	D8	PEG10000	15	214,2857143	3	AS	0,18	30	4	NaCitrat pH4	0,1	50	6	AmFor	0,1	25	22	319,2857143	180,7142857	10
45	D9	PEG10000	15	214,2857143	3	AS	0,2	33,33333333	4	NaCitrat pH4	0,1	50	6	AmTar	0,1	50	23	347,6190476	152,3809524	10
46	D10	PEG10000	15	214,2857143	3	AS	0,2	33,33333333	4	NaCitrat pH4	0,1	50	6	AmTar	0,1	50	23	347,6190476	152,3809524	10
47	D11	PEG10000	15	214,2857143	3	AS	0,18	30	4	NaCitrat pH4	0,1	50	6	AmTar	0,1	50	23	344,2857143	155,7142857	10
48	D12	PEG10000	15	214,2857143	3	AS	0,18	30	4	NaCitrat pH4	0,1	50	6	AmTar	0,1	50	23	344,2857143	155,7142857	10

Table 3.6.1 pPEG7 Screen Conditions 49-96

Source	1	2	3, 24	4	5, 12	6	7	8	9	10	11	13	14	15	16	17	18	19	20	21	22	23
Stock	PEG3350	PEG8000	PEG10000	AS	NaOAc pH4.75	NaCitrat pH4	Anion-Mix1	Anion-Mix2	Anion-Mix3	Wasser	Wasser2	AmNO3	NaI	NaBr	AnioMix5	AnioMix6	AmCl	AmBr	AmI	AmAc	AmFor	AmTar
Cstock	50	35	35	3	0,25	1	100	100	100			5	1	1	100	100	1	1	1	1	2	1
Vges	500																					

Number (Destiny)	Well	Prec	Cprec	Vprec	Source	Salt	Csalt	Vsalt	Source	Buffer	Cbuffer	Vbuffer	Source	Additive	Cadditive	Vadditive		Vsum	Vwater	Source
49	E1	PEG10000	15	214,2857143	3	AmNO3	0,4	40	13	NaCitrat pH4	0,1	50	6	Anion Mix 2	10	50	8	354,2857143	145,7142857	11
50	E2	PEG10000	15	214,2857143	3	AmNO3	0,4	40	13	NaCitrat pH4	0,1	50	6	Anion Mix 2	10	50	8	354,2857143	145,7142857	11
51	E3	PEG10000	15	214,2857143	3	AmNO3	0,35	35	13	NaCitrat pH4	0,1	50	6	Anion Mix 2	10	50	8	349,2857143	150,7142857	11
52	E4	PEG10000	15	214,2857143	3	AmNO3	0,35	35	13	NaCitrat pH4	0,1	50	6	Anion Mix 2	10	50	8	349,2857143	150,7142857	11
53	E5	PEG10000	15	214,2857143	3	AmNO3	0,4	40	13	NaCitrat pH4	0,1	50	6	NaI	0,1	50	14	354,2857143	145,7142857	11
54	E6	PEG10000	15	214,2857143	3	AmNO3	0,4	40	13	NaCitrat pH4	0,1	50	6	NaI	0,1	50	14	354,2857143	145,7142857	11
55	E7	PEG10000	15	214,2857143	3	AmNO3	0,35	35	13	NaCitrat pH4	0,1	50	6	NaI	0,1	50	14	349,2857143	150,7142857	11
56	E8	PEG10000	15	214,2857143	3	AmNO3	0,35	35	13	NaCitrat pH4	0,1	50	6	NaI	0,1	50	14	349,2857143	150,7142857	11
57	E9	PEG10000	15	214,2857143	3	AmNO3	0,4	40	13	NaCitrat pH4	0,1	50	6	NaBr	0,1	50	15	354,2857143	145,7142857	11
58	E10	PEG10000	15	214,2857143	3	AmNO3	0,4	40	13	NaCitrat pH4	0,1	50	6	NaBr	0,1	50	15	354,2857143	145,7142857	11
59	E11	PEG10000	15	214,2857143	3	AmNO3	0,35	35	13	NaCitrat pH4	0,1	50	6	NaBr	0,1	50	15	349,2857143	150,7142857	11
60	E12	PEG10000	15	214,2857143	3	AmNO3	0,35	35	13	NaCitrat pH4	0,1	50	6	NaBr	0,1	50	15	349,2857143	150,7142857	11
61	F1	PEG10000	15	214,2857143	3	AmNO3	0,4	40	13	NaCitrat pH4	0,1	50	6	AnioMix5	10	50	16	354,2857143	145,7142857	11
62	F2	PEG10000	15	214,2857143	3	AmNO3	0,4	40	13	NaCitrat pH4	0,1	50	6	AnioMix5	10	50	16	354,2857143	145,7142857	11
63	F3	PEG10000	15	214,2857143	3	AmNO3	0,35	35	13	NaCitrat pH4	0,1	50	6	AnioMix5	10	50	16	349,2857143	150,7142857	11
64	F4	PEG10000	15	214,2857143	3	AmNO3	0,35	35	13	NaCitrat pH4	0,1	50	6	AnioMix5	10	50	16	349,2857143	150,7142857	11
65	F5	PEG10000	15	214,2857143	3	AmNO3	0,4	40	13	NaCitrat pH4	0,1	50	6	AnioMix6	10	50	17	354,2857143	145,7142857	11
66	F6	PEG10000	15	214,2857143	3	AmNO3	0,4	40	13	NaCitrat pH4	0,1	50	6	AnioMix6	10	50	17	354,2857143	145,7142857	11
67	F7	PEG10000	15	214,2857143	3	AmNO3	0,35	35	13	NaCitrat pH4	0,1	50	6	AnioMix6	10	50	17	349,2857143	150,7142857	11
68	F8	PEG10000	15	214,2857143	3	AmNO3	0,35	35	13	NaCitrat pH4	0,1	50	6	AnioMix6	10	50	17	349,2857143	150,7142857	11
69	F9	PEG10000	15	214,2857143	24	AmNO3	0,4	40	13	NaCitrat pH4	0,1	50	6	AmCl	0,1	50	18	354,2857143	145,7142857	11
70	F10	PEG10000	15	214,2857143	24	AmNO3	0,4	40	13	NaCitrat pH4	0,1	50	6	AmCl	0,1	50	18	354,2857143	145,7142857	11
71	F11	PEG10000	15	214,2857143	24	AmNO3	0,35	35	13	NaCitrat pH4	0,1	50	6	AmCl	0,1	50	18	349,2857143	150,7142857	11
72	F12	PEG10000	15	214,2857143	24	AmNO3	0,35	35	13	NaCitrat pH4	0,1	50	6	AmCl	0,1	50	18	349,2857143	150,7142857	11
73	G1	PEG10000	15	214,2857143	24	AmNO3	0,4	40	13	NaCitrat pH4	0,1	50	6	AmBr	0,1	50	19	354,2857143	145,7142857	11
74	G2	PEG10000	15	214,2857143	24	AmNO3	0,4	40	13	NaCitrat pH4	0,1	50	6	AmBr	0,1	50	19	354,2857143	145,7142857	11
75	G3	PEG10000	15	214,2857143	24	AmNO3	0,35	35	13	NaCitrat pH4	0,1	50	6	AmBr	0,1	50	19	349,2857143	150,7142857	11
76	G4	PEG10000	15	214,2857143	24	AmNO3	0,35	35	13	NaCitrat pH4	0,1	50	6	AmBr	0,1	50	19	349,2857143	150,7142857	11
77	G5	PEG10000	15	214,2857143	24	AmNO3	0,4	40	13	NaCitrat pH4	0,1	50	6	AmI	0,1	50	20	354,2857143	145,7142857	11
78	G6	PEG10000	15	214,2857143	24	AmNO3	0,4	40	13	NaCitrat pH4	0,1	50	6	AmI	0,1	50	20	354,2857143	145,7142857	11
79	G7	PEG10000	15	214,2857143	24	AmNO3	0,35	35	13	NaCitrat pH4	0,1	50	6	AmI	0,1	50	20	349,2857143	150,7142857	11
80	G8	PEG10000	15	214,2857143	24	AmNO3	0,35	35	13	NaCitrat pH4	0,1	50	6	AmI	0,1	50	20	349,2857143	150,7142857	11
81	G9	PEG10000	15	214,2857143	24	AmNO3	0,4	40	13	NaCitrat pH4	0,1	50	6	AmSO4	0,1	16,666667	13	320,952381	179,047619	11
82	G10	PEG10000	15	214,2857143	24	AmNO3	0,4	40	13	NaCitrat pH4	0,1	50	6	AmSO4	0,1	16,666667	13	320,952381	179,047619	11
83	G11	PEG10000	15	214,2857143	24	AmNO3	0,35	35	13	NaCitrat pH4	0,1	50	6	AmSO4	0,1	16,666667	13	315,952381	184,047619	11
84	G12	PEG10000	15	214,2857143	24	AmNO3	0,35	35	13	NaCitrat pH4	0,1	50	6	AmSO4	0,1	16,666667	13	315,952381	184,047619	11
85	H1	PEG10000	15	214,2857143	24	AmNO3	0,4	40	13	NaCitrat pH4	0,1	50	6	AmAc	0,1	50	21	354,2857143	145,7142857	11
86	H2	PEG10000	15	214,2857143	24	AmNO3	0,4	40	13	NaCitrat pH4	0,1	50	6	AmAc	0,1	50	21	354,2857143	145,7142857	11
87	H3	PEG10000	15	214,2857143	24	AmNO3	0,35	35	13	NaCitrat pH4	0,1	50	6	AmAc	0,1	50	21	349,2857143	150,7142857	11
88	H4	PEG10000	15	214,2857143	24	AmNO3	0,35	35	13	NaCitrat pH4	0,1	50	6	AmAc	0,1	50	21	349,2857143	150,7142857	11
89	H5	PEG10000	15	214,2857143	24	AmNO3	0,4	40	13	NaCitrat pH4	0,1	50	6	AmFor	0,1	25	22	329,2857143	170,7142857	11
90	H6	PEG10000	15	214,2857143	24	AmNO3	0,4	40	13	NaCitrat pH4	0,1	50	6	AmFor	0,1	25	22	329,2857143	170,7142857	11
91	H7	PEG10000	15	214,2857143	24	AmNO3	0,35	35	13	NaCitrat pH4	0,1	50	6	AmFor	0,1	25	22	324,2857143	175,7142857	11
92	H8	PEG10000	15	214,2857143	24	AmNO3	0,35	35	13	NaCitrat pH4	0,1	50	6	AmFor	0,1	25	22	324,2857143	175,7142857	11
93	H9	PEG10000	15	214,2857143	24	AmNO3	0,4	40	13	NaCitrat pH4	0,1	50	6	AmTar	0,1	50	23	354,2857143	145,7142857	11
94	H10	PEG10000	15	214,2857143	24	AmNO3	0,4	40	13	NaCitrat pH4	0,1	50	6	AmTar	0,1	50	23	354,2857143	145,7142857	11
95	H11	PEG10000	15	214,2857143	24	AmNO3	0,35	35	13	NaCitrat pH4	0,1	50	6	AmTar	0,1	50	23	349,2857143	150,7142857	11
96	H12	PEG10000	15	214,2857143	24	AmNO3	0,35	35	13	NaCitrat pH4	0,1	50	6	AmTar	0,1	50	23	349,2857143	150,7142857	11
				10285,71429				1800				2400				2166,6667		16652,38095	7347,619048	

Table 3.6.2 PACT premier ™ Cacodylate free

Conditions 1-48 MD 1-29-CF

Number	96-well plates	Salt	Buffer	Precipitant
1	A1		0.1M SPG buffer pH 4	25% w/v PEG 1500
2	A2		0.1M SPG buffer pH 5	25% w/v PEG 1500
3	A3		0.1M SPG buffer pH 6	25% w/v PEG 1500
4	A4		0.1M SPG buffer pH 7	25% w/v PEG 1500
5	A5		0.1M SPG buffer pH 8	25% w/v PEG 1500
6	A6		0.1M SPG buffer pH 9	25% w/v PEG 1500
7	A7	0.2M Sodium chloride	0.1M Sodium acetate pH 5	20% w/v PEG 6000
8	A8	0.2M Ammonium chloride	0.1M Sodium acetate pH 5	20% w/v PEG 6000
9	A9	0.2M Lithium chloride	0.1M Sodium acetate pH 5	20% w/v PEG 6000
10	A10	0.2M Magnesium chloride	0.1M Sodium acetate pH 5	20% w/v PEG 6000
11	A11	0.2M Calcium chloride	0.1M Sodium acetate pH 5	20% w/v PEG 6000
12	A12	0.01M Zinc chloride	0.1M Sodium acetate pH 5	20% w/v PEG 6000
13	B1		0.1M MIB buffer pH 4	25% w/v PEG 1500
14	B2		0.1M MIB buffer pH 5	25% w/v PEG 1500
15	B3		0.1M MIB buffer pH 6	25% w/v PEG 1500
16	B4		0.1M MIB buffer pH 7	25% w/v PEG 1500
17	B5		0.1M MIB buffer pH 8	25% w/v PEG 1500
18	B6		0.1M MIB buffer pH 9	25% w/v PEG 1500
19	B7	0.2M Sodium chloride	0.1M MES pH 6	20% w/v PEG 6000
20	B8	0.2M Ammonium chloride	0.1M MES pH 6	20% w/v PEG 6000
21	B9	0.2M Lithium chloride	0.1M MES pH 6	20% w/v PEG 6000
22	B10	0.2M Magnesium chloride	0.1M MES pH 6	20% w/v PEG 6000
23	B11	0.2M Calcium chloride	0.1M MES pH 6	20% w/v PEG 6000
24	B12	0.01M Zinc chloride	0.1M MES pH 6	20% w/v PEG 6000
25	C1		0.1M PCB buffer pH 4	25% w/v PEG 1500
26	C2		0.1M PCB buffer pH 5	25% w/v PEG 1500
27	C3		0.1M PCB buffer pH 6	25% w/v PEG 1500
28	C4		0.1M PCB buffer pH 7	25% w/v PEG 1500
29	C5		0.1M PCB buffer pH 8	25% w/v PEG 1500
30	C6		0.1M PCB buffer pH 9	25% w/v PEG 1500
31	C7	0.2M Sodium chloride	0.1M Hepes pH 7	20% w/v PEG 6000
32	C8	0.2M Ammonium chloride	0.1M Hepes pH 7	20% w/v PEG 6000
33	C9	0.2M Lithium chloride	0.1M Hepes pH 7	20% w/v PEG 6000
34	C10	0.2M Magnesium chloride	0.1M Hepes pH 7	20% w/v PEG 6000
35	C11	0.2M Calcium chloride	0.1M Hepes pH 7	20% w/v PEG 6000
36	C12	0.01M Zinc chloride	0.1M Hepes pH 7	20% w/v PEG 6000
37	D1		0.1M MMT buffer pH 4	25% w/v PEG 1500
38	D2		0.1M MMT buffer pH 5	25% w/v PEG 1500
39	D3		0.1M MMT buffer pH 6	25% w/v PEG 1500
40	D4		0.1M MMT buffer pH 7	25% w/v PEG 1500
41	D5		0.1M MMT buffer pH 8	25% w/v PEG 1500
42	D6		0.1M MMT buffer pH 9	25% w/v PEG 1500
43	D7	0.2M Sodium chloride	0.1M Tris pH 8	20% w/v PEG 6000
44	D8	0.2M Ammonium chloride	0.1M Tris pH 8	20% w/v PEG 6000
45	D9	0.2M Lithium chloride	0.1M Tris pH 8	20% w/v PEG 6000
46	D10	0.2M Magnesium chloride	0.1M Tris pH 8	20% w/v PEG 6000
47	D11	0.2M Calcium chloride	0.1M Tris pH 8	20% w/v PEG 6000
48	D12		0.1M Tris pH 8	20% w/v PEG 6000

Table 3.6.2 PACT premier ™ Cacodylate free

Conditions 49-96 MD 1-29-CF

Number	96-well plates	Salt	Buffer	Precipitant
49	E1	0.2M Sodium fluoride		20% w/v PEG 3350
50	E2	0.2M Sodium bromide		20% w/v PEG 3350
51	E3	0.2M Sodium iodide		20% w/v PEG 3350
52	E4	0.2M Potassium thiocyanate		20% w/v PEG 3350
53	E5	0.2M Sodium nitrate		20% w/v PEG 3350
54	E6	0.2M Sodium formate		20% w/v PEG 3350
55	E7	0.2M Sodium acetate		20% w/v PEG 3350
56	E8	0.2M Sodium sulphate		20% w/v PEG 3350
57	E9	0.2M Potassium/sodium tartrate		20% w/v PEG 3350
58	E10	0.2M Sodium/potassium phosphate		20% w/v PEG 3350
59	E11	0.2M Sodium citrate		20% w/v PEG 3350
60	E12	0.2M Sodium malonate		20% w/v PEG 3350
61	F1	0.2M Sodium fluoride	0.1M Bis Tris propane pH 6.5	20% w/v PEG 3350
62	F2	0.2M Sodium bromide	0.1M Bis Tris propane pH 6.5	20% w/v PEG 3350
63	F3	0.2M Sodium iodide	0.1M Bis Tris propane pH 6.5	20% w/v PEG 3350
64	F4	0.2M Potassium thiocyanate	0.1M Bis Tris propane pH 6.5	20% w/v PEG 3350
65	F5	0.2M Sodium nitrate	0.1M Bis Tris propane pH 6.5	20% w/v PEG 3350
66	F6	0.2M Sodium formate	0.1M Bis Tris propane pH 6.5	20% w/v PEG 3350
67	F7	0.2M Sodium acetate	0.1M Bis Tris propane pH 6.5	20% w/v PEG 3350
68	F8	0.2M Sodium sulphate	0.1M Bis Tris propane pH 6.5	20% w/v PEG 3350
69	F9	0.2M Potassium/sodium tartrate	0.1M Bis Tris propane pH 6.5	20% w/v PEG 3350
70	F10	0.2M Sodium/potassium phosphate	0.1M Bis Tris propane pH 6.5	20% w/v PEG 3350
71	F11	0.2M Sodium citrate	0.1M Bis Tris propane pH 6.5	20% w/v PEG 3350
72	F12	0.2M Sodium malonate	0.1M Bis Tris propane pH 6.5	20% w/v PEG 3350
73	G1	0.2M Sodium fluoride	0.1M Bis Tris propane pH 7.5	20% w/v PEG 3350
74	G2	0.2M Sodium bromide	0.1M Bis Tris propane pH 7.5	20% w/v PEG 3350
75	G3	0.2M Sodium iodide	0.1M Bis Tris propane pH 7.5	20% w/v PEG 3350
76	G4	0.2M Potassium thiocyanate	0.1M Bis Tris propane pH 7.5	20% w/v PEG 3350
77	G5	0.2M Sodium nitrate	0.1M Bis Tris propane pH 7.5	20% w/v PEG 3350
78	G6	0.2M Sodium formate	0.1M Bis Tris propane pH 7.5	20% w/v PEG 3350
79	G7	0.2M Sodium acetate	0.1M Bis Tris propane pH 7.5	20% w/v PEG 3350
80	G8	0.2M Sodium sulphate	0.1M Bis Tris propane pH 7.5	20% w/v PEG 3350
81	G9	0.2M Potassium/sodium tartarte	0.1M Bis Tris propane pH 7.5	20% w/v PEG 3350
82	G10	0.2M Sodium/potassium phosphate	0.1M Bis Tris propane pH 7.5	20% w/v PEG 3350
83	G11	0.2M Sodium citrate	0.1M Bis Tris propane pH 7.5	20% w/v PEG 3350
84	G12	0.2M Sodium malonate	0.1M Bis Tris propane pH 7.5	20% w/v PEG 3350
85	H1	0.2M Sodium fluoride	0.1M Bis Tris propane pH 8.5	20% w/v PEG 3350
86	H2	0.2M Sodium bromide	0.1M Bis Tris propane pH 8.5	20% w/v PEG 3350
87	H3	0.2M Sodium iodide	0.1M Bis Tris propane pH 8.5	20% w/v PEG 3350
88	H4	0.2M Potassium thiocyanate	0.1M Bis Tris propane pH 8.5	20% w/v PEG 3350
89	H5	0.2M Sodium nitrate	0.1M Bis Tris propane pH 8.5	20% w/v PEG 3350
90	H6	0.2M Sodium formate	0.1M Bis Tris propane pH 8.5	20% w/v PEG 3350
91	H7	0.2M Sodium acetate	0.1M Bis Tris propane pH 8.5	20% w/v PEG 3350
92	H8	0.2M Sodium sulphate	0.1M Bis Tris propane pH 8.5	20% w/v PEG 3350
93	H9	0.2M Potassium/sodium tartrate	0.1M Bis Tris propane pH 8.5	20% w/v PEG 3350
94	H10	0.2M Sodium/potassium phosphate	0.1M Bis Tris propane pH 8.5	20% w/v PEG 3350
95	H11	0.2M Sodium citrate	0.1M Bis Tris propane pH 8.5	20% w/v PEG 3350
96	H12	0.2M Sodium malonate	0.1M Bis Tris propane pH 8.5	20% w/v PEG 3350

4 Results

4.1 Secondary Structure Analysis

S-layer proteins are highly flexible and particularly possess numerous disordered regions, as so far analyzed [246, 247]. Both simulated prediction (web server prediction) and experimental methods (CD spectroscopy) were combined to obtain information about the disorder regions and the secondary structure of the target S-layer proteins, respectively.

4.1.1 Flexible regions prediction

4.1.1.1 SlfB

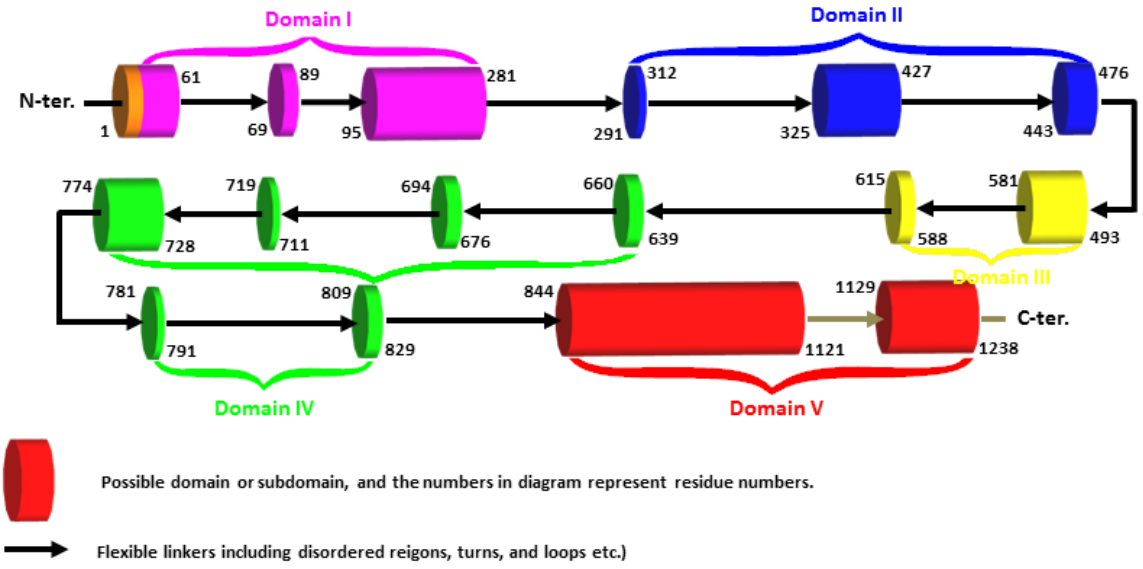

Disordered Regions	1	2	3	4	5	6	7	8	9	10	11	12	13	14	15
	61	89	281	312	427	476	581	615	660	694	719	774	791	829	1121
Residue No.	-	-	-	-	-	-	-	-	-	-	-	-	-	-	-
	69	95	291	321	443	493	588	639	676	711	728	781	809	844	1129

Figure 4.1.1.1a Secondary structure predicted for slfB, as calculated by the server PredictionProtein.

Figure 4.1.1.1a shows the results obtained by using the server "PredictProtein" to identify particular potentially disordered regions in slfB. The corresponding topology diagram is divided into five domains including Domain I shown in pink, Domain II in blue,

Domain III in yellow, Domain IV pointed out in green and Domain V colored in red. The signal peptide is shown in orange. A 3D model of slfB was obtained by using the I-Tasser server and is shown in Figure 4.1.1.1b. The program I-Tasser generated a model by homology modeling procedures using homologues PDB models. The top 10 of them included the structures 3pyw from *B. anthracis* (A common domain of S-layer proteins, the SLH domain, contributes to a three-helical bundle at the spindle base, whereas another α-helix and its connecting loops generate the three prongs [1], with a homology of 22% compared to our target protein) and 4aq1 from *G. stearothermophilus* [45] (The unique full length S-layer protein structure so far, SbsB, has 30% homology compared to slfB and slp-B53). They are summarized in the left table of Figure 4.1.1.1b.

Top 10 threading templates for slfB used by I-TASSER

Rank	PDB Hit	Iden1	Iden2	Cov.	Norm. Z-score
1	4acqA[245]	0.11	019	0.92	2.01
2	4aq1A[45]	0.17	0.14	0.54	7.97
3	3prxB[246]	0.08	0.20	0.85	1.39
4	4aq1A	0.14	0.14	0.57	3.49
5	4aq1A	0.12	0.14	0.57	1.68
6	4aq1A	0.14	0.14	0.54	6.12
7	2pn5A[247]	0.08	0.17	0.94	1.16
8	3pywA[1]	0.26	0.03	0.14	7.06
9	2pn5A	0.09	0.17	0.92	1.83
10	3pywA	0.23	0.03	0.14	5.45
Evaluation	C-score=-1.10, TM-score=0.58±0.14				

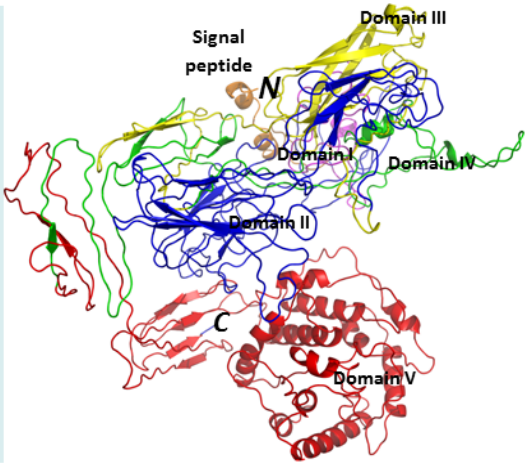

Figure 4.1.1.1b 3D structure prediction of slfB using I-TASSER (4acq [248], 4aq1 [45], 3prx [249], 2pn5 [250], 3pyw [1]). (a) Rank of templates represents the top ten threading templates used by I-TASSER. (b) Ident1 is the percentage sequence identity of the templates in the threading aligned region with the query sequence. (c) Ident2 is the percentage sequence identity of the whole template chains with query sequence. (d) Cov. represents the coverage of the threading alignment and is equal to the number of aligned residues divided by the length of query protein. (e) Norm. Z-score is the normalized Z-score of the threading alignments. Alignment with a Normalized Z-score >1 mean a good alignment and vice versa. (f) C-score is a confidence score for estimating the quality of predicted models by I-TASSER. C-score is typically in the range of [-5,2], where a C-score of higher value signifies a model with a high confidence and vice-versa. (g) TM-score is a measure of global structural similarity between query and template protein.

Several domains of the modeled structures are highlighted with different colors as shown in Figure 4.1.1.1b.

4.1.1.2 Slp-B53

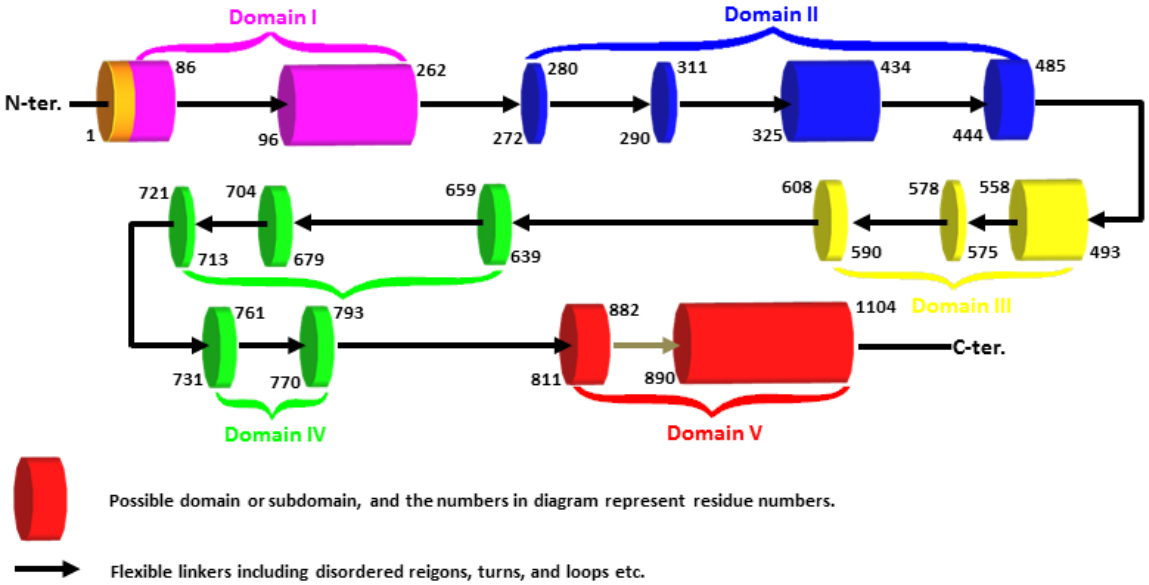

Disordered Regions	1	2	3	4	5	6	7	8	9	10	11	12	13	14	15
	86	262	280	311	434	485	558	578	608	659	704	721	761	793	882
Residue No.	-	-	-	-	-	-	-	-	-	-	-	-	-	-	-
	96	272	290	325	444	493	575	590	639	679	713	731	770	811	890

Figure 4.1.1.2a Secondary structure predicted for slp-B53, as calculated by the server PredictionProtein.

Similar to the results described for slfB, figure 4.1.1.2a indicates the secondary structure distribution of slp-B53. In parallel, five domains are also represented by different colors. For slp-B53, the 3D structure has also been built using the I-Tasser server and was based on multiple-*threading* alignments, as shown in Figure 4.1.1.2b. The domains corresponding to the results of the prediction using the server “PredictionProtein” were marked out with the identical colors.

Top 10 threading templates for slp-B53 used by I-TASSER

Rank	PDB Hit	Iden1	Iden2	Cov.	Norm. Z-score
1	3syjA[248]	0.13	0.17	0.8	1.65
2	4aq1A	0.18	0.18	0.58	8.33
3	3syjA	0.10	0.17	0.82	1.35
4	4aq1A	0.14	0.18	0.65	3.89
5	4aq1A	0.12	0.18	0.65	1.76
6	4aq1A	0.16	0.18	0.59	5.97
7	3syjA	0.09	0.17	0.83	1.04
8	3pywA	0.28	0.04	0.16	6.90
9	4gleA[249]	0.11	0.15	0.84	7.60
10	3pywA	0.24	0.04	0.16	5.70

Evaluation: C-score=-1.10, TM-score=0.58 ± 0.14

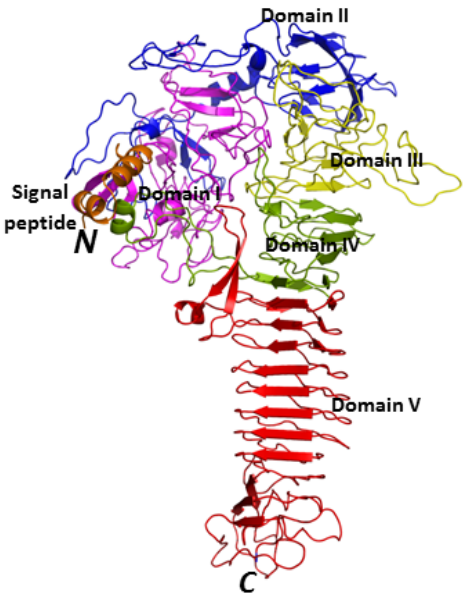

Figure 4.1.1.2b 3D structure prediction of slp-B53 using I-TASSER (3syj [251], 4gle [252]). (a) Rank of templates represents the top ten threading templates used by I-TASSER. (b) Ident1 is the percentage sequence identity of the templates in the threading aligned region with the query sequence. (c) Ident2 is the percentage sequence identity of the whole template chains with query sequence. (d) Cov. represents the coverage of the threading alignment and is equal to the number of aligned residues divided by the length of query protein. (e) Norm. Z-score is the normalized Z-score of the threading alignments. Alignment with a Normalized Z-score >1 mean a good alignment and vice versa. (f) C-score is a confidence score for estimating the quality of predicted models by I-TASSER. C-score is typically in the range of [-5,2], where a C-score of higher value signifies a model with a high confidence and vice-versa. (g) TM-score is a measure of global structural similarity between query and template protein.

4.1.2 Secondary structure determination by CD measurements

4.1.2.1 SlfB

The experimental CD results of the slfB measurements demonstrated that the contents of the slfB α-helical structures varied slightly from 22% to 23%$^{Mg2+}$ and 18%$^{Ca2+}$ upon the addition of cations, respectively (see Figure 4.1.2.1 and Table 4.1.2.1).

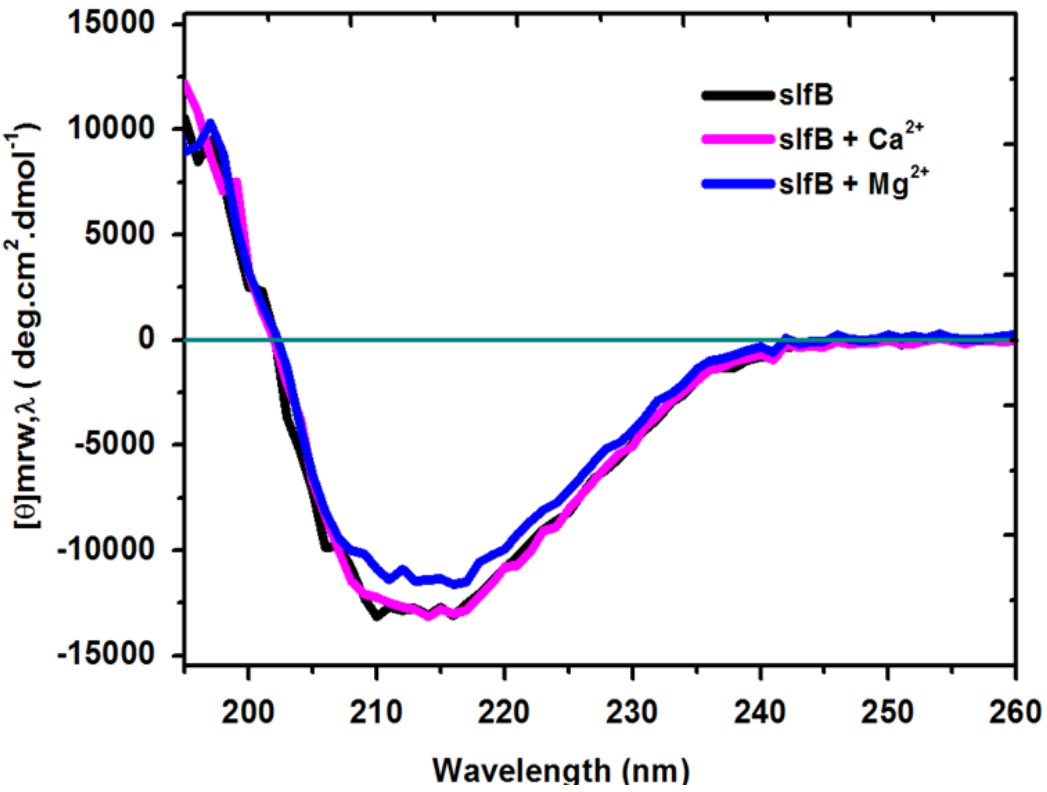

Figure4.1.2.1 Secondary structure determination of slfB by CD spectroscopy.

However, the content of β-sheet shows a slight change and the disordered regions (turns, loops and flexible linkers etc.) decreased distinctly upon the addition of those two cations (see Table 4.1.2.1). The disordered regions cover half of the full length slfB.

Table 4.1.2.1 Secondary structure evaluation of slfB by CD measurements.

Sample	Algorithms	Helix [%]	β-sheet [%]	Disordered [%]
+	[1]Selcon3/[2]CDSSTR/[3]ContinII	23/21/22	30/34/28	53/46/52
Water	mean	22	31	50
+	Selcon3/CDSSTR/ContinII	20/18/17	25/36/32	51/48/48
$CaSO_4$	mean	18	32	49
+	Selcon3/CDSSTR/ContinII	28/20/21	27/35/35	49/44/47
$MgSO_4$	mean	23	30	46

1. Sreerama, N.,*et al.*, *Protein science,* 1999. 2. Manavalan, P. *et al., Analytical biochemistry,* 1987. 3. Van Stokkum, I.H., *et al., Analytical biochemistry*, 1990.

4.1.2.2 Slp-B53

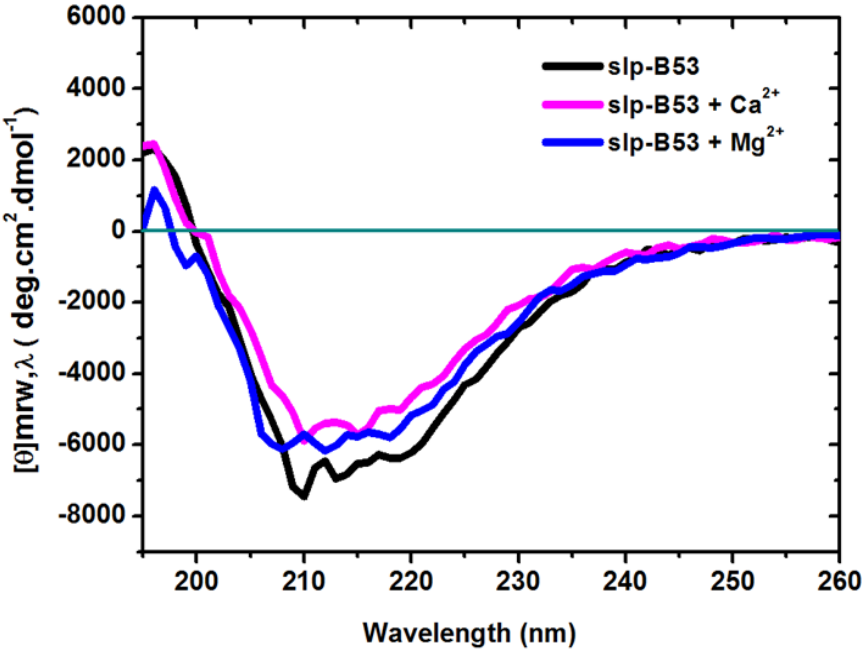

Figure 4.1.2.2 Secondary structure determination of slp-B53 by CD spectroscopy.

The CD data of slp-B53 indicated that the contents of the α-helical structures decreased significantly from approx. 20% upon the addition of cations to 14%$^{Mg2+}$ and 10%$^{Ca2+}$ respectively, as shown in Figure 4.1.2.2 and summarized in Table 4.1.2.2.

Table 4.1.2.2 Secondary structure evaluation of slp-B53 by CD measurements.

Sample	Algorithms	Helix [%]	β-sheet [%]	Disordered [%]
+	[1]Selcon3/[2]CDSSTR/[3]ContinII	20/19/20	27/33/26	54/49/55
Water	mean	20	29	53
+	Selcon3/CDSSTR/ContinII	13/7/11	34/40/36	55/53/54
$CaSO_4$	mean	10	36	54
+	Selcon3/CDSSTR/ContinII	16/9/16	30/38/29	54/53/55
$MgSO_4$	mean	14	32	54

1. Sreerama, N.,*et al.*, *Protein science,* 1999. 2. Manavalan, P. *et al., Analytical biochemistry,* 1987. 3. Van Stokkum, I.H., *et al., Analytical biochemistry*, 1990.

The results further revealed that the contents of β-sheet clearly increased a few percentage points upon the addition of those two cations. The percentage of disordered regions, however, essentially remained unchanged and comprised about 54%.

4.2 S-layer Protein Processing Prior to Investigation

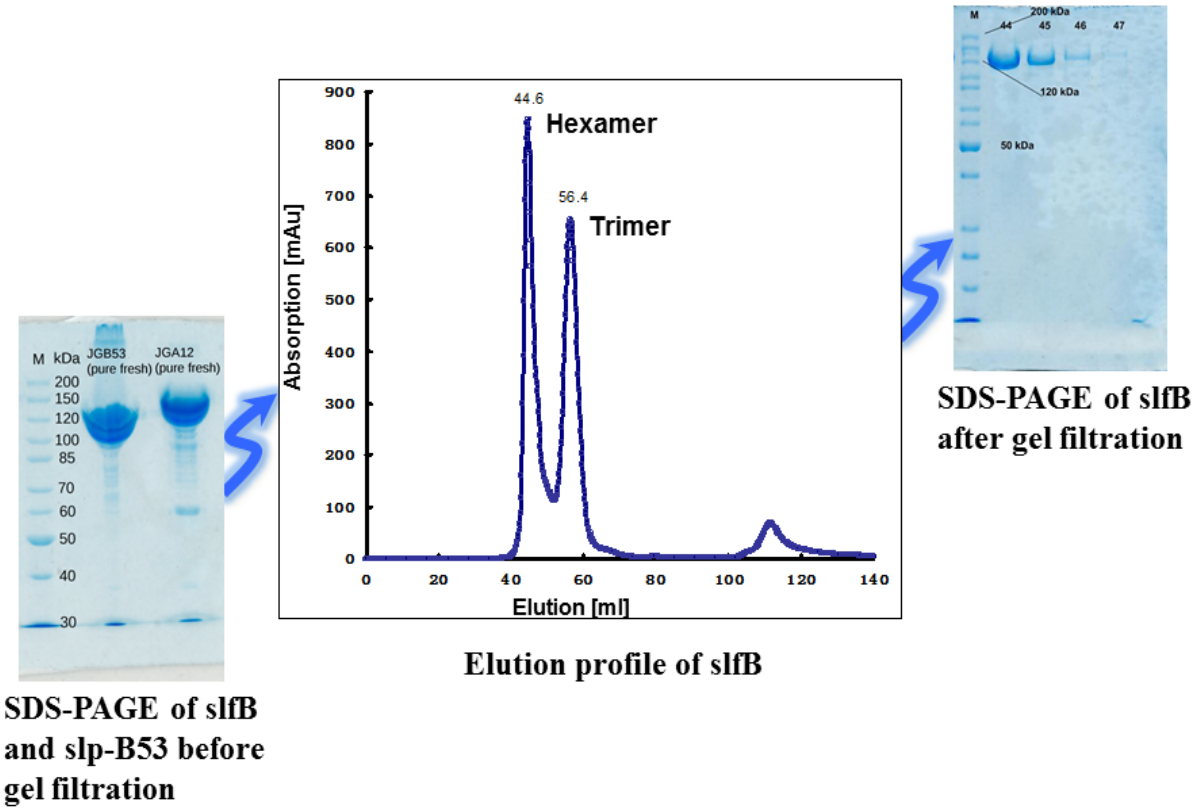

Figure 4.2.1 Basic workflow for processing proteins aggregation.

After long distance transportation and long time storage, an aggregation of proteins is observed. Therefore, prior to performing all subsequent experiments, gel filtrations of slfB and slp-B53 were carried out. Figure 4.2.1 presents the process for slfB by using superdex 200 SEC (size exclusion) chromatography.

The molecular weight of slfB as estimated from the calibration plot of SDS-PAGE was 129 kDa. The superdex 200 elution profile shows that the protein elutes with an apparent molecular weight of 370 kDa, which could possibly indicate a trimer formation (129 kDa × 3 =387 kDa) (Figure 4.2.1).

4.3 Formation of S-layers Observed by AFM

As previously mentioned S-layer proteins have the ability to self-assemble into certain crystalline lattices and therefore build up the S-layers.

4.3.1 AFM of slfB

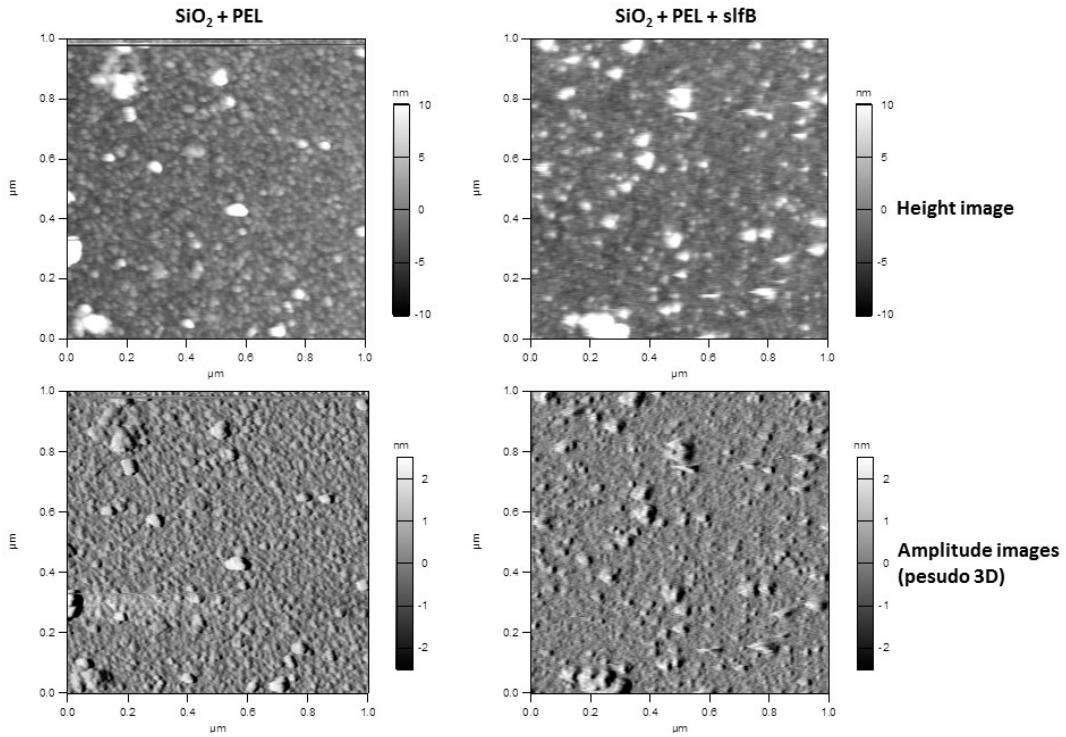

Figure 4.3.1a 2D-crystallization of slfB with ultra-pure water (1x1 µm).

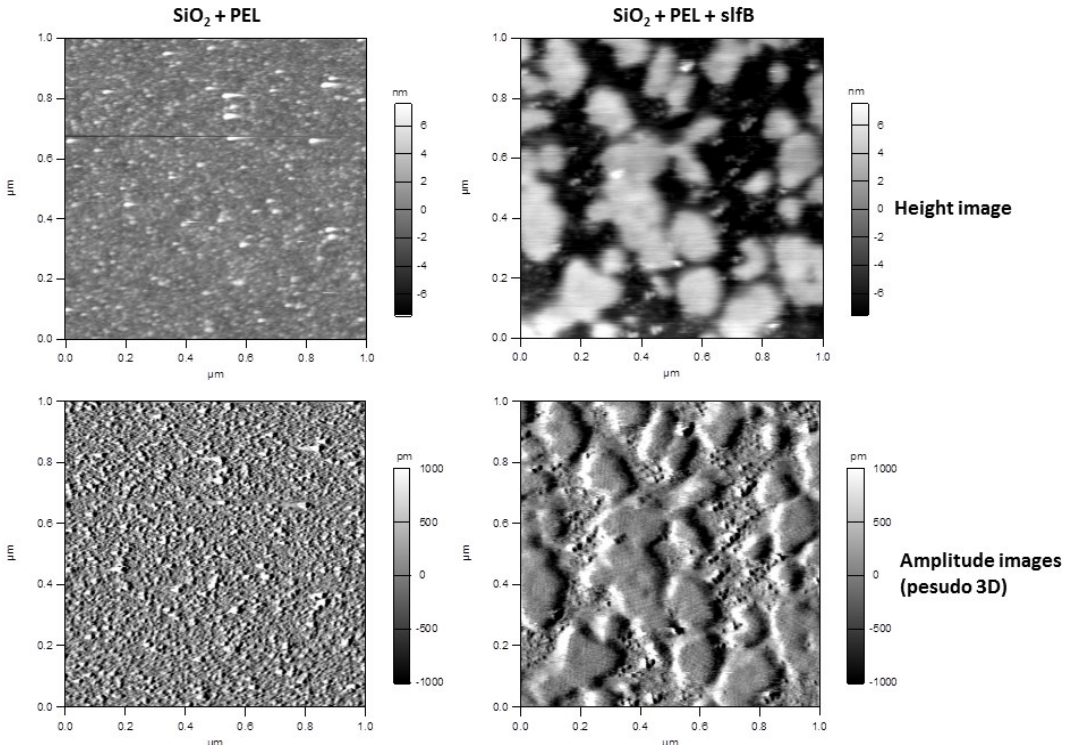

Figure 4.3.1b 2D-crystallization of slfB with 75 mM NaCl and 25 mM Tris/HCl pH 7.4 (1x1 µm).

AFM experiments of slfB provide images of S-layer *via* self-assembly (see Figure 4.3.1). No significant difference can be observed between the control (SiO_2 + PEL) and the test samples (SiO_2 + PEL+ slfB) in ultra-pure water. No 2D-crystal structure can be recognized with any type of symmetry (see Figure 4.3.1a).

However, compared to the trial without any buffer, tetragonal S-layer crystals have been clearly observed on the surface using the appropriate buffer (75 mM NaCl and 25mM Tris/HCl at pH 7.4) (see Figure 4.3.1b).

4.3.2 AFM of slp-B53

Quite similar to the AFM trials of slfB, neither in the blank control (SiO_2 + PEL) nor in the test samples (SiO_2 + PEL+ slp-B53) any S-layer formation could be observed for slp-B53 in ultra-pure water, as can be seen in the experimental images (buffer free) as shown in Figure 4.3.2.

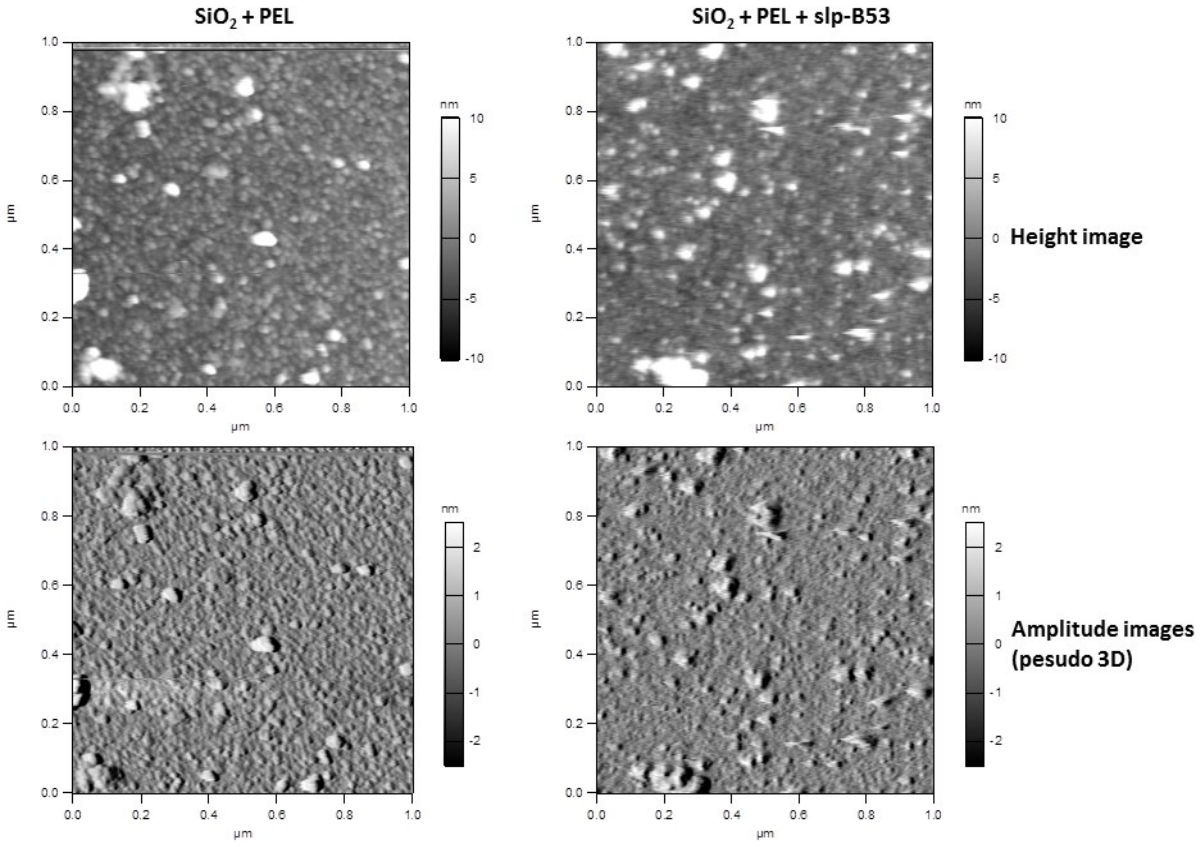

Figure 4.3.2a 2D-crystallization of slp-B53 with ultra-pure water (1x1 µm).

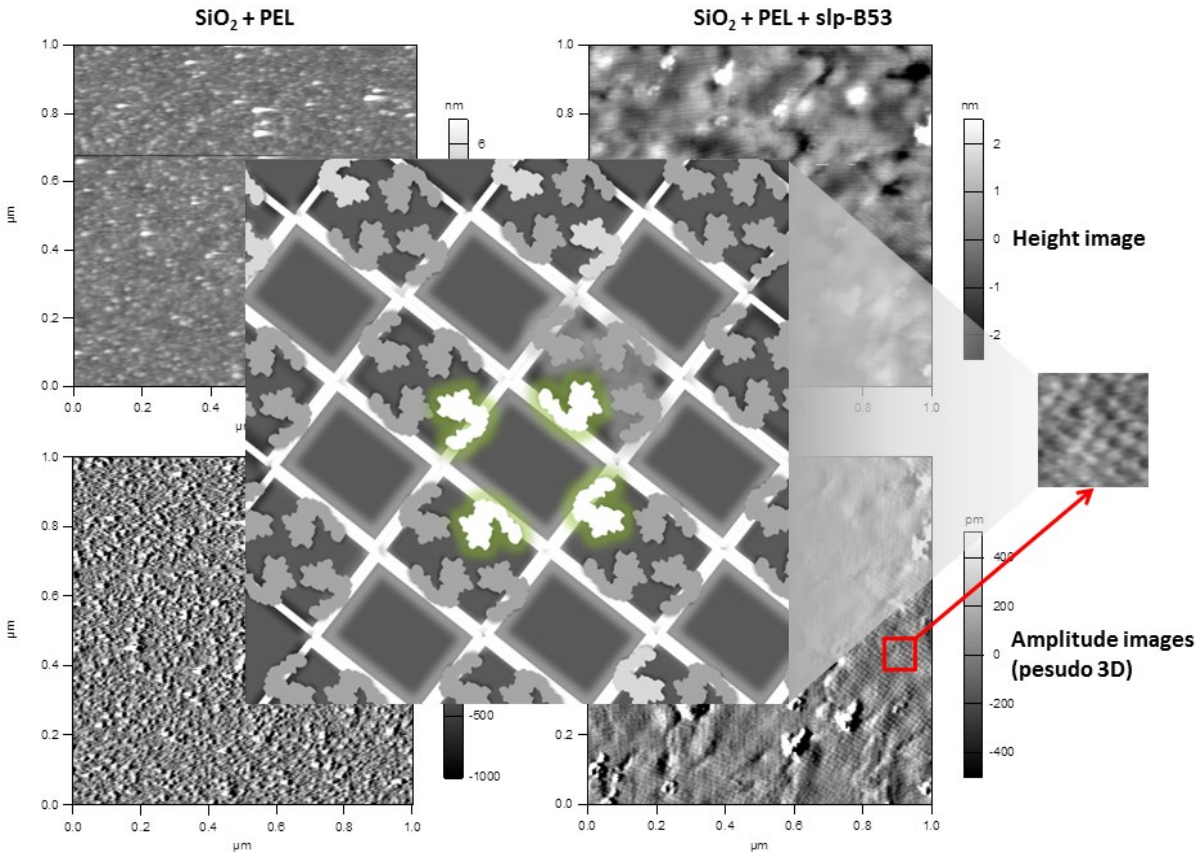

Figure 4.3.2b 2D-crystallization of slp-B53 with 75 mM NaCl and 25 mM Tris/HCl pH 7.4 (1x1 µm).

Significant S-layer crystals (p4 symmetry) for slp-B53 were formed on the surface of the suitable buffer, as shown in Figure 4.3.2b. For the purpose of stereoscopic understanding the self-assembly symmetry, a simulated picture was inserted in Figure 4.3.2b. As can be clearly seen, one unit consisted of four single molecules.

4.4 DLS Measurements

Additionally, DLS measurements were performed to assess the size and the stability of S-layer proteins with and without the addition of bivalent cations in appropriate buffer solutions. DLS experiments of sllfB demostrated that the protein is stable as a monomer for 24 hours, after that the aggregation of the protein was observed (Figure 4.4.1A). Upon the addition of 100 mM Ca^{2+} at pH 7.4, oligomers could be observed after approx. 15 minutes, which were formed by the aggregation of sllfB (R_H= 12-45 nm) (Figure 4.4.1B). However, after addition of Mg^{2+}, the monodispersity of sllfB could be maintained

for up to 7 days (Figure 4.4.1C).

4.4.1 DLS experiments of slfB

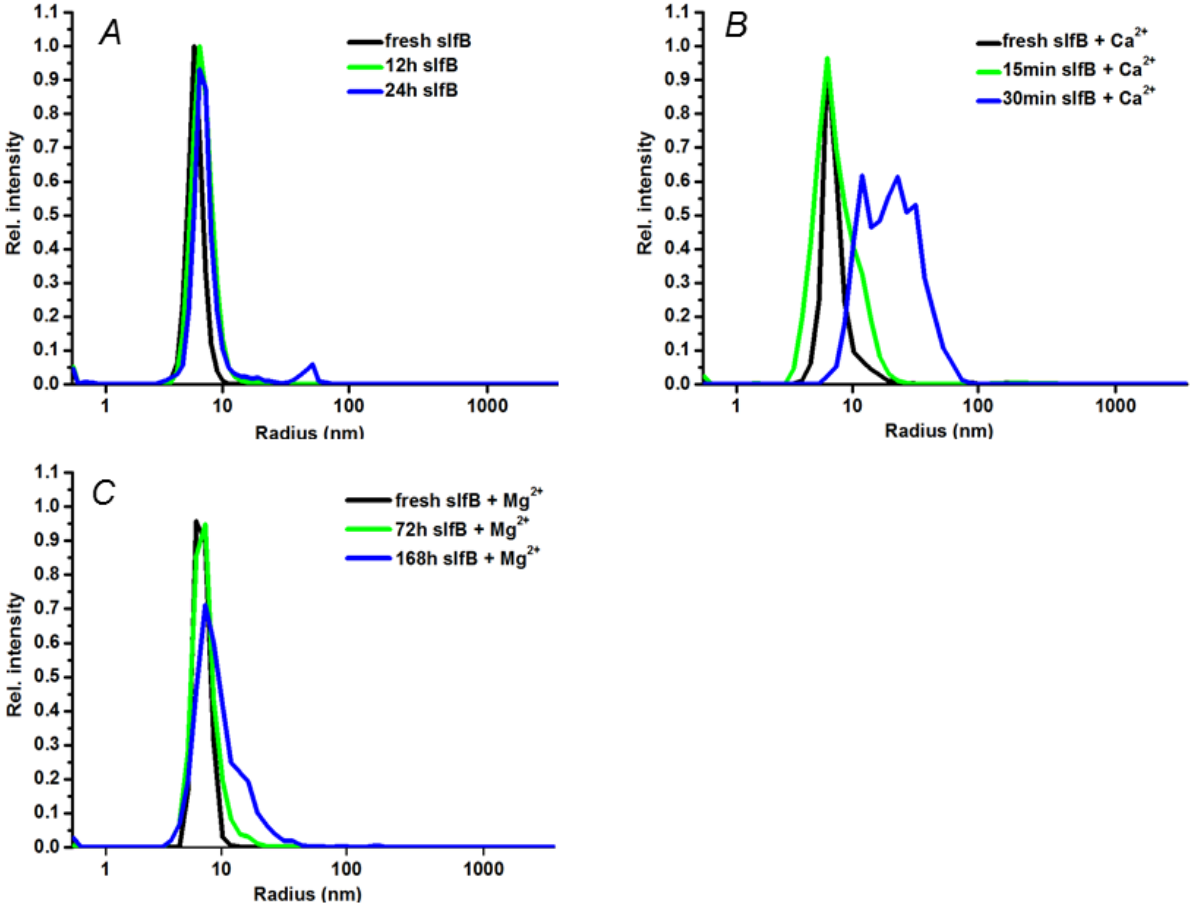

Figure 4.4.1 Analysis of the influence of bivalent cations on the monodispersity of slfB as observed by DLS measurements.

4.4.2 DLS experiments of slp-B53

The DLS data of slp-B53 showed that its monodisperse status can maintain only one hour, after this, the aggregation of protein occurs, as shown in Figure 4.4.2A. Upon the addition of 100 mM Ca^{2+} at pH 7.4, a distinct increase of R_H indicating the formation of slp-B53 oligomer (R_H =20-50 nm) can be determined after approx. 30 minutes (Figure 4.4.2B). However, after addition of Mg^{2+}, the DLS experiments indicated that the monomeric hydrodynamic radius of slp-B53 remains stable for up to 168 hours (Figure 4.4.2C).

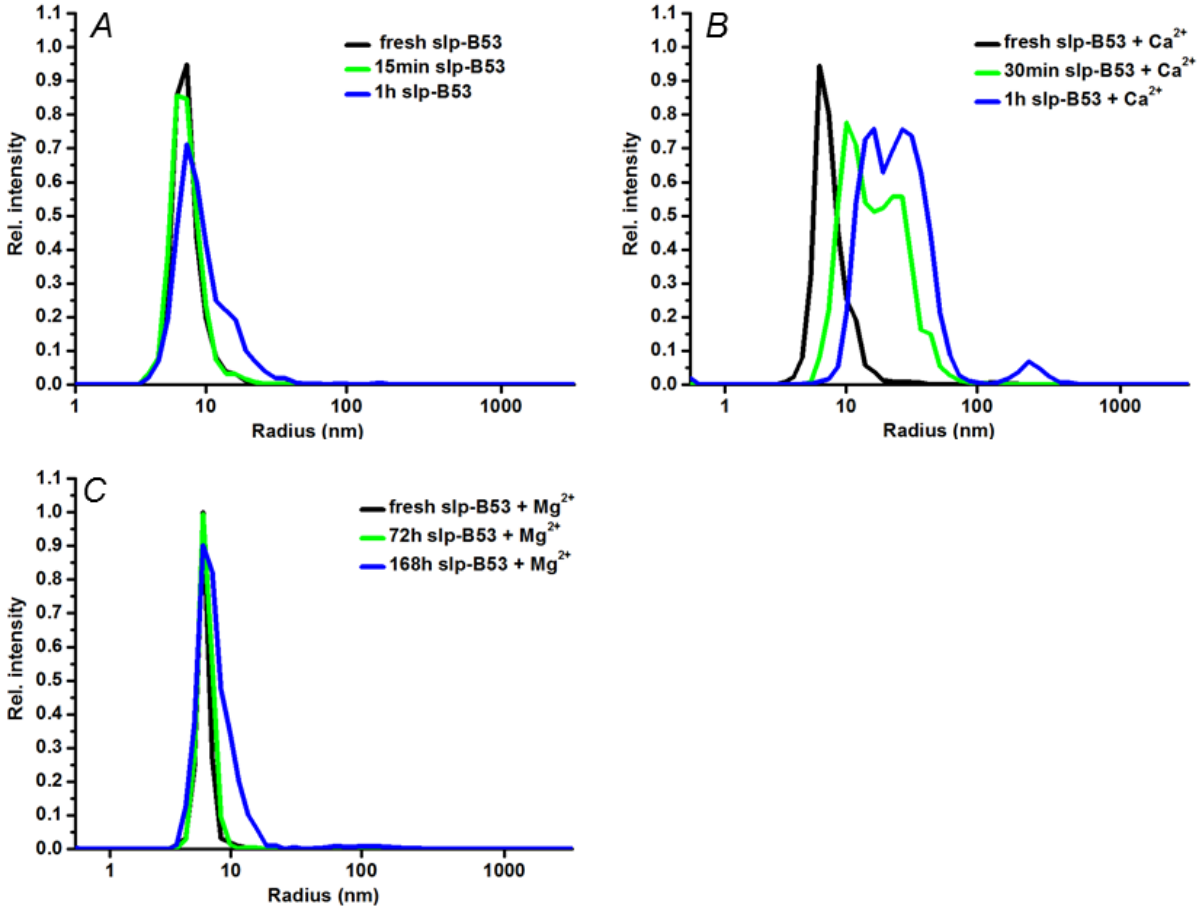

Figure 4.4.2 Analysis of the influence of bivalent cations on the monodispersity of slp-B53 by DLS.

4.5 SAXS Measurements

SAXS was applied to analyze the shape and shape variation of the proteins.

4.5.1 SAXS measurements of slfB

Based on the intensity function of the scattering angle, the scattering patterns are significant differenct between the protein slfB with and without bound bivalent cations, as shown in Figure 4.5.1a-A. Also the pair distribution function (*P(R)*) of slfB SAXS data shows substantial variations as analyzed using the program GNOM, such as upon addition of bivalent cations the D_{max} of slfB has been obviously increased (Figure 4.5.1a-B).

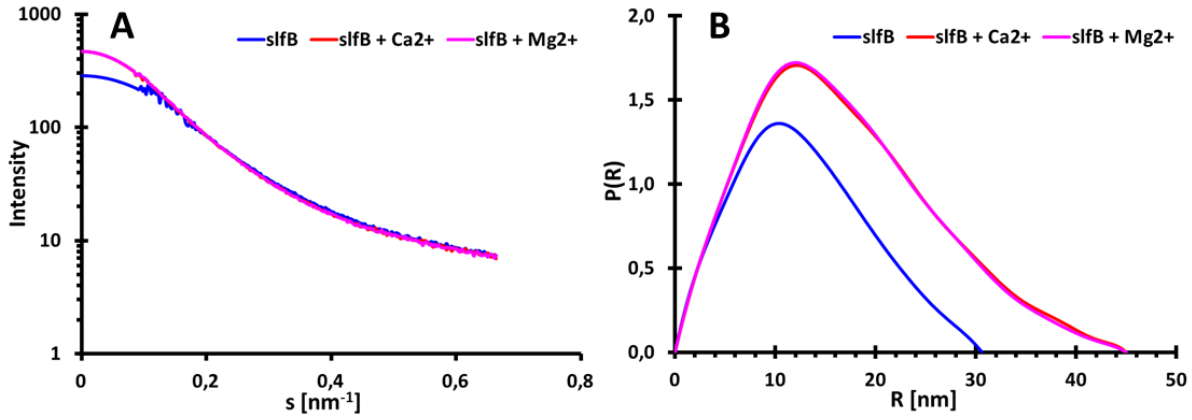

Figure 4.5.1a Left picture-A: The experimental scattering of slfB. Right picture-B: *P(R)* functions calculated from experimental scattering by GNOM.

The *ab-initio* slfB model, as calculated from *P(R)* of SAXS data by the program DAMMIF, implicates a D_{max} of 31 nm and a width ranging from 15.5 nm to 18.9 nm, as shown in Figure 4.5.1b-A, as well as a molecular weight of 730 kDa, given in Table 4.5.1. The pattern of slfB upon the addition of Ca^{2+} showed significant changes. The D_{max} was increased to 44 nm and the molecular weight was calculated to be 3180 kDa. The appearance of this model is demonstrated in Figure 4.5.1b-B. The calculated model structure of slfB after Mg^{2+}-binding differs significantly, which changed the D_{max} to 48 nm, the width range to 19 nm - 31 nm and the molecular weight to 3840 kDa. Figure 4.5.1b-C shows the shape of the protein under this condition.

All corresponding parameters of these three models are summarized in Table 4.5.1, respectively.

Table 4.5.1 Parameters of slfB SAXS models.

Parameters / Samples	R_g[nm]	*I (0)*	D_{max}[nm]	V[nm³]	*MM*[kDa]
slfB	9.1 ± 1.6	326	31	-	730
slfB + Ca^{2+}	9.0 ± 3.0	336	44	-	3180
slfB + Mg^{2+}	-	-	48	-	3860

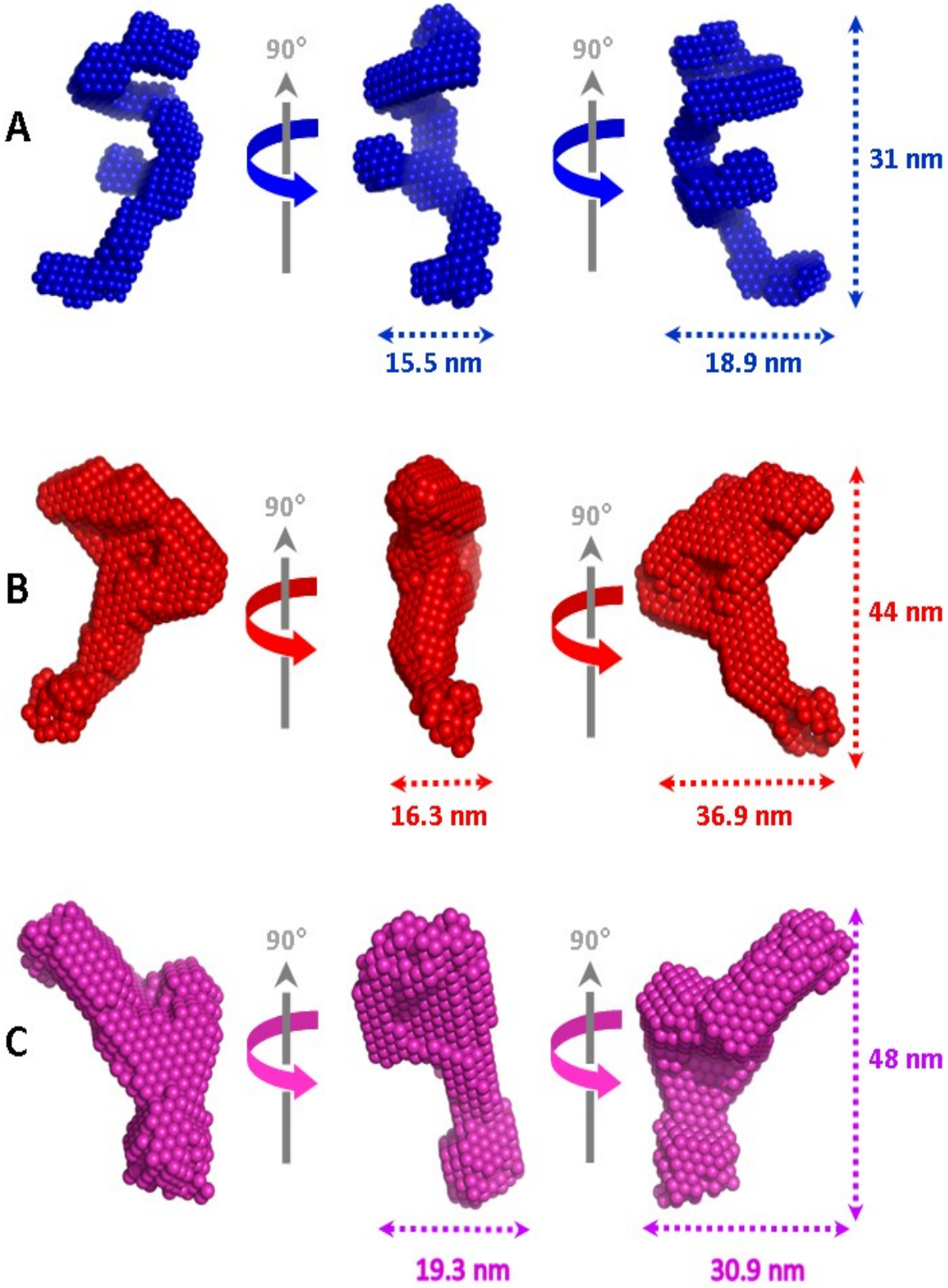

Figure 4.5.1b SAXS models of slfB generated by DAMMIF. A) SAXS models of slfB without bivalent cations. B) SAXS models of slfB with bound Ca^{2+}. C) SAXS models of slfB with bound Mg^{2+}.

4.5.2 SAXS measurements of slp-B53

Unlike the performance of slfB in solution, the scattering patterns of slp-B53 are highly similar between the samples with and without bound bivalent cations, as shown in Figure 4.5.2a-A. The program GNOM computed that the *P(R)*) of the respective sample presents slight variations, such as the increase of D_{max} (Figure 4.5.2a-B).

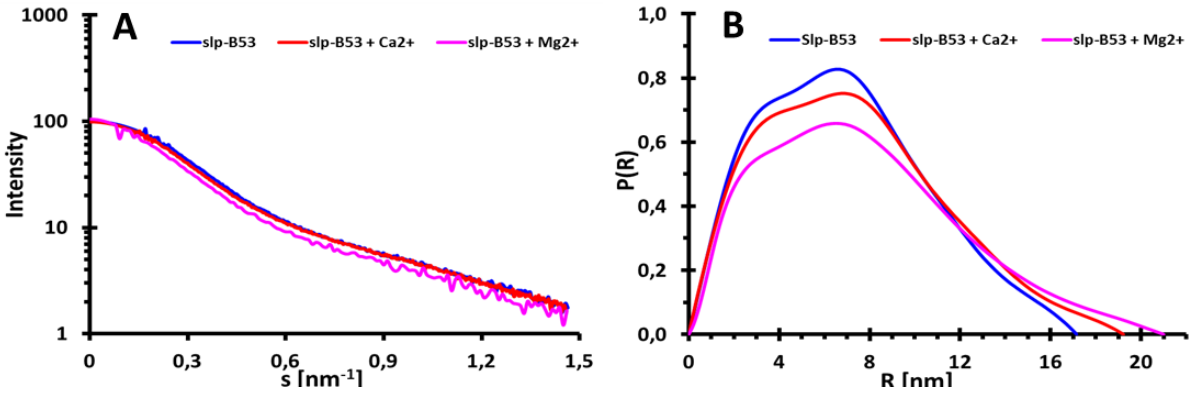

Figure 4.5.2a Left picture-A: The experimental scattering of slp-B53. Right picture-B: *P(R)* functions calculated from experimental scattering by GNOM.

The *ab-initio* slp-B53 reconstructions obtained from *P(R)* by the program DAMMIF is shown in Figure 4.5.2b. The model without addition of bivalent cations resembles an elongated and band molecular shape with a D_{max} of 17 nm and a radius of gyration R_g of 5.0 ± 0.60 nm, as shown in Figure 4.5.2b-A and summarized in Table 4.5.2. The shape with bound Ca^{2+} is highly similar compared to the shape obtained under the cation free condition. However, some distinct changes of the shape parameters can be observed, such as the variation of the width, D_{max} (19 nm) and R_g (6.1 ± 0.37 nm), as shown in Figure 4.5.2b-B and also summarized in Table 4.5.2.

The shape with bound Ca^{2+} is highly similar compared to the shape obtained under a cation free condition. However, some distinct changes of the shape parameters can be observed such as the variation of the width, D_{max} (19 nm) and R_g (6.1 ± 0.37 nm), as shown in Figure 4.5.2b-B and also summarized in Table 4.5.2. In contrast, the slp-B53 occupied with Mg^{2+} displays significant differences. The overall shape is shown in Figure

4.5.2b-C. It presents a maximum diameter of 21 nm and a corresponding molecular weight of 113 kDa. The R_g was altered to 5.9 ± 0.65 nm.

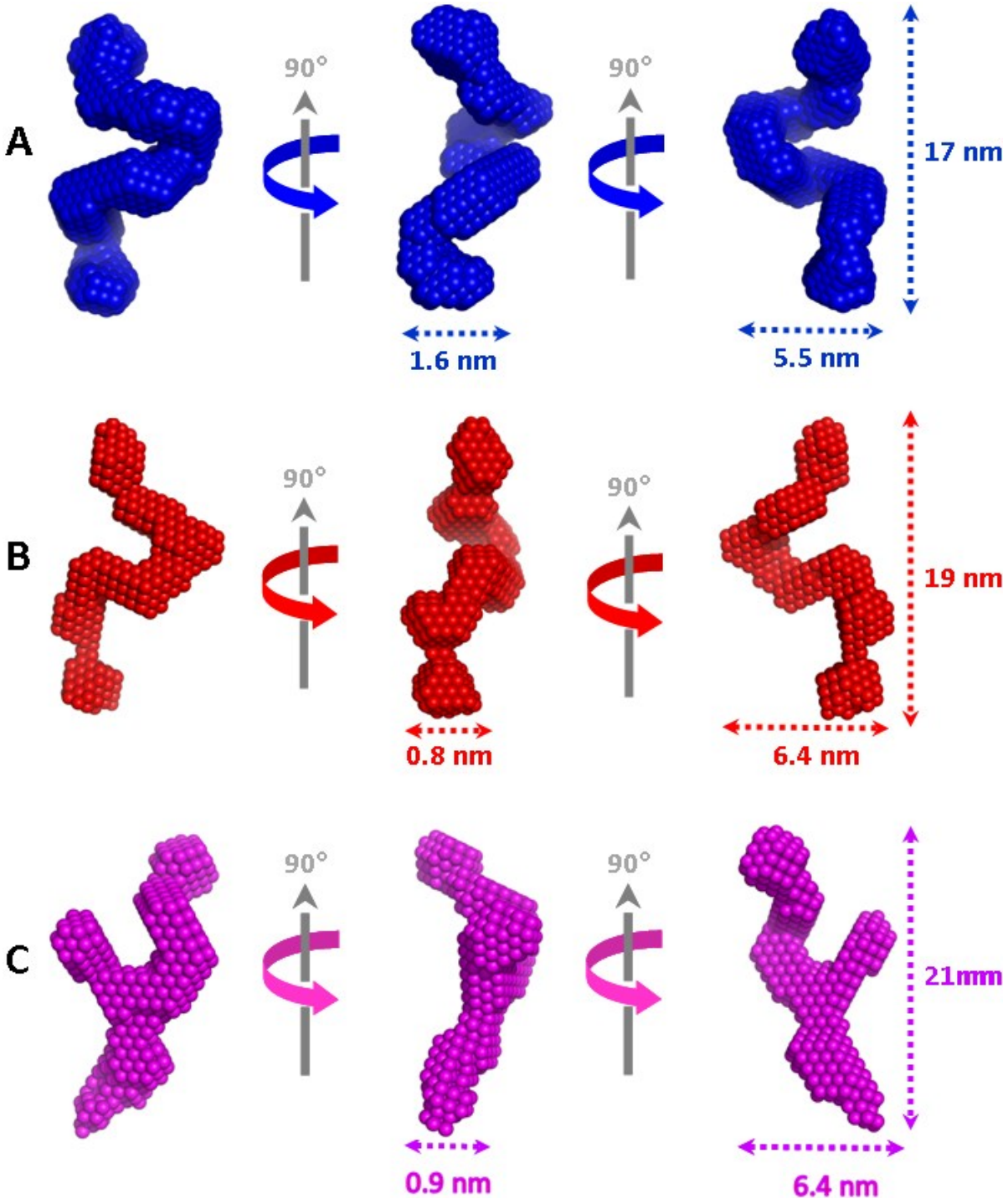

Figure 4.5.2b SAXS models of slp-B53 generated by DAMMIF. A) SAXS models of slp-B53 without bivalent cations. B) SAXS models of slp-B53 with bound Mg^{2+}. C) SAXS models of slp-B53 with bound Mg^{2+}.

Structural parameters including *Rg, D_{max}, I(0), V,* as well as MM of the three models are summarized in Table 4.5.2.

Table 4.5.2 Parameters of SAXS slp-B53 models.

Parameters / Samples	R_g[nm]	*I (0)*	D_{max}[nm]	V[nm³]	*MM*[kDa]
slp-B53	5.0 ± 0.6	107	17	240	116
slp-B53 + Ca^{2+}	6.1 ± 0.37	92	19	225	135
slp-B53 + Mg^{2+}	5.9 ± 0.65	111	21	242	113

4.6 Crystallization Experiments of S-layer Proteins

As described previously, SDS-PAGE analysis shows that the purity of the proteins is high enough for crystallization after the gel filtration run (Figure 4.2.1). Both proteins also present good monodisperse DLS patterns in a buffer of 75 mM NaCl 25 mM Tris, pH 7.4 containing 100 mM Mg^{2+}. The concentration of two target proteins best suited for crystallization is around 10 mg/mL, estimated by following PCT (pre-crystallization test). Both sIfB and slp-B53 were screened with the Honeybee 961 robot against numerous common commercial screens (Nextal Classic suite, JCSG suite, PACT suite, Morpheus suite, Ammonium Sulfate suite, Stura Footprint and Macrosol suite and Compass suite) and additionally with the self-designed pPEG screen series. For each screen two plates were prepared: One was incubated at 20°C and the other at 4°C to evaluate the temperature dependence of the protein phase diagram. After one week, the incubation plates were analyzed manually by using microscopy techniques. Thus, possible crystallization conditions could be identified. Afterwards, optimization of the crystallization was performed based on the analysis of the screen trials.

4.6.1 Crystallization screening of sIfB

No crystallization growth could be identified after screening of sIfB using the common

commercial screens. Fortunately, under the condition of a self-designed pPEG7 screen, many small crystals with needle- or sea urchin-like shapes were clearly displayed, as shown in Figure 4.6.1. Table 3.6.1 shows the compound contents of the pPEG7 screen.

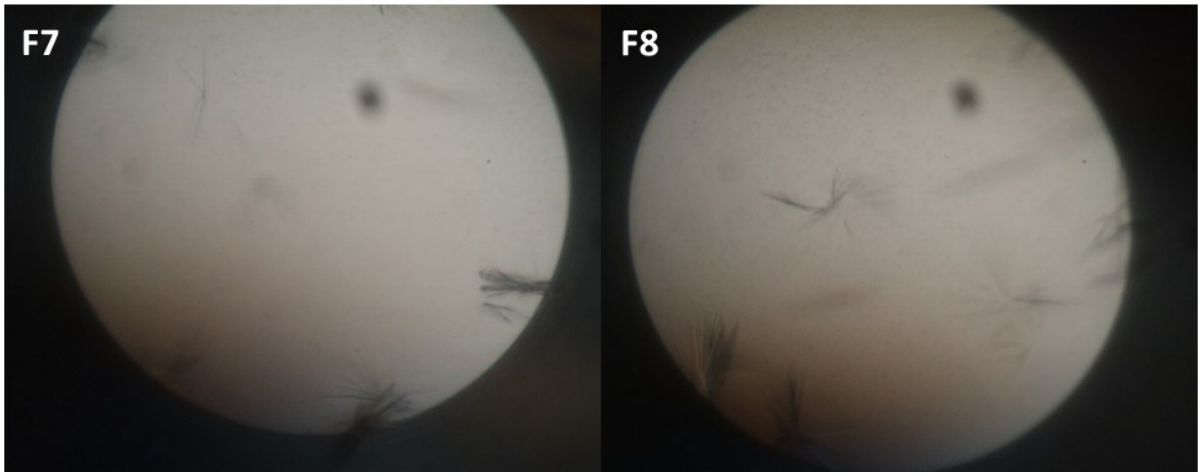

Figure 4.6.1 Results experienced from previous *pPEG7* crystallization screening of slfB. Crystals grew in conditions: 15% PEG 10000 (w/v), 0.35 M ammonium nitrate, 0.1 M sodium citrate-buffer (pH 4.0), 10% Anion-Mix6 (Anions of 0.07 M I^- (NH_4I) and 0.08 M of Br^- (NH_4Br)).

4.6.2 Crystallization optimization of slfB

Based on the results of the pPEG 7 suite, almost all crystallization methods including vapor diffusion methods (sitting drop, hanging drop), seeding and Granada Crystallization Box (GCB) & Capillaries (counter-diffusion method) were performed to optimize the crystallization of slfB against each screen trial. Unfortunately, the initial results could not be significant improved.

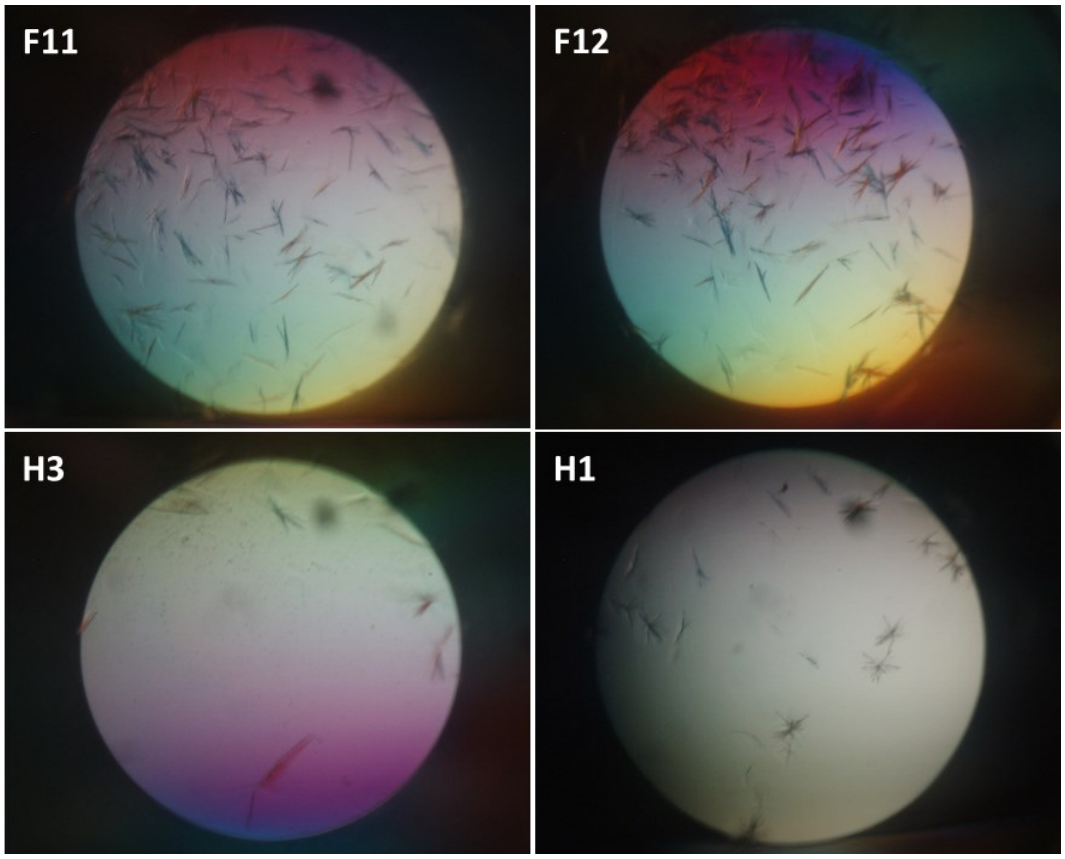

Figure 4.6.2 Slight improved crystals grown from the optimization screens, F11, F12 and H3 of *Liu2_Alcohols Screen and H1 of Liu3_Ethylene Glycols Screen*, respectively. The conditions are the following: F11 and F12) 14% PEG 10000 (w/v), 0.35 M ammonium nitrate, 0.1 M sodium citrate-buffer (pH 4.0), 10% Anion-Mix2 (Anions of 0.06 M I^- (NH_4I), 0.09 M of Br^- (NH_4Br)), 10% Glycerol. H3) 14% PEG 10000 (w/v), 0.4 M ammonium nitrate, 0.1 M sodium citrate-buffer (pH 4.0), 10% Anion-Mix6 (Anions of 0.08 M I^- (NH_4I), 0.07 M of Br^- (NH_4Br)), 20 mM Alcohol Mixture (1,6-hexanediol, 1,4-butanediol, 2,3-butanediol, 1,3-butanediol, 2,3-butanediol, 1-propanol, 2-propanol). H1) 14% PEG 10000 (w/v), 0.4 M ammonium nitrate, 0.1 M sodium citrate-buffer (pH 4.0), 10% Anion-Mix6 (Anions of 0.08 M I^- (NH_4I), 0.07 M of Br^- (NH_4Br)), 30 mM ethylene glycols.

4.6.3 Crystallization screening of slp-B53

Unfortunately, all tested screening solutions have not provided any condition suitable for crystal growth of slp-B53. Only under the condition of E7, F9, G10 and H9 from the PACT suite, some typically liquid-liquid phase separation (LLPS) or oils-like droplets as described in the crystallization tutorials 3 by Teresa Bergfors, could be detected. Figure 4.6.3a shows some screening results of slp-B53.

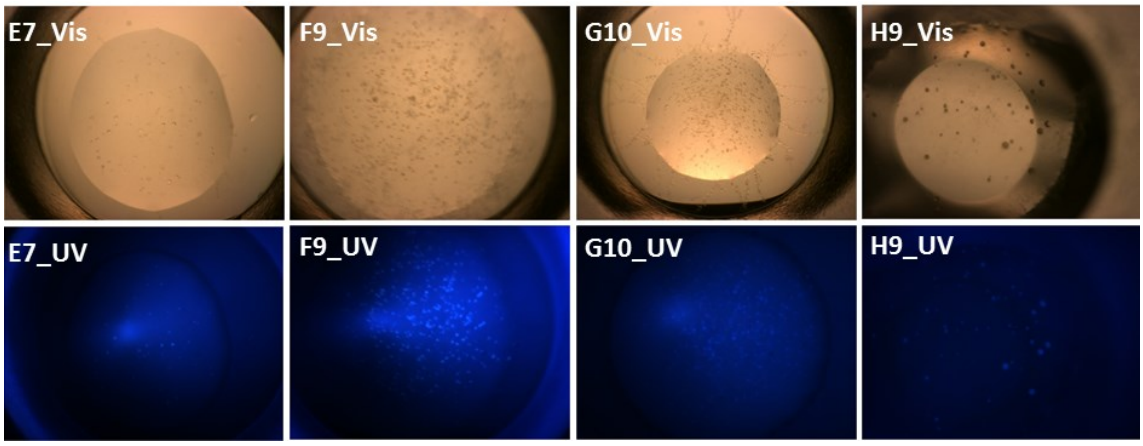

Figure 4.6.3a Liquid-liquid phase separations (LLPS) were obtained in conditions E7, F9, G10 and H9 of the crystallization PACT screen. The strong UV-fluorescence (lower pictures) shows that the LLPS formation is due to protein accumulation. Conditions are the following: E7) 20% w/v PEG 3350, 0.2 M NaOAC; F9) 20% w/v PEG 3350, 0.2M Potassium/sodium tartrate, 0.1M Bis Tris propane, pH 6.5; G10) 20% w/v PEG 3350, 0.2M Sodium/potassium phosphate, 0.1M Bis Tris propane, pH 7.5; H9) 20% w/v PEG 3350, 0.2 M Potassium/sodium tartrate, 0.1M Bis Tris propane, pH 8.5.

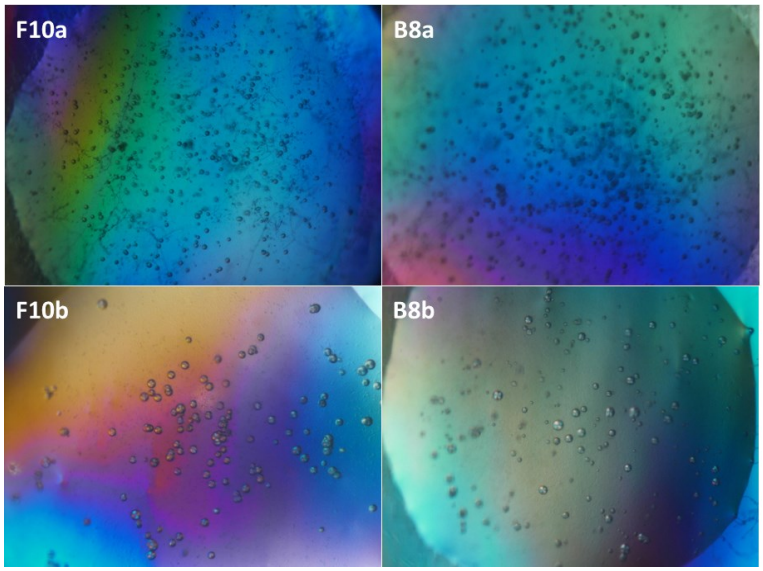

Figure 4.6.3b No essential improvement could be detected for the LLPS of slp-B53 using the self-designed screen PACT_E7 and _H9, respectively. The upper pictures display the screens using the crystallization robot Honeybee 961 and the lower pictures show products gained by manual crystallization methods. F10 is derived from the self-designed screen- PACT_E7 and B8 originates from the self-designed screen- PACT_H9. Conditions were: F10) 18% w/v PEG 3350, 0.18 M NaOAC; H9) 14% w/v PEG 3350, 0.18 M Potassium/sodium tartrate, 0.1M Bis Tris propane, pH 6.5.

In order to obtain crystal growth of slp-B53, various crystallization methods and different recipes based on the possible conditions of the PACT suite were applied. However, no crystals have been observed so far. According to the protein phase diagram, a reduction of protein and precipitant concentration has also been considered. Some results using manual or automated screen optimization are shown in Figure 4.6.3b.

5 Discussion

5.1 Basic Symmetry of Target Proteins

5.1.1 Secondary structure analysis

Theoretical secondary structure predictions and 3D models of slfB and slp-B53 show a high flexibility due to the high content of disordered regions. Online servers (ProteinPredict and I-TASSER) predicted that the disordered regions are present in the regions between the 600^{th}-800^{th} amino acid residues. It is most probable that the flexible elements (flexible linkers, turns and random coils) are enriched in this area. Thus, it allows to propose a shape of the S-layers as shown in Figure 5.1.2, highlighting two functional important domains (color labeled in gray and purple). Usually, it was defined as an anchoring region that contains SLH domains, like Domain I of the topology diagrams shown in the present work. All other remaining domains, except the orange signal peptide, support the self-assembly of the protein.

The variation of α-helices, β-sheets and disordered region contents influenced by bivalent cation-binding demonstrated on the basis of CD experiments, that the addition of bivalent cations affect not only the key secondary elements, but also influence the naturally unfolded regions (including turns, disordered regions and random coils etc.) of the target proteins. Moreover, as the disordered regions account for the half of the full length proteins (slfB and slp-B53), it is not surprising that the entire protein is very flexible.

5.1.2 Analysis of S-layer formation

As summarized before, S-layer proteins have the ability to self-assemble in accordance to distinct crystalline lattices. AFM experiments show that both S-layer proteins from *L. sphaericus* self-assemble, based on a p4 symmetry (see Figure 4.3.1b and Figure 4.3.2b).

A slight blurring in the sample both of sIfB and slp-B53 without buffer can be explained by the contamination of the cantilever. It is very likely that protein is adsorbed on the surface. The reason for failing a 2D-S-layer lattice detection can possibly be explained by either insufficient time during AFM cantilever scanning or that water might be unsuitable for formation of oriented matrixes (see Figure 4.3.1a). However, tetragonal S-layer crystallites with the so called p4 symmetry were clearly observed on the surface of the solution, using the buffer 75 mM NaCl and 25mM Tris at pH 7.4 (see Figure 4.3.1b and Figure 4.3.2b). The driving force to orient the protein molecule to form the regular lattice might be related with ionic bonds, van der Waals and molecular interactions upon the addition of the cation Na^+, as a monodisperse performance was observed by DLS measurements using this buffer condition.

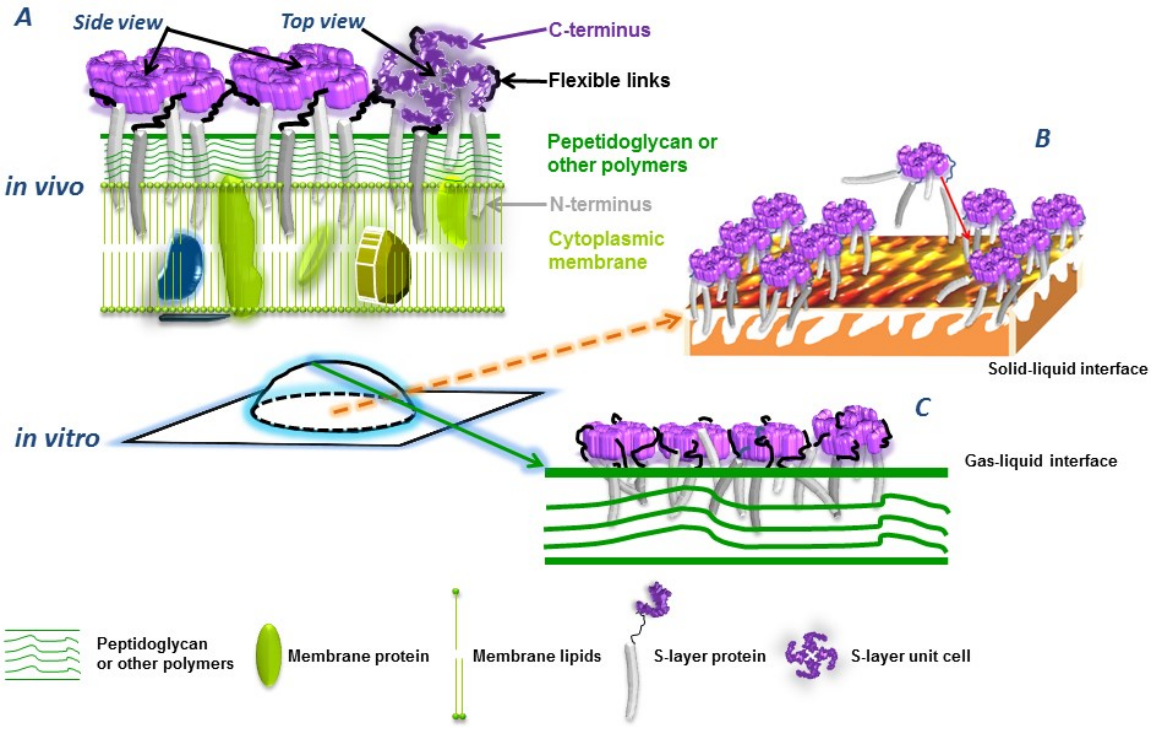

Figure 5.1.2 Scheme indicating the shape of S-layers self-assembly. Figure 5.1.2A serves to demonstrate the shape of S-layers self-assembly scheme in vivo. Figure 5.1.2B shows the mimic formation diagram of an S-layer at a solid-liquid interface. The respective diagram displaying the formation of S-layers in solution is shown in Figure 5.1.2C.

In combination with the above mentioned AFM and CD experimental results, the formation of S-layers could be interpreted as shown in the simulation diagram in Figure

5.1.2A. In vivo, one domain that contains SLH profiles presents the positively charged N-terminus, which binds to the negatively charged secondary cell wall polymer, thus being responsible for anchoring. Another domain is located at the C-terminus of the protein, facing to the extracellular space. The C-terminal domain including several sub-domains interacts with the counterparts of neighboring S-layer proteins, thus self-forming the S-layers. These two functional important domains are connected by flexible linkers. The highly adaptable linker domains explain why S-layer proteins are highly flexible and capable to adapt conformations, allowing them to interact with surrounding S-layer proteins to form the stable 2D S-layer structures as a result. The conclusions of the AFM experiments were used to predict a self-assembly of slp-B53 towards forming S-layers, as shown in Figure 5.1.2B and 5.1.2C.

5.2 Dynamics and Structure of S-layer Proteins

5.2.1 Monodispersity as analyzed by DLS measurements

At 293K slfB is stable in its buffer at pH 7.4 for approx. 24 hours. It was proved that an ionic bond between Na^+ and the protein molecule can be broken within one day. For slp-B53, however, the ionic bond is weaker than that of slfB. Thus, it is stable as a monomer for only one hour. Upon addition of 100 mM Ca^{2+} at pH 7.4, the oligomeric aggregation of both slfB and slp-B53 proteins occurred within one hour. However, whilst adding Mg^{2+} into the target protein solutions, both slfB and slp-B53 were very stable up to 7 days as monomers (see Figure 4.4.1C and Figure 4.4.2C). There is an indication that Mg^{2+} can not only improve the monodispersity of the proteins, but also can strengthen the balance of intermolecular forces. It can be assumed that the uptake of Mg^{2+} induces conformational changes of interdomains, leading to the self-assembly sites A and B buried in the center of protein, which enables the intermolecular interact weaken, thus maintains the monodisperse (Figure 5.2.1). Instead of maintaining stable monodisperse protein molecules in solution, as observed after binding of Ca^{2+}, uptake and binding of this cation results in a complete exposure of the self-assembly sites that allows

intermolecular interaction between S-layer proteins, promoting the lattice formation as shown in Figure 5.2.1. Without any cations adding, S-layer protein can present any shape in initial stage. It is a dynamic process as shown in Figure 5.2.1. When the protein shape which self-assembly sites were exposured on the surface of protein, the lattice will be formed like shown in Figure 5.2.1, but these lattices are not very stable after diluting the sample solution, the lattices will disappear.

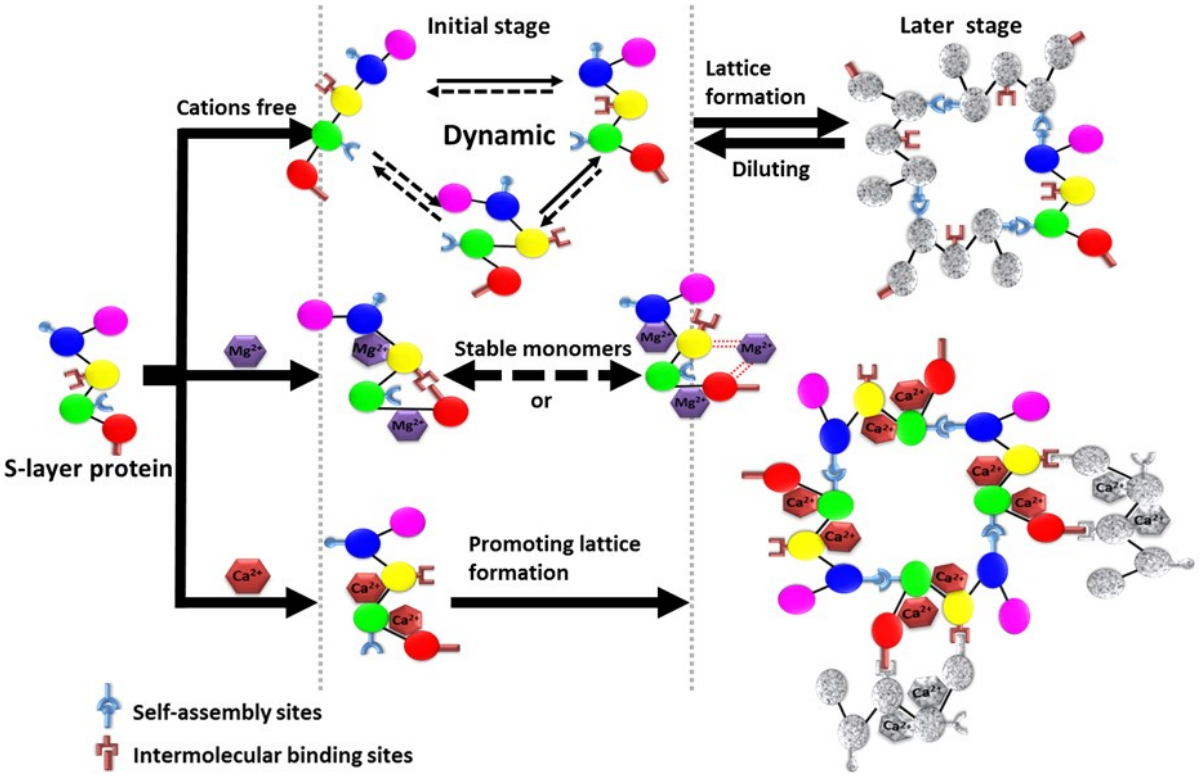

Figure 5.2.1 Schematic diagram showing the influence of bivalent cations on slfB and slp-B53 self-assembly. The addition of cations induces the possible shape variation of flexible S-layer proteins. The mechanism about influence of bivalent cations on S-layer proteins assembly was proposed.

Undoubtedly, SbsB, the unique S-layer protein of which the full length 3D structure has been solved, as reported, nanobodies were enabled by the addition of Ca^{2+}. There are at least 7 Ca^{2+} binding sites (2 sharing Ca^{2+} binding sites and 3 common Ca^{2+} sites) of SbsB, based on the analysis of crystal structures. Ca^{2+} promotes the structure formation and thereby possibly facilitates the crystallization of SbsB. These two target proteins obviously prefer the second possibility, presenting an oligomeric aggregation. However, after the addition of Mg^{2+}, not only the maintenance of the monodispersity could be

detected, but also a contribution to crystallization effects of S-layer proteins was observed, similar to the role of Ca^{2+} in SbsB solutions.

Obviously, the addition of Mg^{2+} helps to maintain the monodispersity of samples in opposite to the promotion of aggregation by the addition of Ca^{2+}, due to the presence of multiple Ca^{2+} binding sites as previously discussed and shown in Figure 5.2.1. Certainly, self-assembly of S-layer proteins can also occur in the absence of bivalent cations as pointed out in Figure 4.3.1b and Figure 4.3.2b (AFM images). In such a case, with the formation of the S-layer, protein aggregation also takes place simultaneously due to the possible intertwining of flexible linkers or other ions (Na^{+}) effect.

5.2.2 Analysis of SAXS experiments

It can be speculated that the main reason for the formation of slfB oligomers is, that the protein solution still contains small amounts of Ca^{2+}, which was not completely removed during purification of the protein. DLS results show that the hydrodynamic radius of slfB is approx. 10 nm (the normal single molecule R_H is 6 nm). When bivalent cations were introduced into the protein, varying degrees of aggregation were observed, respectively. This strongly indicates that some ion binding sites still exist and possess high affinity to the cations, which leads to oligomer formation. From different SAXS models of slfB oligomers, it can be concluded that different ions added induce different effects on the protein intermolecular binding behavior in solution.

The elongated and band molecular shape of slp-B53 in a solution free bivalent cations was analyzed at the first time in the present work (Figure 4.5.2b-A). The shape of slp-B53 with bound Ca^{2+} is highly similar compared to the shape obtained under cation free condition (see Figure 4.5.2b-A and -B). It appears like the elongated shape was stretched even longer, as shown in Figure 4.5.2b-B. In contrast, the slp-B53 bound with Mg^{2+} undergoes substantial changes. The overall shape possesses a bifurcated region and its structure is significantly more compact than the structures obtained without bivalent cations or in the presence of Ca^{2+} (see Figure 4.5.2b-C). Due to its actual molecular weight of 116 kDa, a monomeric state is presumed throughout the courses of these

experimental series, thus, the reliability about above slp-B53 models analysis was enhanced.

In summary, the SAXS experiments revealed that ubiquitous bivalent metal ions have a substantial influence on the structure and conformation of the S-layer proteins. Mg^{2+} ions stabilize the monomeric form of the S-layer protein, as became evident in DLS experiments, by changing the native conformation of the S-layer proteins from *L. sphaericus.* Ca^{2+} ions support the aggregation of the S-layer protein upon storage, due to the existence of multiple Ca^{2+}-binding sites.

5.3 Analysis of crystallization experiments

For the initially grown small needle crystals of slfB and for the LLPS of slp-B53, no significant improvement on their crystallization behavior could be achieved by using the self-designed screens comprising the F7, 8 of the pPEG7 and the E7, H9 of the PACT conditions, respectively. Almost all the methods which could be imaged such as variation of protein and precipitant concentration, selected temperature incubation, changes in the type of precipitant, pH value altering and the introduction of additives as well as the application of seeding methods and counter diffusion (Granada Crystallization Box (GCB) & Capillaries), were applied to grow crystal. Even the use of the special material SDB to assist crystallization, but in the end it still can not obtain any crystals suitable for X-ray diffraction analysis. It can be speculated that the molecular mass of protein is too big and with an elongated shape, the crystal nucleation is not very stable. Also the fact that these proteins contain many disordered regions resulting in its high flexibility, might hinder the initial protein molecules arrangement in a certain direction. Particularly, the ability of these proteins to self-assemble in a 2D-crystalline form is evolutionarily favored, which strongly interferes with the formation of 3D crystals. Hence, to try to stabilize the monodispersity of individual proteins (addition of bivalent cations) and to avoid the proteins self-assembly into 2D crystal lattices is the key to solve the difficulties in obtaining suitable 3D crystals.

5.4 General Discussion and Outlook

S-layers represent a suitable model system for studying self-assembly processes at the molecular level. The p4 symmetry of S-layers from *B. sphearicus* represents the basic assembly form. The S-layer proteins are favorable to bind ions rather than similar molecules in case bivalent cations are present in the solution. The addition of Mg^{2+} is a really good option to enhance the monodispersity of S-layers. The secondary structure of S-layer proteins contains many turns, loops and disorder regions, which are flexible and lack secondary structural elements. The outer shape of the S-layer protein, as investigated, is elongated and contains several distinct domains confirmed by SAXS. CD-spectroscopy, AFM and SAXS results also demonstrate why obtaining a structure of atomic resolution is so challenging in the case of S-layer proteins: Not only 2D-crystallization behavior is favored over 3D-crystallization by evolution, but also the high content of disordered regions (flexible linkers) as well as the elongated structure of the protein with two domains at C- and N-terminus, respectively, leads to a high intermolecular flexibility. This is detrimental to 3D-crystallization as discussed in the SAXS experimental section. In future structure determination from very thin, almost 2D-crystals, such as S-layers, might be possible at free-electron X-ray lasers as LCLS (SLAC, Menlo Park, USA), SACLA (Spring8, Japan) or the European XFEL (Hamburg, Germany, under construction) applying the methods of serial femtosecond crystallography [253, 254]. The analysis of atomic structures from crystal fragments *via* digestion using special enzymes is another alternative option.

6 Summary - Zusammenfassung

6.1 Summary

The formation of stable and functional surface layers via self-assembly of so-called surface layer proteins on the cell surface is a dynamic and complex process. S-layers facilitate a number of important biological functions, e.g. they provide cellular wall protection, mediate selective exchange of molecules and therefore function as molecular sieves. Further, S-layers selectively bind several metals partly with high affinity, e.g. uranium, palladium and gold. Most of the current research projects analyzing the surface structure and function of surface layers focus on the crystalline arrays of proteinaceous subunits of archaea and bacteria.

To investigate the structure function relationship and the dynamics of the S-layer proteins assembly of sIfB and slp-B53 from *L. sphaericus*, complementary analytical techniques and methods were applied: i) The secondary structure of the S-layer proteins was analyzed by CD-spectroscopy, ii) The two dimensional structure of S-layer assemblies was analyzed by AFM, iii) The dynamics and the time resolved assembly of S-layers were followed applying DLS techniques, iv) SAXS was applied to gain insights into the three dimensional structures.

In conclusion, the secondary structure composition of the S-layer proteins investigated contains a substantial amount of turns, loops and disordered regions. The S-layer proteins from *L. sphearicus* build p4 symmetry as a basic assembly form. The addition of Mg^{2+} or Ca^{2+} has a significant influence on the monodispersity of S-layer proteins. A SAXS analysis further showed that the molecular shapes of sIfB and slp-B53 are mainly elongated and contain several domains.

The data obtained provide important insight to understand the mechanism of the S-layer self-assembly in context with the binding of bivalent cations. The results obtained highlight potential applications of S-layer proteins in the field of micro- and

nano-materials. Possible ways to obtain X-ray suitable crystals for high resolution 3D structure analysis of such proteins are summarized.

6.2 Zusammenfassung

Die Ausbildung von stabilen und funktionellen *S-Layern* durch Selbstassemblierung von sogenannten *S-Layer* Proteinen ist ein dynamischer und komplexer Prozess. *S-Layer* unterstützen und ermöglichen eine Vielzahl von wichtigen biologischen Funktionen. Sie tragen zum Schutz der Zellwand bei und ermöglichen den selektiven Austausch von Molekülen; sie fungieren damit als molekulares Sieb. Des Weiteren binden *S-Layer* selektiv und zum Teil hochaffin verschiedene Metallionen wie Uran, Palladium und Gold. Die meisten derzeitigen Forschungsprojekte, die die Oberflächenstrukturen und die Funktion von *S-Layern* analysieren, fokussieren sich auf die kristalline Anordnung der Protein-Untereinheiten von Archaeen und Bakterien.

Um die Struktur und Dynamik-Funktions-Beziehung der *S-Layer* Assemblierung von slfB und slp-B53 von *L. sphaericus* zu untersuchen, wurden im Rahmen dieser Arbeit komplementäre analytische Techniken und Methoden verwendet: i) Die Sekundärstruktur der *S-layer* Proteine wurde mittels CD-Spektroskopie analysiert, ii) Die zweidimensionale Struktur der *S-layer* Anordnung wurde mit AFM untersucht, iii) Die Dynamik und die zeitaufgelöste Assemblierung des *S-layers* wurden mit DLS Techniken verfolgt, iv) SAXS wurde angewendet, um Informationon über die dreidimensionalen Strukturen zu erhalten.

Die Sekundärstrukturzusammensetzung der untersuchten *S-layer* Proteine ist geprägt von einem signifikanten Anteil flexibler ungeordneter Regionen. Die *S-layer* Proteine aus *L. sphearicus* bauen als elementare Assemblierungsform eine p4 Symmetrie auf. Die Anwesenheit von Mg^{2+} oder Ca^{2+} hat einen signifikanten Einfluss auf die Monodispersität von *S-layer* Proteinen. Eine SAXS-Analyse zeigte weiterhin, dass slfB and slp-B53 elongierte Multi-Domänen-Proteine sind.

Die erhaltenen Ergebnisse geben Aufschluss über potentielle Anwendungen von *S-Layer*

Proteinen für den Bereich von Mikro- und Nanomaterialien. Die Daten liefern wertvolle Informationen, um den Mechanismus der *S-Layer* Selbstassemblierung im Kontext der Bindung von bivalenten Kationen zu verstehen. Es werden mögliche Lösungsansätze vorgestellt, mit denen hochauflösende 3D-Strukturinformationen von *S-Layer*- und ähnlichen Proteinen erhalten werden können.

7 References

1. Kern, J., et al., *Structure of surface layer homology (SLH) domains from Bacillus anthracis surface array protein.* Journal of Biological Chemistry, 2011. **286**(29): p. 26042-26049.
2. Schuster, B. and U.B. Sleytr, *Composite S-layer lipid structures.* Journal of structural biology, 2009. **168**(1): p. 207-216.
3. Engelhardt, H., *Are S-layers exoskeletons? The basic function of protein surface layers revisited.* Journal of structural biology, 2007. **160**(2): p. 115-124.
4. Györvary, E.S., et al., *Self-assembly and recrystallization of bacterial S-layer proteins at silicon supports imaged in real time by atomic force microscopy.* Journal of Microscopy, 2003. **212**(3): p. 300-306.
5. Sleytr, U.B., *Crystalline bacterial cell surface proteins*. Molecular biology intelligence group. 1996, Austin, TX: R.G. Landes Co. 6 , 230 p.
6. Sleytr, U.B., et al., *Self-assembling Protein Systems: Microbial S-layers.* Biopolymers Online, 2002.
7. Åvall-Jääskeläinen, S. and A. Palva, *Lactobacillus surface layers and their applications.* Fems Microbiology Reviews, 2005. **29**(3): p. 511-529.
8. Claus, H., et al., *Molecular organization of selected prokaryotic S-layer proteins.* Canadian journal of microbiology, 2005. **51**(9): p. 731-743.
9. Roberts, K., et al., *Cell wall glycoproteins: structure and function.* Journal of Cell Science, 1985. **1985**(Supplement 2): p. 105-127.
10. Beveridge, T.J. and L.L. Graham, *Surface layers of bacteria.* Microbiological reviews, 1991. **55**(4): p. 684.
11. Holt, S. and E. Leadbetter, *Comparative ultrastructure of selected aerobic spore-forming bacteria: a freeze-etching study.* Bacteriological reviews, 1969. **33**(2): p. 346.
12. Sleytr, U.B. and A.M. Glauert, *Analysis of regular arrays of subunits on bacterial surfaces; evidence for a dynamic process of assembly.* Journal of ultrastructure research, 1975. **50**(1): p. 103-116.
13. Sleytr, U.B., *Regular arrays of macromolecules on bacterial cell walls: structure, chemistry, assembly, and function.* International review of cytology, 1978. **53**: p. 1-64.
14. Sleytr, U.B. and P. Messner, *Crystalline surface layers on bacteria.* Annual Reviews in Microbiology, 1983. **37**(1): p. 311-339.
15. Sleytr, U. and P. Messner, *Self-assembly of crystalline bacterial cell surface layers (S-layers).* Electron microscopy of subcellular dynamics. CRC Press, Inc., Boca Raton, Fla, 1989: p. 13-31.
16. Baumeister, W., I. Wildhaber, and B.M. Phipps, *Principles of organization in eubacterial and archaebacterial surface proteins.* Canadian journal of microbiology, 1989. **35**(1): p. 215-227.
17. Müller, D., W. Baumeister, and A. Engel, *Conformational change of the hexagonally packed intermediate layer of Deinococcus radiodurans monitored by atomic force microscopy.* Journal of bacteriology, 1996. **178**(11): p. 3025-3030.

18. Beveridge, T.J. and S.F. Koval, *Advances in bacterial paracrystalline surface layers*. Vol. 252. 1993: Plenum Pub Corp.
19. Hovmöller, S., *Crystallographic image processing applications for S-layers.* NATO ASI SERIES A LIFE SCIENCES, 1993. **252**: p. 13-13.
20. Sleytr, U.B., et al., *Occurrence, location, ultrastructure and morphogenesis of S-layers.* Crystalline Bacterial Cell Surface Proteins, 1996: p. 5-33.
21. Müller, D.J., W. Baumeister, and A. Engel, *Controlled unzipping of a bacterial surface layer with atomic force microscopy.* Proceedings of the National Academy of Sciences, 1999. **96**(23): p. 13170-13174.
22. Sleytr, U.B., et al., *Crystalline bacterial cell surface layers (S layers): from supramolecular cell structure to biomimetics and nanotechnology.* Angewandte Chemie International Edition, 1999. **38**(8): p. 1034-1054.
23. Horejs, C., et al., *Structure prediction of an S-layer protein by the mean force method.* The Journal of chemical physics, 2008. **128**: p. 065106.
24. Sára, M. and U.B. Sleytr, *S-layer proteins.* Journal of bacteriology, 2000. **182**(4): p. 859-868.
25. Pum, D., M. Sára, and U. Sleytr, *Structure, surface charge, and self-assembly of the S-layer lattice from Bacillus coagulans E38-66.* Journal of bacteriology, 1989. **171**(10): p. 5296-5303.
26. Sleytr, U.B., *Heterologous reattachment of regular arrays of glycoproteins on bacterial surfaces*. 1975: Nature Publishing Group.
27. Sleytr, U.B., et al., *Crystalline bacterial cell surface proteins*. 1996: Academic Press.
28. Horejs, C., et al., *Atomistic structure of monomolecular surface layer self-assemblies: toward functionalized nanostructures.* ACS nano, 2011. **5**(3): p. 2288-2297.
29. Kern, J. and O. Schneewind, *BslA, the S-layer adhesin of B. anthracis, is a virulence factor for anthrax pathogenesis.* Molecular microbiology, 2010. **75**(2): p. 324-332.
30. Sabet, M., et al., *The surface (S-) layer is a virulence factor of Bacteroides forsythus.* Microbiology, 2003. **149**(12): p. 3617-3627.
31. Kokka, R.P., N.A. Vedros, and J.M. Janda, *Electrophoretic analysis of the surface components of autoagglutinating surface array protein-positive and surface array protein-negative Aeromonas hydrophila and Aeromonas sobria.* Journal of clinical microbiology, 1990. **28**(10): p. 2240-2247.
32. Dooley, J., et al., *Isolation and biochemical characterization of the S-layer protein from a pathogenic Aeromonas hydrophila strain.* Journal of bacteriology, 1988. **170**(6): p. 2631-2638.
33. Ishiguro, E., et al., *Loss of virulence during culture of Aeromonas salmonicida at high temperature.* Journal of bacteriology, 1981. **148**(1): p. 333-340.
34. Geisse, N.A., *AFM and combined optical techniques.* Materials today, 2009. **12**(7): p. 40-45.
35. Lipfert, J. and S. Doniach, *Small-angle X-ray scattering from RNA, proteins, and protein complexes.* Annu. Rev. Biophys. Biomol. Struct., 2007. **36**: p. 307-327.
36. Sarkar, S.K., *NMR spectroscopy and its application to biomedical research*. 1996,

Amsterdam ; New York: Elsevier. xviii, 387 p.
37. Glatter, O. and O. Kratky, *Small angle X-ray scattering*. Vol. 102. 1982: Academic press London.
38. Pollmann, K., et al., *Novel surface layer protein genes in Bacillus sphaericus associated with unusual insertion elements.* Microbiology, 2005. **151**(9): p. 2961-2973.
39. Putnam, C.D., et al., *X-ray solution scattering (SAXS) combined with crystallography and computation: defining accurate macromolecular structures, conformations and assemblies in solution.* Quarterly reviews of biophysics, 2007. **40**(03): p. 191-285.
40. Svergun, D.I. and M.H. Koch, *Small-angle scattering studies of biological macromolecules in solution.* Reports on Progress in Physics, 2003. **66**(10): p. 1735.
41. Svergun, D.I. and M.H. Koch, *Advances in structure analysis using small-angle scattering in solution.* Current opinion in structural biology, 2002. **12**(5): p. 654-660.
42. Svergun, D.I., M.V. Petoukhov, and M.H. Koch, *Determination of domain structure of proteins from X-ray solution scattering.* Biophysical journal, 2001. **80**(6): p. 2946-2953.
43. Svergun, D., *Restoring low resolution structure of biological macromolecules from solution scattering using simulated annealing.* Biophysical journal, 1999. **76**(6): p. 2879-2886.
44. Sarkar, S.K., *NMR spectroscopy and its application to biomedical research*. 1996: Elsevier Science.
45. Baranova, E., et al., *SbsB structure and lattice reconstruction unveil Ca2+ triggered S-layer assembly.* Nature, 2012.
46. Messner, P. and U. Sleytr, *Separation and purification of S-layers from gram-positive and gram-negative bacteria.* Bacterial cell surface techniques. John Wiley & Sons, Chichester, United Kingdom, 1988: p. 97-104.
47. Schuster, B., et al., *Nanotechnology with S-layer proteins*, in *Protein Nanotechnology*. 2005, Springer. p. 101-123.
48. Koval, S. and R. Murray, *The isolation of surface array proteins from bacteria.* Canadian journal of biochemistry and cell biology, 1984. **62**(11): p. 1181-1189.
49. Sleytr, U.B., *Heterologous reattachment of regular arrays of glycoproteins on bacterial surfaces.* 1975.
50. König, H., H. Claus, and A. Varma, *Prokaryotic cell wall compounds.* 2010.
51. Sleytr, U.B., et al., *Crystalline bacterial cell surface layers.* Molecular microbiology, 1993. **10**(5): p. 911-916.
52. Sleytr, U.B., et al., *Characterization and use of crystalline bacterial cell surface layers.* Progress in surface science, 2001. **68**(7): p. 231-278.
53. Sumper, M. and F.T. Wieland, *Bacterial glycoproteins.* New Comprehensive Biochemistry, 1995. **29**: p. 455-473.
54. Messner, P. and C. Schäffer, *Prokaryotic glycoproteins*, in *Fortschritte der Chemie organischer Naturstoffe/Progress in the Chemistry of Organic Natural Products*. 2003, Springer. p. 51-124.
55. Lupas, A., et al., *Domain structure of the Acetogenium kivui surface layer revealed by electron crystallography and sequence analysis.* Journal of bacteriology, 1994. **176**(5): p. 1224-1233.

56. Sára, M., *Conserved anchoring mechanisms between crystalline cell surface S-layer proteins and secondary cell wall polymers in Gram-positive bacteria?* Trends in microbiology, 2001. **9**(2): p. 47-49.
57. Mader, C., et al., *Interaction of the crystalline bacterial cell surface layer protein SbsB and the secondary cell wall polymer of Geobacillus stearothermophilus PV72 assessed by real-time surface plasmon resonance biosensor technology.* Journal of bacteriology, 2004. **186**(6): p. 1758-1768.
58. Huber, C., et al., *The three S-layer-like homology motifs of the S-layer protein SbpA of Bacillus sphaericus CCM 2177 are not sufficient for binding to the pyruvylated secondary cell wall polymer.* Molecular microbiology, 2005. **55**(1): p. 197-205.
59. Ferner-Ortner, J., et al., *High-affinity interaction between the S-layer protein SbsC and the secondary cell wall polymer of Geobacillus stearothermophilus ATCC 12980 determined by surface plasmon resonance technology.* Journal of bacteriology, 2007. **189**(19): p. 7154-7158.
60. Schäffer, C. and P. Messner, *The structure of secondary cell wall polymers: how Gram-positive bacteria stick their cell walls together.* Microbiology, 2005. **151**(3): p. 643-651.
61. Egelseer, E.-M., et al., *Genetically engineered S-layer proteins and S-layer-specific heteropolysaccharides as components of a versatile molecular construction kit for applications in nanobiotechnology*, in *NanoBioTechnology*. 2008, Springer. p. 55-86.
62. Mesnage, S., et al., *The S-layer homology domain as a means for anchoring heterologous proteins on the cell surface of Bacillus anthracis.* Journal of applied microbiology, 1999. **87**(2): p. 256-260.
63. Howorka, S., et al., *Surface-accessible residues in the monomeric and assembled forms of a bacterial surface layer protein.* Journal of Biological Chemistry, 2000. **275**(48): p. 37876-37886.
64. Jarosch, M., et al., *Analysis of the structure–function relationship of the S-layer protein SbsC of Bacillus stearothermophilus ATCC 12980 by producing truncated forms.* Microbiology, 2001. **147**(5): p. 1353-1363.
65. Sokolova, T., et al., *Carboxydobrachium pacificum gen. nov., sp. nov., a new anaerobic, thermophilic, CO-utilizing marine bacterium from Okinawa Trough.* International journal of systematic and evolutionary microbiology, 2001. **51**(1): p. 141-149.
66. Eichler, J. and M.W. Adams, *Posttranslational protein modification in Archaea.* Microbiology and Molecular Biology Reviews, 2005. **69**(3): p. 393-425.
67. Messner, P., et al., *S-layer nanoglycobiology of bacteria.* Carbohydrate research, 2008. **343**(12): p. 1934-1951.
68. Blaser, M.J., *Editorial Response: Campylobacter fetus: Emerging Infection and Model System for Bacterial Pathogenesis at Mucosal Surfaces.* Clinical Infectious Diseases, 1998. **27**(2): p. 256-258.
69. Sleytr, U., et al., *Molecular nanotechnology and nanobiotechnology with two-dimensional protein crystals (S-layers).* Nano-surface chemistry, 2001: p. 333-389.
70. Sleytr, U.B., et al., *Crystalline bacterial cell surface layers (S-layers): a versatile*

self-assembly system. 2000: Marcel Dekker: New York.
71. Sleytr, U.B., *I. Basic and applied S-layer research: an overview1.* Fems Microbiology Reviews, 1997. **20**(1-2): p. 5-12.
72. Sleytr, U.B. and T.J. Beveridge, *Bacterial S-layers.* Trends in microbiology, 1999. **7**(6): p. 253-260.
73. Delcour, J., et al., *The biosynthesis and functionality of the cell-wall of lactic acid bacteria*, in *Lactic Acid Bacteria: Genetics, Metabolism and Applications*. 1999, Springer. p. 159-184.
74. Navarre, W.W. and O. Schneewind, *Surface proteins of gram-positive bacteria and mechanisms of their targeting to the cell wall envelope.* Microbiology and Molecular Biology Reviews, 1999. **63**(1): p. 174-229.
75. Ton-That, H., L.A. Marraffini, and O. Schneewind, *Protein sorting to the cell wall envelope of Gram-positive bacteria.* Biochimica et Biophysica Acta (BBA)-Molecular Cell Research, 2004. **1694**(1): p. 269-278.
76. Johannis P. Kamerling, G.-J.B., Yuan Ch. Lee, Akemi Suzuki, Naoyuki Taniguchi, Alphons G.J. Voragen, *Comprehensive Glycoscience (From Chemistry to Systems Biology).* 2007: p. 123-179.
77. Baumeister, W. and G. Lembcke, *Structural features of archaebacterial cell envelopes.* Journal of bioenergetics and biomembranes, 1992. **24**(6): p. 567-575.
78. Messner, P. and U.B. Sleytr, *Crystalline bacterial cell-surface layers.* Adv Microb Physiol, 1992. **33**: p. 213-75.
79. Etienne-Toumelin, I., et al., *Characterization of the Bacillus anthracis S-layer: cloning and sequencing of the structural gene.* Journal of bacteriology, 1995. **177**(3): p. 614-620.
80. Mesnage, S., et al., *Molecular characterization of the Bacillus anthracis main S-layer component: evidence that it is the major cell-associated antigen.* Molecular microbiology, 1997. **23**(6): p. 1147-1155.
81. Redmond, C., et al., *Identification of proteins in the exosporium of Bacillus anthracis.* Microbiology, 2004. **150**(2): p. 355-363.
82. Williams, D.D. and C.L. Turnbough, *Surface layer protein EA1 is not a component of Bacillus anthracis spores but is a persistent contaminant in spore preparations.* Journal of bacteriology, 2004. **186**(2): p. 566-569.
83. Kelly, C.P. and J.T. LaMont, *Clostridium difficile infection.* Annual review of medicine, 1998. **49**: p. 375.
84. Borriello, S., et al., *Virulence factors of Clostridium difficile.* Review of Infectious Diseases, 1990. **12**(Supplement 2): p. S185-S191.
85. Mukherjee, K., et al., *Proteins released during high toxin production in Clostridium difficile.* Microbiology, 2002. **148**(7): p. 2245-2253.
86. Calabi, E., et al., *Molecular characterization of the surface layer proteins from Clostridium difficile.* Molecular microbiology, 2001. **40**(5): p. 1187-1199.
87. Karjalainen, T., et al., *Molecular and genomic analysis of genes encoding surface-anchored proteins from Clostridium difficile.* Infection and immunity, 2001. **69**(5): p. 3442-3446.
88. Savariau-Lacomme, M.-P., et al., *Transcription and analysis of polymorphism in a cluster of*

genes encoding surface-associated proteins of Clostridium difficile. Journal of bacteriology, 2003. **185**(15): p. 4461-4470.

89. Eidhin, D.N., et al., *Sequence and phylogenetic analysis of the gene for surface layer protein, slpA, from 14 PCR ribotypes of Clostridium difficile.* Journal of medical microbiology, 2006. **55**(1): p. 69-83.
90. Karjalainen, T., et al., *Clostridium difficile genotyping based on slpA variable region in S-layer gene sequence: an alternative to serotyping.* Journal of clinical microbiology, 2002. **40**(7): p. 2452-2458.
91. Calabi, E. and N. Fairweather, *Patterns of sequence conservation in the S-layer proteins and related sequences in Clostridium difficile.* Journal of bacteriology, 2002. **184**(14): p. 3886-3897.
92. Cachat, E. and F.G. Priest, *Lactobacillus suntoryeus sp. nov., isolated from malt whisky distilleries.* International journal of systematic and evolutionary microbiology, 2005. **55**(1): p. 31-34.
93. Naser, S.M., et al., *Lactobacillus suntoryeus Cachat and Priest 2005 is a later synonym of Lactobacillus helveticus (Orla-Jensen 1919) Bergey et al. 1925 (Approved Lists 1980).* International journal of systematic and evolutionary microbiology, 2006. **56**(2): p. 355-360.
94. Reniero, R., et al., *Surface proteins in enteric lactobacilli.* Ann Microbiol, 1990. **40**: p. 83-91.
95. Ventura, M., et al., *Identification and characterization of novel surface proteins in Lactobacillus johnsonii and Lactobacillus gasseri.* Applied and Environmental Microbiology, 2002. **68**(12): p. 6172-6181.
96. Jakava-Viljanen, M., et al., *Isolation of three new surface layer protein genes (slp) from Lactobacillus brevis ATCC 14869 and characterization of the change in their expression under aerated and anaerobic conditions.* Journal of bacteriology, 2002. **184**(24): p. 6786-6795.
97. Narita, J., et al., *Improvement of protein production in lactic acid bacteria using 5'-untranslated leader sequence of slpA from Lactobacillus acidophilus.* Applied microbiology and biotechnology, 2006. **73**(2): p. 366-373.
98. Smit, E., et al., *The S-layer Protein of< i> Lactobacillus acidophilus</i> ATCC 4356: Identification and Characterisation of Domains Responsible for S-protein Assembly and Cell Wall Binding.* Journal of molecular biology, 2001. **305**(2): p. 245-257.
99. Smit, E. and P.H. Pouwels, *One repeat of the cell wall binding domain is sufficient for anchoring the Lactobacillus acidophilus surface layer protein.* Journal of bacteriology, 2002. **184**(16): p. 4617-4619.
100. Verbelen, C., et al., *Exploring the molecular forces within and between CbsA S-layer proteins using single molecule force spectroscopy.* Ultramicroscopy, 2007. **107**(10): p. 1004-1011.
101. Van der Mei, H., et al., *Cell surface hydrophobicity is conveyed by S-layer proteins—a study in recombinant lactobacilli.* Colloids and Surfaces B: Biointerfaces, 2003. **28**(2): p. 127-134.
102. Vadillo-Rodríguez, V., et al., *Dynamic cell surface hydrophobicity of Lactobacillus strains*

with and without surface layer proteins. Journal of bacteriology, 2004. **186**(19): p. 6647-6650.

103. Vadillo-Rodriguez, V., et al., *Role of lactobacillus cell surface hydrophobicity as probed by AFM in adhesion to surfaces at low and high ionic strength.* Colloids and Surfaces B: Biointerfaces, 2005. **41**(1): p. 33-41.
104. Jakava-Viljanen, M. and A. Palva, *Isolation of surface (S) layer protein carrying< i> Lactobacillus</i> species from porcine intestine and faeces and characterization of their adhesion properties to different host tissues.* Veterinary microbiology, 2007. **124**(3): p. 264-273.
105. Hollmann, A., et al., *Characterization of liposomes coated with S-layer proteins from lactobacilli.* Biochimica et Biophysica Acta (BBA)-Biomembranes, 2007. **1768**(3): p. 393-400.
106. Messner, P., F. Hollaus, and U.B. Sleytr, *Paracrystalline cell wall surface layers of different Bacillus stearothermophilus strains.* International journal of systematic bacteriology, 1984. **34**(2): p. 202-210.
107. Messner, P., D. Pum, and U.B. Sleytr, *Characterization of the ultrastructure and the self-assembly of the surface layer of< i> Bacillus stearothermophilus</i> strain NRS 2004/3a.* Journal of ultrastructure and molecular structure research, 1986. **97**(1): p. 73-88.
108. Messner, P. and U.B. Sleytr, *Bacterial surface layer glycoproteins.* Glycobiology, 1991. **1**(6): p. 545-551.
109. Messner, P. and U.B. Sleytr, *Crystalline bacterial cell-surface layers.* Adv. Microb. Physiol, 1992. **33**: p. 213-275.
110. Schäffer, C., et al., *The surface layer (S-layer) glycoprotein of Geobacillus stearothermophilus NRS 2004/3a Analysis of its glycosylation.* Journal of Biological Chemistry, 2002. **277**(8): p. 6230-6239.
111. Novotny, R., et al., *Genetic organization of chromosomal S-layer glycan biosynthesis loci of Bacillaceae.* Glycoconjugate journal, 2003. **20**(7-8): p. 435-447.
112. Novotny, R., et al., *S-layer glycan-specific loci on the chromosome of Geobacillus stearothermophilus NRS 2004/3a and dTDP-L-rhamnose biosynthesis potential of G. stearothermophilus strains.* Microbiology, 2004. **150**(4): p. 953-965.
113. Szymanski, C.M. and B.W. Wren, *Protein glycosylation in bacterial mucosal pathogens.* Nature Reviews Microbiology, 2005. **3**(3): p. 225-237.
114. Steiner, K., et al., *New insights into the glycosylation of the surface layer protein SgsE from Geobacillus stearothermophilus NRS 2004/3a.* Journal of bacteriology, 2006. **188**(22): p. 7914-7921.
115. Steiner, K., et al., *Functional characterization of the initiation enzyme of S-layer glycoprotein glycan biosynthesis in Geobacillus stearothermophilus NRS 2004/3a.* Journal of bacteriology, 2007. **189**(7): p. 2590-2598.
116. Bindila, L., et al., *Sequencing of O-glycopeptides derived from an S-layer glycoprotein of Geobacillus stearothermophilus NRS 2004/3a containing up to 51 monosaccharide residues at a single glycosylation site by Fourier transform ion cyclotron resonance infrared multiphoton dissociation mass spectrometry.* Analytical chemistry, 2007. **79**(9): p.

3271-3279.
117. Egelseer, E.M., et al., *Characterization of an S-layer glycoprotein produced in the course of S-layer variation of Bacillus stearothermophilus ATCC 12980 and sequencing and cloning of the sbsD gene encoding the protein moiety.* Archives of microbiology, 2001. **177**(1): p. 70-80.
118. Sára, M., et al., *Identification of two binding domains, one for peptidoglycan and another for a secondary cell wall polymer, on the N-terminal part of the S-layer protein SbsB from Bacillus stearothermophilus PV72/p2.* Journal of bacteriology, 1998. **180**(24): p. 6780-6783.
119. Kuen, B., U.B. Sleytr, and W. Lubitz, *Sequence analysis of the< i> sbsA</i> gene encoding the 130-kDa surface-layer protein of< i> Bacillus stearothermophilus</i> strain PV72.* Gene, 1994. **145**(1): p. 115-120.
120. Sára, M., et al., *Dynamics in oxygen-induced changes in S-layer protein synthesis from Bacillus stearothermophilus PV72 and the S-layer-deficient variant T5 in continuous culture and studies of the cell wall composition.* Journal of bacteriology, 1996. **178**(7): p. 2108-2117.
121. Rünzler, D., et al., *Biophysical characterization of the entire bacterial surface layer protein SbsB and its two distinct functional domains.* Journal of Biological Chemistry, 2004. **279**(7): p. 5207-5215.
122. Ilk, N., et al., *Molecular characterization of the S-layer gene, sbpA, of Bacillus sphaericus CCM 2177 and production of a functional S-layer fusion protein with the ability to recrystallize in a defined orientation while presenting the fused allergen.* Applied and Environmental Microbiology, 2002. **68**(7): p. 3251-3260.
123. Merroun, M.L., et al., *Complexation of uranium by cells and S-layer sheets of Bacillus sphaericus JG-A12.* Applied and Environmental Microbiology, 2005. **71**(9): p. 5532-5543.
124. Sakakibara, J., et al., *Loss of adherence ability to human gingival epithelial cells in S-layer protein-deficient mutants of Tannerella forsythensis.* Microbiology, 2007. **153**(3): p. 866-876.
125. Walker, S., S. Smith, and J. Smit, *Isolation and comparison of the paracrystalline surface layer proteins of freshwater caulobacters.* Journal of bacteriology, 1992. **174**(6): p. 1783-1792.
126. Ford, M.J., J.F. Nomellini, and J. Smit, *S-layer anchoring and localization of an S-layer-associated protease in Caulobacter crescentus.* Journal of bacteriology, 2007. **189**(6): p. 2226-2237.
127. Smit, J., et al., *The S-layer of Caulobacter crescentus: three-dimensional image reconstruction and structure analysis by electron microscopy.* Journal of bacteriology, 1992. **174**(20): p. 6527.
128. Tu, Z.C., et al., *Structure and genotypic plasticity of the Campylobacter fetus sap locus.* Molecular microbiology, 2003. **48**(3): p. 685-698.
129. Tu, Z.-C., et al., *Campylobacter fetus of reptile origin as a human pathogen.* Journal of clinical microbiology, 2004. **42**(9): p. 4405-4407.
130. Grogono-Thomas, R., et al., *Role of S-layer protein antigenic diversity in the immune*

responses of sheep experimentally challenged with Campylobacter fetus subsp. fetus. Infection and immunity, 2003. **71**(1): p. 147-154.

131. Sleytr, U., *Morphopoietic and functional aspects of regular protein membranes present on prokaryotic cell walls*, in *Cytomorphogenesis in Plants*. 1981, Springer. p. 3-26.
132. Shenton, W., et al., *Synthesis of cadmium sulphide superlattices using self-assembled bacterial S-layers.* Nature, 1997. **389**(6651): p. 585-587.
133. Dieluweit, S., D. Pum, and U. Sleytr, *Formation of a gold superlattice on an S-layer with square lattice symmetry.* Supramolecular Science, 1998. **5**(1): p. 15-19.
134. Mertig, M., et al., *Fabrication of highly oriented nanocluster arrays by biomolecular templating.* The European Physical Journal D-Atomic, Molecular, Optical and Plasma Physics, 1999. **9**(1): p. 45-48.
135. Pum, D., M. Sára, and U. Sleytr, *Two-dimensional (glyco) protein crystals as patterning elements and immobilisation matrices for the development of biosensors*, in *Immobilised Macromolecules: Application Potentials*. 1993, Springer. p. 141-160.
136. Neubauer, A., D. Pum, and U. Sleytr, *An amperometric glucose sensor based on isoporous crystalline protein membranes as immobilization matrix.* Analytical letters, 1993. **26**(7): p. 1347-1360.
137. Völlenkle, C., et al., *Construction of a functional S-layer fusion protein comprising an immunoglobulin G-binding domain for development of specific adsorbents for extracorporeal blood purification.* Applied and Environmental Microbiology, 2004. **70**(3): p. 1514-1521.
138. Sleytr, U.B., et al., *S-layers as a tool kit for nanobiotechnological applications.* FEMS microbiology letters, 2007. **267**(2): p. 131-144.
139. Sleytr, U.B., et al., *S-Layers as a basic building block in a molecular construction kit.* Febs Journal, 2007. **274**(2): p. 323-334.
140. Schäffer, C., et al., *Novel Biocatalysts Based on S-Layer Self-Assembly of Geobacillus Stearothermophilus NRS 2004/3a: A Nanobiotechnological Approach.* Small, 2007. **3**(9): p. 1549-1559.
141. Tschiggerl, H., et al., *Exploitation of the S-layer self-assembly system for site directed immobilization of enzymes demonstrated for an extremophilic laminarinase from< i> Pyrococcus furiosus</i>.* Journal of biotechnology, 2008. **133**(3): p. 403-411.
142. Tschiggerl, H., et al., *Display of a peptide mimotope on a crystalline bacterial cell surface layer (S-layer) lattice for diagnosis of Epstein–Barr virus infection.* Bioconjugate chemistry, 2008. **19**(4): p. 860-865.
143. Ford, L.A. and R.L. Thune, *Immunization of channel catfish with a crude, acid-extracted preparation of motile aeromonad S-layer protein.* Biomedical letters, 1992. **47**(188): p. 355-362.
144. Messner, P., F.M. Unger, and U.B. Sleytr, *Vaccine development based on S-layer technology.* Crystalline Bacterial Cell surface Proteins. Austin: RG Landes Company, 1996: p. 161-73.
145. Riedmann, E.M., et al., *Construction of recombinant S-layer proteins (rSbsA) and their expression in bacterial ghosts–a delivery system for the nontypeable Haemophilus*

influenzae antigen Omp26. FEMS Immunology & Medical Microbiology, 2003. **37**(2-3): p. 185-192.

146. Bhatnagar, P., et al., *Anti-tumor effects of the bacterium Caulobacter crescentus in murine tumor models.* Cancer biology & therapy, 2006. **5**(5): p. 485-491.
147. Georgiou, G., et al., *Display of heterologous proteins on the surface of microorganisms: from the screening of combinatorial libraries to live recombinant vaccines.* Nature biotechnology, 1997. **15**(1): p. 29-34.
148. Toporowski, J.R.N.M.C. and J. Smit, *Secretion or Presentation of Recombinant Proteins and Peptides Mediated by the S-layer of Caulobacter crescentus.* Protein expression technologies: current status and future trends, 2004: p. 477.
149. Simon, B., et al., *Recombinant vaccines against infectious hematopoietic necrosis virus: production line by the Caulobacter crescentus S-layer protein secretion system and evaluation in laboratory trials.* Dis Aqua Org, 2001. **44**: p. 400-402.
150. Sára, M. and U. Sleytr, *Molecular sieving through S layers of Bacillus stearothermophilus strains.* Journal of bacteriology, 1987. **169**(9): p. 4092-4098.
151. Sára, M. and U.B. Sleytr, *Production and characteristics of ultrafiltration membranes with uniform pores from two-dimensional arrays of proteins.* Journal of Membrane Science, 1987. **33**(1): p. 27-49.
152. Moll, D., et al., *S-layer-streptavidin fusion proteins as template for nanopatterned molecular arrays.* Proceedings of the National Academy of Sciences, 2002. **99**(23): p. 14646-14651.
153. Huber, C., et al., *Heterotetramers Formed by an S-Layer–Streptavidin Fusion Protein and Core-Streptavidin as a Nanoarrayed Template for Biochip Development.* Small, 2006. **2**(1): p. 142-150.
154. Breitwieser, A., et al., *A recombinant bacterial cell surface (S-layer)-major birch pollen allergen-fusion protein (rSbsC/Bet v1) maintains the ability to self-assemble into regularly structured monomolecular lattices and the functionality of the allergen.* Protein engineering, 2002. **15**(3): p. 243-249.
155. Pleschberger, M., et al., *Generation of a functional monomolecular protein lattice consisting of an S-layer fusion protein comprising the variable domain of a camel heavy chain antibody.* Bioconjugate chemistry, 2003. **14**(2): p. 440-448.
156. Pleschberger, M., et al., *An S-layer heavy chain camel antibody fusion protein for generation of a nanopatterned sensing layer to detect the prostate-specific antigen by surface plasmon resonance technology.* Bioconjugate chemistry, 2004. **15**(3): p. 664-671.
157. Naik, R.R., et al., *Biomimetic synthesis and patterning of silver nanoparticles.* Nature materials, 2002. **1**(3): p. 169-172.
158. Küpcü, S., M. Sára, and U.B. Sleytr, *Chemical modification of crystalline ultrafiltration membranes and immobilization of macromolecules.* Journal of Membrane Science, 1991. **61**: p. 167-175.
159. Küpcü, S., M. Sára, and U.B. Sleytr, *Influence of covalent attachment of low molecular weight substances on the rejection and adsorption properties of crystalline proteinaceous ultrafiltration membranes.* Desalination, 1993. **90**(1): p. 65-76.

160. Weygand, M., et al., *Coupling of protein sheet crystals (S-layers) to phospholipid monolayersBasis of a presentation given at Materials Chemistry Discussion No. 2, 13–15 September 1999, University of Nottingham, UK.* Journal of Materials Chemistry, 2000. **10**(1): p. 141-148.
161. Wetzer, B., et al., *S-layer reconstitution at phospholipid monolayers.* Langmuir, 1998. **14**(24): p. 6899-6906.
162. Schuster, B. and U.B. Sleytr, *Biomimetic S-layer supported lipid membranes.* Current Nanoscience, 2006. **2**(2): p. 143-152.
163. Schuster, B., *Biomimetic design of nanopatterned membranes.* NanoBiotechnology, 2005. **1**(2): p. 153-164.
164. Bäuerlein, E., *Biomineralization of Unicellular Organisms: An Unusual Membrane Biochemistry for the Production of Inorganic Nano-and Microstructures.* Angewandte Chemie International Edition, 2003. **42**(6): p. 614-641.
165. Beveridge, T.J., *Bacterial cell wall structure and implications for interactions with metal ions and minerals.* J Nucl Radiochem Sci, 2005. **6**(1): p. 7-10.
166. Ehrlich, H.L., *Geomicrobiology: its significance for geology.* Earth-Science Reviews, 1998. **45**(1): p. 45-60.
167. Beveridge, T.J., *Role of cellular design in bacterial metal accumulation and mineralization.* Annual Reviews in Microbiology, 1989. **43**(1): p. 147-171.
168. Mera, M.U., et al., *The membrane-induced proton motive force influences the metal binding ability of Bacillus subtilis cell walls.* Applied and Environmental Microbiology, 1992. **58**(12): p. 3837-3844.
169. Fahmy, K., et al., *Secondary Structure and Pd< sup>(II)</sup> Coordination in S-Layer Proteins from< i> Bacillus sphaericus</i> Studied by Infrared and X-Ray Absorption Spectroscopy.* Biophysical journal, 2006. **91**(3): p. 996-1007.
170. Pollmann, K., et al., *Metal binding by bacteria from uranium mining waste piles and its technological applications.* Biotechnology advances, 2006. **24**(1): p. 58-68.
171. Hanert, H.H., *The genus Siderocapsa (and other iron-and manganese-oxidizing eubacteria)*, in *The prokaryotes*. 2006, Springer. p. 1005-1015.
172. Istok, J., et al., *In situ bioreduction of technetium and uranium in a nitrate-contaminated aquifer.* Environmental Science & Technology, 2004. **38**(2): p. 468-475.
173. Nevin, K.P., K.T. Finneran, and D.R. Lovley, *Microorganisms associated with uranium bioremediation in a high-salinity subsurface sediment.* Applied and Environmental Microbiology, 2003. **69**(6): p. 3672-3675.
174. Suzuki, Y., et al., *Microbial populations stimulated for hexavalent uranium reduction in uranium mine sediment.* Applied and Environmental Microbiology, 2003. **69**(3): p. 1337-1346.
175. Anderson, R.T., et al., *Stimulating the in situ activity of Geobacter species to remove uranium from the groundwater of a uranium-contaminated aquifer.* Applied and Environmental Microbiology, 2003. **69**(10): p. 5884-5891.
176. Nyman, J.L., et al., *Heterogeneous response to biostimulation for U (VI) reduction in replicated sediment microcosms.* Biodegradation, 2006. **17**(4): p. 303-316.

177. Wan, J., et al., *Reoxidation of bioreduced uranium under reducing conditions.* Environmental Science & Technology, 2005. **39**(16): p. 6162-6169.
178. Geissler, A., et al., *Biogeochemical changes induced in uranium mining waste pile samples by uranyl nitrate treatments under anaerobic conditions.* Geobiology, 2009. **7**(3): p. 282-294.
179. Merroun, M.L., et al., *Bio-precipitation of uranium by two bacterial isolates recovered from extreme environments as estimated by potentiometric titration, TEM and X-ray absorption spectroscopic analyses.* Journal of hazardous materials, 2011. **197**: p. 1-10.
180. Selenska-Pobell, S., et al., *Selective accumulation of heavy metals by three indigenous Bacillus strains, B. cereus, B. megaterium and B. sphaericus, from drain waters of a uranium waste pile.* FEMS Microbiology Ecology, 1999. **29**(1): p. 59-67.
181. Raff, J., et al., *Biosorption of uranium and copper by biocers.* Chemistry of Materials, 2003. **15**(1): p. 240-244.
182. Creamer, N., et al., *Novel supported Pd hydrogenation bionanocatalyst for hybrid homogeneous/heterogeneous catalysis.* Catalysis Today, 2007. **128**(1): p. 80-87.
183. Lederer, F.L., et al., *Identification of multiple putative S-layer genes partly expressed by Lysinibacillus sphaericus JG-B53.* Microbiology, 2013. **159**(Pt 6): p. 1097-1108.
184. Lopez, A.E., et al., *Surface dependence of protein nanocrystal formation.* Small, 2010. **6**(3): p. 396-403.
185. Györvary, E.S., et al., *Biomimetic nanostructure fabrication: nonlithographic lateral patterning and self-assembly of functional bacterial S-layers at silicon supports.* Nano letters, 2003. **3**(3): p. 315-319.
186. Georgieva, R., et al., *Permeability and conductivity of red blood cell templated polyelectrolyte capsules coated with supplementary layers.* Langmuir, 2004. **20**(5): p. 1895-1900.
187. Balkundi, S.S., et al., *Encapsulation of Bacterial Spores in Nanoorganized Polyelectrolyte Shells†.* Langmuir, 2009. **25**(24): p. 14011-14016.
188. Franz, B., et al., *Layer-by-Layer Nano-Encapsulation of Microbes: Controlled Cell Surface Modification and Investigation of Substrate Uptake in Bacteria.* Macromolecular bioscience, 2010. **10**(2): p. 164-172.
189. Kelly, S.M. and N.C. Price, *The use of circular dichroism in the investigation of protein structure and function.* Current protein and peptide science, 2000. **1**(4): p. 349-384.
190. Johnson Jr, W.C., *Secondary structure of proteins through circular dichroism spectroscopy.* Annual review of biophysics and biophysical chemistry, 1988. **17**(1): p. 145-166.
191. Greenfield, N.J., *Methods to estimate the conformation of proteins and polypeptides from circular dichroism data.* Analytical biochemistry, 1996. **235**(1): p. 1-10.
192. Venyaminov, S.Y. and J.T. Yang, *Determination of protein secondary structure*, in *Circular dichroism and the conformational analysis of biomolecules*. 1996, Springer. p. 69-107.
193. Sreerama, N. and R.W. Woody, *Estimation of protein secondary structure from circular dichroism spectra: comparison of CONTIN, SELCON, and CDSSTR methods with an expanded reference set.* Analytical biochemistry, 2000. **287**(2): p. 252-260.
194. Sreerama, N. and R.W. Woody, *On the analysis of membrane protein circular dichroism*

spectra. Protein science, 2004. **13**(1): p. 100-112.
195. Sreerama, N., S.Y. Venyaminov, and R.W. Woody, *Estimation of the number of α-helical and β-strand segments in proteins using circular dichroism spectroscopy.* Protein science, 1999. **8**(2): p. 370-380.
196. Manavalan, P. and W.C. Johnson Jr, *Variable selection method improves the prediction of protein secondary structure from circular dichroism spectra.* Analytical biochemistry, 1987. **167**(1): p. 76-85.
197. Van Stokkum, I.H., et al., *Estimation of protein secondary structure and error analysis from circular dichroism spectra.* Analytical biochemistry, 1990. **191**(1): p. 110-118.
198. Gadegaard, N., *Atomic force microscopy in biology: technology and techniques.* Biotechnic & Histochemistry, 2006. **81**(2-3): p. 87-97.
199. Lapshin, R.V., *Feature-oriented scanning methodology for probe microscopy and nanotechnology.* Nanotechnology, 2004. **15**(9): p. 1135.
200. Lapshin, R.V., *Automatic drift elimination in probe microscope images based on techniques of counter-scanning and topography feature recognition.* Measurement Science and Technology, 2007. **18**(3): p. 907.
201. Yurov, V.Y. and A. Klimov, *Scanning tunneling microscope calibration and reconstruction of real image: Drift and slope elimination.* Review of scientific instruments, 1994. **65**(5): p. 1551-1557.
202. Lapshin, R.V., *Analytical model for the approximation of hysteresis loop and its application to the scanning tunneling microscope.* Review of scientific instruments, 1995. **66**(9): p. 4718-4730.
203. Binnig, G., C.F. Quate, and C. Gerber, *Atomic force microscope.* Physical review letters, 1986. **56**(9): p. 930.
204. Hool, G.A. and N.C. Johnson, *Handbook of Building Construction: Data for Architects, Designing and Constructing Engineers, and Contractors*. Vol. 2. 1920: McGraw-Hill Book Company, Incorporated.
205. Holler, F., D. Skoog, and S. Crouch, *Principles of instrumental analysis.* Belmont: Thomson, 2007.
206. Lang, K., et al., *Conducting atomic force microscopy for nanoscale tunnel barrier characterization.* Review of scientific instruments, 2004. **75**(8): p. 2726-2731.
207. Bryant, P., R. Miller, and R. Yang, *Scanning tunneling and atomic force microscopy combined.* Applied physics letters, 1988. **52**(26): p. 2233-2235.
208. Willemsen, O.H., et al., *Biomolecular interactions measured by atomic force microscopy.* Biophysical journal, 2000. **79**(6): p. 3267-3281.
209. Chung, K.-H. and D.-E. Kim, *Wear characteristics of diamond-coated atomic force microscope probe.* Ultramicroscopy, 2007. **108**(1): p. 1-10.
210. Xu, X. and A. Raman, *Comparative dynamics of magnetically, acoustically, and Brownian motion driven microcantilevers in liquids.* Journal of Applied Physics, 2007. **102**(3): p. 034303-034303-8.
211. Giessibl, F.J., *High-speed force sensor for force microscopy and profilometry utilizing a quartz tuning fork.* Applied physics letters, 1998. **73**(26): p. 3956-3958.

212. Nishida, S., et al., *Photothermal excitation and laser Doppler velocimetry of higher cantilever vibration modes for dynamic atomic force microscopy in liquid.* Review of scientific instruments, 2008. **79**(12): p. 123703-123703-4.
213. Rugar, D., H. Mamin, and P. Guethner, *Improved fiber-optic interferometer for atomic force microscopy.* Applied physics letters, 1989. **55**(25): p. 2588-2590.
214. Goddenhenrich, T., et al., *Force microscope with capacitive displacement detection.* Journal of Vacuum Science & Technology A: Vacuum, Surfaces, and Films, 1990. **8**(1): p. 383-387.
215. Giessibl, F. and B. Trafas, *Piezoresistive cantilevers utilized for scanning tunneling and scanning force microscope in ultrahigh vacuum.* Review of scientific instruments, 1994. **65**(6): p. 1923-1929.
216. Gross, L., et al., *The chemical structure of a molecule resolved by atomic force microscopy.* Science, 2009. **325**(5944): p. 1110-1114.
217. Giessibl, F.J., *Advances in atomic force microscopy.* Reviews of modern physics, 2003. **75**(3): p. 949.
218. Roiter, Y. and S. Minko, *AFM single molecule experiments at the solid-liquid interface: in situ conformation of adsorbed flexible polyelectrolyte chains.* Journal of the American Chemical Society, 2005. **127**(45): p. 15688-15689.
219. Zhong, Q., et al., *Fractured polymer/silica fiber surface studied by tapping mode atomic force microscopy.* Surface Science Letters, 1993. **290**(1): p. L688-L692.
220. Sugimoto, Y., et al., *Chemical identification of individual surface atoms by atomic force microscopy.* Nature, 2007. **446**(7131): p. 64-67.
221. Berne, B.J., *Dynamic light scattering: with applications to chemistry, biology and physics*. 1976: DoverPublications. com.
222. Liu, J., et al., *Selecting Temperature for Protein Crystallization Screens Using the Temperature Dependence of the Second Virial Coefficient.* PloS one, 2011. **6**(3): p. e17950.
223. CHAYEN, N., et al., *Size and shape determination of proteins in solution by a noninvasive depolarized dynamic light scattering instrument.* Annals of the New York Academy of Sciences, 2004. **1027**(1): p. 20-27.
224. Koch, M.H., P. Vachette, and D.I. Svergun, *Small-angle scattering: a view on the properties, structures and structural changes of biological macromolecules in solution.* Quarterly reviews of biophysics, 2003. **36**(02): p. 147-227.
225. Hura, G.L., et al., *Robust, high-throughput solution structural analyses by small angle X-ray scattering (SAXS).* Nature methods, 2009. **6**(8): p. 606-612.
226. Glatter, O., *A new method for the evaluation of small-angle scattering data.* Journal of Applied Crystallography, 1977. **10**(5): p. 415-421.
227. Semenyuk, A. and D. Svergun, *GNOM-a program package for small-angle scattering data processing.* Journal of Applied Crystallography, 1991. **24**(5): p. 537-540.
228. Bax, A. and A. Grishaev, *Weak alignment NMR: a hawk-eyed view of biomolecular structure.* Current opinion in structural biology, 2005. **15**(5): p. 563-570.
229. Amadei, A., A. Linssen, and H.J. Berendsen, *Essential dynamics of proteins.* Proteins:

Structure, Function, and Bioinformatics, 1993. **17**(4): p. 412-425.
230. Van Aalten, D., et al., *Protein dynamics derived from clusters of crystal structures.* Biophysical journal, 1997. **73**(6): p. 2891-2896.
231. Brooks, B. and M. Karplus, *Normal modes for specific motions of macromolecules: application to the hinge-bending mode of lysozyme.* Proceedings of the National Academy of Sciences, 1985. **82**(15): p. 4995-4999.
232. Lindahl, E. and M. Delarue, *Refinement of docked protein–ligand and protein–DNA structures using low frequency normal mode amplitude optimization.* Nucleic acids research, 2005. **33**(14): p. 4496-4506.
233. Levitt, M., C. Sander, and P.S. Stern, *Protein normal-mode dynamics: trypsin inhibitor, crambin, ribonuclease and lysozyme.* Journal of molecular biology, 1985. **181**(3): p. 423-447.
234. Smith, P.E., et al., *Internal mobility of the basic pancreatic trypsin inhibitor in solution: a comparison of NMR spin relaxation measurements and molecular dynamics simulations.* Journal of molecular biology, 1995. **246**(2): p. 356-365.
235. Tirion, M.M., *Large amplitude elastic motions in proteins from a single-parameter, atomic analysis.* Physical review letters, 1996. **77**(9): p. 1905.
236. Hinsen, K., *Analysis of domain motions by approximate normal mode calculations.* Proteins Structure Function and Genetics, 1998. **33**(3): p. 417-429.
237. Atilgan, A., et al., *Anisotropy of fluctuation dynamics of proteins with an elastic network model.* Biophysical journal, 2001. **80**(1): p. 505-515.
238. Suhre, K. and Y.-H. Sanejouand, *ElNemo: a normal mode web server for protein movement analysis and the generation of templates for molecular replacement.* Nucleic acids research, 2004. **32**(suppl 2): p. W610-W614.
239. Delarue, M. and P. Dumas, *On the use of low-frequency normal modes to enforce collective movements in refining macromolecular structural models.* Proceedings of the National Academy of Sciences of the United States of America, 2004. **101**(18): p. 6957-6962.
240. Karplus, M. and J.A. McCammon, *Molecular dynamics simulations of biomolecules.* Nature Structural & Molecular Biology, 2002. **9**(9): p. 646-652.
241. MacKerell, A.D., et al., *All-atom empirical potential for molecular modeling and dynamics studies of proteins.* The Journal of Physical Chemistry B, 1998. **102**(18): p. 3586-3616.
242. Binder, K. and D.W. Heermann, *Monte Carlo simulation in statistical physics: an introduction*. 2010: Springer.
243. Hansmann, U.H. and Y. Okamoto, *New Monte Carlo algorithms for protein folding.* Current opinion in structural biology, 1999. **9**(2): p. 177-183.
244. Maiorov, V. and R. Abagyan, *A new method for modeling large-scale rearrangements of protein domains.* Proteins Structure Function and Genetics, 1997. **27**(3): p. 410-424.
245. Drenth, J., *Principles of Protein X-ray Crystallography, 1995.* Ref Type: Serial (Book, Monograph).
246. Dunker, A.K., et al., *Function and structure of inherently disordered proteins.* Current opinion in structural biology, 2008. **18**(6): p. 756-764.

247. Dyson, H.J. and P.E. Wright, *Intrinsically unstructured proteins and their functions.* Nature Reviews Molecular Cell Biology, 2005. **6**(3): p. 197-208.
248. Marrero, A., et al., *The Crystal Structure of Human α2-Macroglobulin Reveals a Unique Molecular Cage.* Angewandte Chemie International Edition, 2012. **51**(14): p. 3340-3344.
249. Laursen, N.S., et al., *Substrate recognition by complement convertases revealed in the C5–cobra venom factor complex.* The EMBO journal, 2011. **30**(3): p. 606-616.
250. Baxter, R.H., et al., *Structural basis for conserved complement factor-like function in the antimalarial protein TEP1.* Proceedings of the National Academy of Sciences, 2007. **104**(28): p. 11615-11620.
251. Meng, G., et al., *Crystal structure of the Haemophilus influenzae Hap adhesin reveals an intercellular oligomerization mechanism for bacterial aggregation.* The EMBO journal, 2011. **30**(18): p. 3864-3874.
252. Nishimasu, H., et al., *Structure and function of Zucchini endoribonuclease in piRNA biogenesis.* Nature, 2012. **491**(7423): p. 284-287.
253. Redecke, L., et al., *Natively inhibited trypanosoma brucei cathepsin b structure determined by using an x-ray laser.* Science, 2013. **339**(6116): p. 227-230.
254. Chapman, H.N., et al., *Femtosecond X-ray protein nanocrystallography.* Nature, 2011. **470**(7332): p. 73-77.

8 Appendix

8.1 Self-Designed Screens

Self-designed screens

Suite No.	Screen	Protein
Liu2	*pPEG7 Screen Liu2*	sIfB
Liu3	*pPEG7 Screen Liu3*	sIfB
Self-designed screen _ E7	*PACT Screen Liu1*	sIp-B53
Self-designed screen _ H9	*PACT Screen Liu2*	sIp-B53

Additives mixture used in self designed screens

Additive mixture	Contents
AA-Mix	0.2 M (Glycine, D-lysine, L-serine, D,L-glutamic acids, L-alanine)
Monosaccharides	0.2 M **(**D-glucose, D-mannose, D-galactose, D-oxylose, L-fucose**)**
Anion-Mix2	0.06 M NH4I, 0.09 M NH_4Br
Anion-Mix3	0.07 M NH4I, 0.0**8** M NH_4Br
Anion-Mix5	0.05 M NH4I, 0.10 M NH_4Br
Anion-Mix6	0.08 M NH4I**,** 0.07 M NH_4Br
Alcohols	0.2 M (1,6-hexanediol, 1,4-butanediol, 2,3-butanediol, 1,3-butanediol, 2,3-butanediol, 1-propanol, 2-propanol)
Ethylene glycols	0.3 M Ethylene glycol, triethylene glycols, tetraethylene glycols

8.2 Self designed screen – *pPEG7 series*

Liu2_Alcohols_pPEG7 Screen and Liu3_Ethylene Glycols Screen.

8.3 Self designed screen – *PACT series*

PACT Premier ™_E7 Screen and PACT Premier ™_H9 Screen.

Liu2_Alcohols_pPEG7 Screen Conditions 1-48

Source	1	2	3, 24	4	5, 12	6	7	8	9	10	11	13	14	15	16	17	18	19	20	21	22	23	25		
Stock	PEG3350	PEG8000	PEG10000	AS	NaOAc pH4.75	NaCitrat pH4	Anion-Mi	A-M2(6+9)	Anion-Mix3	Water	Water2	$AmNO_3$	NaI	NaBr	A-M5(5+10)	A-M6(8+7)	AmCl	AmBr	AmI	AmAc	AmFor	AmTar	Alcohols		
Cstock	50	35	35	3	0,25	1	100	100	100			5	1	1	100	100	1	1	1	1	2	1	0,2		
Vges	500																								
							A-M=Anion-Mix		Alcohols=1,6-hexanediol, 1,4-butanediol, 2,3-butanediol, 1,3-butanediol, 2,3-butanediol, 1-propanol, 2-propanol,															
Number	Well	Prec	Cprec	Vprec	Source	Salt	Csalt	Vsalt	Source	Buffer	Cbuffer	Vbuffer	Source	Additive	Cadditive	Vadditive		Cryo	Ccryo	Vcryo	Source	Vsum	Vwater	Source	
1	A1	PEG10000	15	214,2857	3	$AmNO_3$	0,35	35	13	NaCitrat pH4	0,1	50	6	A-M6(8+7)	10	50	17	Alcohol	0	0	25	349,2857	150,7143	10	
2	A2	PEG10000	15	214,2857	3	$AmNO_3$	0,35	35	13	NaCitrat pH4	0,1	50	6	A-M6(8+7)	10	50	17	Alcohol	0	0	25	349,2857	150,7143	10	
3	A3	PEG10000	15	214,2857	3	$AmNO_3$	0,35	35	13	NaCitrat pH4	0,1	50	6	A-M6(8+7)	10	50	17	Alcohol	0	0	25	349,2857	150,7143	10	
4	A4	PEG10000	15	214,2857	3	$AmNO_3$	0,35	35	13	NaCitrat pH4	0,1	50	6	A-M6(8+7)	10	50	17	Alcohol	0	0	25	349,2857	150,7143	10	
5	A5	PEG10000	15	214,2857	3	$AmNO_3$	0,35	35	13	NaCitrat pH4	0,1	50	6	A-M5(5+10)	10	50	16	Alcohol	0	0	25	349,2857	150,7143	10	
6	A6	PEG10000	15	214,2857	3	$AmNO_3$	0,35	35	13	NaCitrat pH4	0,1	50	6	A-M5(5+10)	10	50	16	Alcohol	0	0	25	349,2857	150,7143	10	
7	A7	PEG10000	15	214,2857	3	$AmNO_3$	0,35	35	13	NaCitrat pH4	0,1	50	6	A-M5(5+10)	10	50	16	Alcohol	0	0	25	349,2857	150,7143	10	
8	A8	PEG10000	15	214,2857	3	$AmNO_3$	0,35	35	13	NaCitrat pH4	0,1	50	6	A-M5(5+10)	10	50	16	Alcohol	0	0	25	349,2857	150,7143	10	
9	A9	PEG10000	15	214,2857	3	$AmNO_3$	0,35	35	13	NaCitrat pH4	0,1	50	6	A-M2(6+9)	10	50	8	Alcohol	0	0	25	349,2857	150,7143	10	
10	A10	PEG10000	15	214,2857	3	$AmNO_3$	0,35	35	13	NaCitrat pH4	0,1	50	6	A-M2(6+9)	10	50	8	Alcohol	0	0	25	349,2857	150,7143	10	
11	A11	PEG10000	15	214,2857	3	$AmNO_3$	0,35	35	13	NaCitrat pH4	0,1	50	6	A-M2(6+9)	10	50	8	Alcohol	0	0	25	349,2857	150,7143	10	
12	A12	PEG10000	15	214,2857	3	$AmNO_3$	0,35	35	13	NaCitrat pH4	0,1	50	6	A-M2(6+9)	10	50	8	Alcohol	0	0	25	349,2857	150,7143	10	
13	B1	PEG10000	15	214,2857	3	$AmNO_3$	0,4	40	13	NaCitrat pH4	0,1	50	6	A-M6(8+7)	10	50	17	Alcohol	0	0	25	354,2857	145,7143	10	
14	B2	PEG10000	15	214,2857	3	$AmNO_3$	0,4	40	13	NaCitrat pH4	0,1	50	6	A-M6(8+7)	10	50	17	Alcohol	0	0	25	354,2857	145,7143	10	
15	B3	PEG10000	15	214,2857	3	$AmNO_3$	0,4	40	13	NaCitrat pH4	0,1	50	6	A-M6(8+7)	10	50	17	Alcohol	0	0	25	354,2857	145,7143	10	
16	B4	PEG10000	15	214,2857	3	$AmNO_3$	0,4	40	13	NaCitrat pH4	0,1	50	6	A-M6(8+7)	10	50	17	Alcohol	0	0	25	354,2857	145,7143	10	
17	B5	PEG10000	15	214,2857	3	$AmNO_3$	0,4	40	13	NaCitrat pH4	0,1	50	6	A-M5(5+10)	10	50	16	Alcohol	0	0	25	354,2857	145,7143	10	
18	B6	PEG10000	15	214,2857	3	$AmNO_3$	0,4	40	13	NaCitrat pH4	0,1	50	6	A-M5(5+10)	10	50	16	Alcohol	0	0	25	354,2857	145,7143	10	
19	B7	PEG10000	15	214,2857	3	$AmNO_3$	0,4	40	13	NaCitrat pH4	0,1	50	6	A-M5(5+10)	10	50	16	Alcohol	0	0	25	354,2857	145,7143	10	
20	B8	PEG10000	15	214,2857	3	$AmNO_3$	0,4	40	13	NaCitrat pH4	0,1	50	6	A-M5(5+10)	10	50	16	Alcohol	0	0	25	354,2857	145,7143	10	
21	B9	PEG10000	15	214,2857	3	$AmNO_3$	0,4	40	13	NaCitrat pH4	0,1	50	6	A-M2(6+9)	10	50	8	Alcohol	0	0	25	354,2857	145,7143	10	
22	B10	PEG10000	15	214,2857	3	$AmNO_3$	0,4	40	13	NaCitrat pH4	0,1	50	6	A-M2(6+9)	10	50	8	Alcohol	0	0	25	354,2857	145,7143	10	
23	B11	PEG10000	15	214,2857	3	$AmNO_3$	0,4	40	13	NaCitrat pH4	0,1	50	6	A-M2(6+9)	10	50	8	Alcohol	0	0	25	354,2857	145,7143	10	
24	B12	PEG10000	15	214,2857	3	$AmNO_3$	0,4	40	13	NaCitrat pH4	0,1	50	6	A-M2(6+9)	10	50	8	Alcohol	0	0	25	354,2857	145,7143	10	
25	C1	PEG10000	16	228,5714	3	$AmNO_3$	0,35	35	13	NaCitrat pH4	0,1	50	6	A-M6(8+7)	10	50	17	Alcohol	0	0	25	363,5714	136,4286	10	
26	C2	PEG10000	16	228,5714	3	$AmNO_3$	0,35	35	13	NaCitrat pH4	0,1	50	6	A-M6(8+7)	10	50	17	Alcohol	0	0	25	363,5714	136,4286	10	
27	C3	PEG10000	16	228,5714	3	$AmNO_3$	0,35	35	13	NaCitrat pH4	0,1	50	6	A-M6(8+7)	10	50	17	Alcohol	0	0	25	363,5714	136,4286	10	
28	C4	PEG10000	16	228,5714	3	$AmNO_3$	0,35	35	13	NaCitrat pH4	0,1	50	6	A-M6(8+7)	10	50	17	Alcohol	0	0	25	363,5714	136,4286	10	
29	C5	PEG10000	16	228,5714	3	$AmNO_3$	0,35	35	13	NaCitrat pH4	0,1	50	6	A-M5(5+10)	10	50	16	Alcohol	0	0	25	363,5714	136,4286	10	
30	C6	PEG10000	16	228,5714	3	$AmNO_3$	0,35	35	13	NaCitrat pH4	0,1	50	6	A-M5(5+10)	10	50	16	Alcohol	0	0	25	363,5714	136,4286	10	
31	C7	PEG10000	16	228,5714	3	$AmNO_3$	0,35	35	13	NaCitrat pH4	0,1	50	6	A-M5(5+10)	10	50	16	Alcohol	0	0	25	363,5714	136,4286	10	
32	C8	PEG10000	16	228,5714	3	$AmNO_3$	0,35	35	13	NaCitrat pH4	0,1	50	6	A-M5(5+10)	10	50	16	Alcohol	0	0	25	363,5714	136,4286	10	
33	C9	PEG10000	16	228,5714	3	$AmNO_3$	0,35	35	13	NaCitrat pH4	0,1	50	6	A-M2(6+9)	10	50	8	Alcohol	0	0	25	363,5714	136,4286	10	
34	C10	PEG10000	16	228,5714	3	$AmNO_3$	0,35	35	13	NaCitrat pH4	0,1	50	6	A-M2(6+9)	10	50	8	Alcohol	0	0	25	363,5714	136,4286	10	
35	C11	PEG10000	16	228,5714	3	$AmNO_3$	0,35	35	13	NaCitrat pH4	0,1	50	6	A-M2(6+9)	10	50	8	Alcohol	0	0	25	363,5714	136,4286	10	
36	C12	PEG10000	16	228,5714	3	$AmNO_3$	0,35	35	13	NaCitrat pH4	0,1	50	6	A-M2(6+9)	10	50	8	Alcohol	0	0	25	363,5714	136,4286	10	
37	D1	PEG10000	14	200	3	$AmNO_3$	0,4	40	13	NaCitrat pH4	0,1	50	6	A-M6(8+7)	10	50	17	Alcohol	0	0	25	340	160	10	
38	D2	PEG10000	14	200	3	$AmNO_3$	0,4	40	13	NaCitrat pH4	0,1	50	6	A-M6(8+7)	10	50	17	Alcohol	0	0	25	340	160	10	
39	D3	PEG10000	14	200	3	$AmNO_3$	0,4	40	13	NaCitrat pH4	0,1	50	6	A-M6(8+7)	10	50	17	Alcohol	0	0	25	340	160	10	
40	D4	PEG10000	14	200	3	$AmNO_3$	0,4	40	13	NaCitrat pH4	0,1	50	6	A-M6(8+7)	10	50	17	Alcohol	0	0	25	340	160	10	
41	D5	PEG10000	14	200	3	$AmNO_3$	0,4	40	13	NaCitrat pH4	0,1	50	6	A-M5(5+10)	10	50	16	Alcohol	0	0	25	340	160	10	
42	D6	PEG10000	14	200	3	$AmNO_3$	0,4	40	13	NaCitrat pH4	0,1	50	6	A-M5(5+10)	10	50	16	Alcohol	0	0	25	340	160	10	
43	D7	PEG10000	14	200	3	$AmNO_3$	0,4	40	13	NaCitrat pH4	0,1	50	6	A-M5(5+10)	10	50	16	Alcohol	0	0	25	340	160	10	
44	D8	PEG10000	14	200	3	$AmNO_3$	0,4	40	13	NaCitrat pH4	0,1	50	6	A-M5(5+10)	10	50	16	Alcohol	0	0	25	340	160	10	
45	D9	PEG10000	14	200	3	$AmNO_3$	0,4	40	13	NaCitrat pH4	0,1	50	6	A-M2(6+9)	10	50	8	Alcohol	0	0	25	340	160	10	
46	D10	PEG10000	14	200	3	$AmNO_3$	0,4	40	13	NaCitrat pH4	0,1	50	6	A-M2(6+9)	10	50	8	Alcohol	0	0	25	340	160	10	
47	D11	PEG10000	14	200	3	$AmNO_3$	0,4	40	13	NaCitrat pH4	0,1	50	6	A-M2(6+9)	10	50	8	Alcohol	0	0	25	340	160	10	
48	D12	PEG10000	14	200	3	$AmNO_3$	0,4	40	13	NaCitrat pH4	0,1	50	6	A-M2(6+9)	10	50	8	Alcohol	0	0	25	340	160	10	

Liu2_Alcohols_pPEG7 Screen Conditions 49-96

Source	1	2	3, 24	4	5, 12	6	7	8	9	10	11	13	14	15	16	17	18	19	20	21	22	23	25	
Stock	PEG3350	PEG8000	PEG10000	AS	NaOAc pH4.75	NaCitrat pH4	Anion-Mi	A-M2(6+9)	Anion-Mix3	Water	Water2	$AmNO_3$	NaI	NaBr	A-M5(5+10)	A-M6(8+7)	AmCl	AmBr	AmI	AmAc	AmFor	AmTar	Alcohols	
Cstock	50	35	35	3	0,25	1	100	100	100			5	1	1	100	100	1	1	1	1	2	1	0,2	
Vges	500																							
							A-M=Anion-Mix		Alcohols=1,6-hexanediol, 1,4-butanediol, 2,3-butanediol, 1,3-butanediol, 2,3-butanediol, 1-propanol, 2-propanol,														
Number	Well	Prec	Cprec	Vprec	Source	Salt	Csalt	Vsalt	Source	Buffer	Cbuffer	Vbuffer	Source	Additive	Cadditive	Vadditive		Cryo	Ccryo	Vcryo	Source	Vsum	Vwater	Source
49	E1	PEG10000	15	214,2857	24	$AmNO_3$	0,35	35	13	NaCitrat pH4	0,1	50	6	A-M6(8+7)	10	50	17	Alcohol	0,02	50	25	399,2857	100,7143	10
50	E2	PEG10000	15	214,2857	24	$AmNO_3$	0,35	35	13	NaCitrat pH4	0,1	50	6	A-M6(8+7)	10	50	17	Alcohol	0,02	50	25	399,2857	100,7143	10
51	E3	PEG10000	15	214,2857	24	$AmNO_3$	0,35	35	13	NaCitrat pH4	0,1	50	6	A-M6(8+7)	10	50	17	Alcohol	0,02	50	25	399,2857	100,7143	10
52	E4	PEG10000	15	214,2857	24	$AmNO_3$	0,35	35	13	NaCitrat pH4	0,1	50	6	A-M6(8+7)	10	50	17	Alcohol	0,02	50	25	399,2857	100,7143	10
53	E5	PEG10000	15	214,2857	24	$AmNO_3$	0,35	35	13	NaCitrat pH4	0,1	50	6	A-M5(5+10)	10	50	16	Alcohol	0,02	50	25	399,2857	100,7143	10
54	E6	PEG10000	15	214,2857	24	$AmNO_3$	0,35	35	13	NaCitrat pH4	0,1	50	6	A-M5(5+10)	10	50	16	Alcohol	0,02	50	25	399,2857	100,7143	10
55	E7	PEG10000	15	214,2857	24	$AmNO_3$	0,35	35	13	NaCitrat pH4	0,1	50	6	A-M5(5+10)	10	50	16	Alcohol	0,02	50	25	399,2857	100,7143	10
56	E8	PEG10000	15	214,2857	24	$AmNO_3$	0,35	35	13	NaCitrat pH4	0,1	50	6	A-M5(5+10)	10	50	16	Alcohol	0,02	50	25	399,2857	100,7143	10
57	E9	PEG10000	15	214,2857	24	$AmNO_3$	0,35	35	13	NaCitrat pH4	0,1	50	6	A-M2(6+9)	10	50	8	Alcohol	0,02	50	25	399,2857	100,7143	10
58	E10	PEG10000	15	214,2857	24	$AmNO_3$	0,35	35	13	NaCitrat pH4	0,1	50	6	A-M2(6+9)	10	50	8	Alcohol	0,02	50	25	399,2857	100,7143	10
59	E11	PEG10000	15	214,2857	24	$AmNO_3$	0,35	35	13	NaCitrat pH4	0,1	50	6	A-M2(6+9)	10	50	8	Alcohol	0,02	50	25	399,2857	100,7143	10
60	E12	PEG10000	15	214,2857	24	$AmNO_3$	0,35	35	13	NaCitrat pH4	0,1	50	6	A-M2(6+9)	10	50	8	Alcohol	0,02	50	25	399,2857	100,7143	10
61	F1	PEG10000	15	214,2857	24	$AmNO_3$	0,4	40	13	NaCitrat pH4	0,1	50	6	A-M6(8+7)	10	50	17	Alcohol	0,02	50	25	404,2857	95,71429	10
62	F2	PEG10000	15	214,2857	24	$AmNO_3$	0,4	40	13	NaCitrat pH4	0,1	50	6	A-M6(8+7)	10	50	17	Alcohol	0,02	50	25	404,2857	95,71429	10
63	F3	PEG10000	15	214,2857	24	$AmNO_3$	0,4	40	13	NaCitrat pH4	0,1	50	6	A-M6(8+7)	10	50	17	Alcohol	0,02	50	25	404,2857	95,71429	10
64	F4	PEG10000	15	214,2857	24	$AmNO_3$	0,4	40	13	NaCitrat pH4	0,1	50	6	A-M6(8+7)	10	50	17	Alcohol	0,02	50	25	404,2857	95,71429	10
65	F5	PEG10000	15	214,2857	24	$AmNO_3$	0,4	40	13	NaCitrat pH4	0,1	50	6	A-M5(5+10)	10	50	16	Alcohol	0,02	50	25	404,2857	95,71429	10
66	F6	PEG10000	15	214,2857	24	$AmNO_3$	0,4	40	13	NaCitrat pH4	0,1	50	6	A-M5(5+10)	10	50	16	Alcohol	0,02	50	25	404,2857	95,71429	10
67	F7	PEG10000	15	214,2857	24	$AmNO_3$	0,4	40	13	NaCitrat pH4	0,1	50	6	A-M5(5+10)	10	50	16	Alcohol	0,02	50	25	404,2857	95,71429	10
68	F8	PEG10000	15	214,2857	24	$AmNO_3$	0,4	40	13	NaCitrat pH4	0,1	50	6	A-M5(5+10)	10	50	16	Alcohol	0,02	50	25	404,2857	95,71429	10
69	F9	PEG10000	15	214,2857	24	$AmNO_3$	0,4	40	13	NaCitrat pH4	0,1	50	6	A-M2(6+9)	10	50	8	Alcohol	0,02	50	25	404,2857	95,71429	10
70	F10	PEG10000	15	214,2857	24	$AmNO_3$	0,4	40	13	NaCitrat pH4	0,1	50	6	A-M2(6+9)	10	50	8	Alcohol	0,02	50	25	404,2857	95,71429	10
71	F11	PEG10000	15	214,2857	24	$AmNO_3$	0,4	40	13	NaCitrat pH4	0,1	50	6	A-M2(6+9)	10	50	8	Alcohol	0,02	50	25	404,2857	95,71429	10
72	F12	PEG10000	15	214,2857	24	$AmNO_3$	0,4	40	13	NaCitrat pH4	0,1	50	6	A-M2(6+9)	10	50	8	Alcohol	0,02	50	25	404,2857	95,71429	10
73	G1	PEG10000	16	228,5714	24	$AmNO_3$	0,35	35	13	NaCitrat pH4	0,1	50	6	A-M6(8+7)	10	50	17	Alcohol	0,02	50	25	413,5714	86,42857	10
74	G2	PEG10000	16	228,5714	24	$AmNO_3$	0,35	35	13	NaCitrat pH4	0,1	50	6	A-M6(8+7)	10	50	17	Alcohol	0,02	50	25	413,5714	86,42857	10
75	G3	PEG10000	16	228,5714	24	$AmNO_3$	0,35	35	13	NaCitrat pH4	0,1	50	6	A-M6(8+7)	10	50	17	Alcohol	0,02	50	25	413,5714	86,42857	10
76	G4	PEG10000	16	228,5714	24	$AmNO_3$	0,35	35	13	NaCitrat pH4	0,1	50	6	A-M6(8+7)	10	50	17	Alcohol	0,02	50	25	413,5714	86,42857	10
77	G5	PEG10000	16	228,5714	24	$AmNO_3$	0,35	35	13	NaCitrat pH4	0,1	50	6	A-M5(5+10)	10	50	16	Alcohol	0,02	50	25	413,5714	86,42857	10
78	G6	PEG10000	16	228,5714	24	$AmNO_3$	0,35	35	13	NaCitrat pH4	0,1	50	6	A-M5(5+10)	10	50	16	Alcohol	0,02	50	25	413,5714	86,42857	10
79	G7	PEG10000	16	228,5714	24	$AmNO_3$	0,35	35	13	NaCitrat pH4	0,1	50	6	A-M5(5+10)	10	50	16	Alcohol	0,02	50	25	413,5714	86,42857	10
80	G8	PEG10000	16	228,5714	24	$AmNO_3$	0,35	35	13	NaCitrat pH4	0,1	50	6	A-M5(5+10)	10	50	16	Alcohol	0,02	50	25	413,5714	86,42857	10
81	G9	PEG10000	16	228,5714	24	$AmNO_3$	0,35	35	13	NaCitrat pH4	0,1	50	6	A-M2(6+9)	10	50	8	Alcohol	0,02	50	25	413,5714	86,42857	10
82	G10	PEG10000	16	228,5714	24	$AmNO_3$	0,35	35	13	NaCitrat pH4	0,1	50	6	A-M2(6+9)	10	50	8	Alcohol	0,02	50	25	413,5714	86,42857	10
83	G11	PEG10000	16	228,5714	24	$AmNO_3$	0,35	35	13	NaCitrat pH4	0,1	50	6	A-M2(6+9)	10	50	8	Alcohol	0,02	50	25	413,5714	86,42857	10
84	G12	PEG10000	16	228,5714	24	$AmNO_3$	0,35	35	13	NaCitrat pH4	0,1	50	6	A-M2(6+9)	10	50	8	Alcohol	0,02	50	25	413,5714	86,42857	10
85	H1	PEG10000	14	200	24	$AmNO_3$	0,4	40	13	NaCitrat pH4	0,1	50	6	A-M6(8+7)	10	50	17	Alcohol	0,02	50	25	390	110	10
86	H2	PEG10000	14	200	24	$AmNO_3$	0,4	40	13	NaCitrat pH4	0,1	50	6	A-M6(8+7)	10	50	17	Alcohol	0,02	50	25	390	110	10
87	H3	PEG10000	14	200	24	$AmNO_3$	0,4	40	13	NaCitrat pH4	0,1	50	6	A-M6(8+7)	10	50	17	Alcohol	0,02	50	25	390	110	10
88	H4	PEG10000	14	200	24	$AmNO_3$	0,4	40	13	NaCitrat pH4	0,1	50	6	A-M6(8+7)	10	50	17	Alcohol	0,02	50	25	390	110	10
89	H5	PEG10000	14	200	24	$AmNO_3$	0,4	40	13	NaCitrat pH4	0,1	50	6	A-M5(5+10)	10	50	16	Alcohol	0,02	50	25	390	110	10
90	H6	PEG10000	14	200	24	$AmNO_3$	0,4	40	13	NaCitrat pH4	0,1	50	6	A-M5(5+10)	10	50	16	Alcohol	0,02	50	25	390	110	10
91	H7	PEG10000	14	200	24	$AmNO_3$	0,4	40	13	NaCitrat pH4	0,1	50	6	A-M5(5+10)	10	50	16	Alcohol	0,02	50	25	390	110	10
92	H8	PEG10000	14	200	24	$AmNO_3$	0,4	40	13	NaCitrat pH4	0,1	50	6	A-M5(5+10)	10	50	16	Alcohol	0,02	50	25	390	110	10
93	H9	PEG10000	14	200	24	$AmNO_3$	0,4	40	13	NaCitrat pH4	0,1	50	6	A-M2(6+9)	10	50	8	Alcohol	0,02	50	25	390	110	10
94	H10	PEG10000	14	200	24	$AmNO_3$	0,4	40	13	NaCitrat pH4	0,1	50	6	A-M2(6+9)	10	50	8	Alcohol	0,02	50	25	390	110	10
95	H11	PEG10000	14	200	24	$AmNO_3$	0,4	40	13	NaCitrat pH4	0,1	50	6	A-M2(6+9)	10	50	8	Alcohol	0,02	50	25	390	110	10
96	H12	PEG10000	14	200	24	$AmNO_3$	0,4	40	13	NaCitrat pH4	0,1	50	6	A-M2(6+9)	10	50	8	Alcohol	0,02	50	25	390	110	10
				10285,71				1800				2400				2400				2400		19285,71	4714,286	

Liu3_Ethylene Glycols Screen Conditions 1-48

Source	1	2	3, 24	4	5, 12	6	7	8	9	10	11	13	14	15	16	17	18	19	20	21	22	23	25
Stock	PEG3350	PEG8000	PEG10000	AS	NaOAc pH4.75	NaCitrat pH4	Anion-Mix1	A-M2(6+9)	Anion-Mix3	Water	Water2	AmNO3	NaI	NaBr	A-M5(5+10)	A-M6(8+7)	AmCl	AmBr	AmI	AmAc	AmFor	AmTar	Ethylene glycols
Cstock	50	35	35	3	0,25	1	100	100	100			5	1	1	100	100	1	1	1	1	2	1	0,3
Vges	500																						

A-M=Anion-Mix

Ethylene glycols=ethylene glycol, triethylene glycols, tetraethylene glycols

Number	Well	Prec	Cprec	Vprec	Source	Salt	Csalt	Vsalt	Source	Buffer	Cbuffer	Vbuffer	Source	Additive	Cadditive	Vadditive		Cryo	Ccryo	Vcryo	Source	Vsum	Vwater	Source
1	A1	PEG10000	15	214,2857143	3	AmNO3	0,35	35	13	NaCitrat pH4	0,1	50	6	A-M6(8+7)	10	50	17	Ethylene glycols	0	0	25	349,2857143	150,7142857	10
2	A2	PEG10000	15	214,2857143	3	AmNO3	0,35	35	13	NaCitrat pH4	0,1	50	6	A-M6(8+7)	10	50	17	Ethylene glycols	0	0	25	349,2857143	150,7142857	10
3	A3	PEG10000	15	214,2857143	3	AmNO3	0,35	35	13	NaCitrat pH4	0,1	50	6	A-M6(8+7)	10	50	17	Ethylene glycols	0	0	25	349,2857143	150,7142857	10
4	A4	PEG10000	15	214,2857143	3	AmNO3	0,35	35	13	NaCitrat pH4	0,1	50	6	A-M6(8+7)	10	50	17	Ethylene glycols	0	0	25	349,2857143	150,7142857	10
5	A5	PEG10000	15	214,2857143	3	AmNO3	0,35	35	13	NaCitrat pH4	0,1	50	6	A-M5(5+10)	10	50	16	Ethylene glycols	0	0	25	349,2857143	150,7142857	10
6	A6	PEG10000	15	214,2857143	3	AmNO3	0,35	35	13	NaCitrat pH4	0,1	50	6	A-M5(5+10)	10	50	16	Ethylene glycols	0	0	25	349,2857143	150,7142857	10
7	A7	PEG10000	15	214,2857143	3	AmNO3	0,35	35	13	NaCitrat pH4	0,1	50	6	A-M5(5+10)	10	50	16	Ethylene glycols	0	0	25	349,2857143	150,7142857	10
8	A8	PEG10000	15	214,2857143	3	AmNO3	0,35	35	13	NaCitrat pH4	0,1	50	6	A-M5(5+10)	10	50	16	Ethylene glycols	0	0	25	349,2857143	150,7142857	10
9	A9	PEG10000	15	214,2857143	3	AmNO3	0,35	35	13	NaCitrat pH4	0,1	50	6	A-M2(6+9)	10	50	8	Ethylene glycols	0	0	25	349,2857143	150,7142857	10
10	A10	PEG10000	15	214,2857143	3	AmNO3	0,35	35	13	NaCitrat pH4	0,1	50	6	A-M2(6+9)	10	50	8	Ethylene glycols	0	0	25	349,2857143	150,7142857	10
11	A11	PEG10000	15	214,2857143	3	AmNO3	0,35	35	13	NaCitrat pH4	0,1	50	6	A-M2(6+9)	10	50	8	Ethylene glycols	0	0	25	349,2857143	150,7142857	10
12	A12	PEG10000	15	214,2857143	3	AmNO3	0,35	35	13	NaCitrat pH4	0,1	50	6	A-M2(6+9)	10	50	8	Ethylene glycols	0	0	25	349,2857143	150,7142857	10
13	B1	PEG10000	15	214,2857143	3	AmNO3	0,4	40	13	NaCitrat pH4	0,1	50	6	A-M6(8+7)	10	50	17	Ethylene glycols	0	0	25	354,2857143	145,7142857	10
14	B2	PEG10000	15	214,2857143	3	AmNO3	0,4	40	13	NaCitrat pH4	0,1	50	6	A-M6(8+7)	10	50	17	Ethylene glycols	0	0	25	354,2857143	145,7142857	10
15	B3	PEG10000	15	214,2857143	3	AmNO3	0,4	40	13	NaCitrat pH4	0,1	50	6	A-M6(8+7)	10	50	17	Ethylene glycols	0	0	25	354,2857143	145,7142857	10
16	B4	PEG10000	15	214,2857143	3	AmNO3	0,4	40	13	NaCitrat pH4	0,1	50	6	A-M6(8+7)	10	50	17	Ethylene glycols	0	0	25	354,2857143	145,7142857	10
17	B5	PEG10000	15	214,2857143	3	AmNO3	0,4	40	13	NaCitrat pH4	0,1	50	6	A-M5(5+10)	10	50	16	Ethylene glycols	0	0	25	354,2857143	145,7142857	10
18	B6	PEG10000	15	214,2857143	3	AmNO3	0,4	40	13	NaCitrat pH4	0,1	50	6	A-M5(5+10)	10	50	16	Ethylene glycols	0	0	25	354,2857143	145,7142857	10
19	B7	PEG10000	15	214,2857143	3	AmNO3	0,4	40	13	NaCitrat pH4	0,1	50	6	A-M5(5+10)	10	50	16	Ethylene glycols	0	0	25	354,2857143	145,7142857	10
20	B8	PEG10000	15	214,2857143	3	AmNO3	0,4	40	13	NaCitrat pH4	0,1	50	6	A-M5(5+10)	10	50	16	Ethylene glycols	0	0	25	354,2857143	145,7142857	10
21	B9	PEG10000	15	214,2857143	3	AmNO3	0,4	40	13	NaCitrat pH4	0,1	50	6	A-M2(6+9)	10	50	8	Ethylene glycols	0	0	25	354,2857143	145,7142857	10
22	B10	PEG10000	15	214,2857143	3	AmNO3	0,4	40	13	NaCitrat pH4	0,1	50	6	A-M2(6+9)	10	50	8	Ethylene glycols	0	0	25	354,2857143	145,7142857	10
23	B11	PEG10000	15	214,2857143	3	AmNO3	0,4	40	13	NaCitrat pH4	0,1	50	6	A-M2(6+9)	10	50	8	Ethylene glycols	0	0	25	354,2857143	145,7142857	10
24	B12	PEG10000	15	214,2857143	3	AmNO3	0,4	40	13	NaCitrat pH4	0,1	50	6	A-M2(6+9)	10	50	8	Ethylene glycols	0	0	25	354,2857143	145,7142857	10
25	C1	PEG10000	16	228,5714286	3	AmNO3	0,35	35	13	NaCitrat pH4	0,1	50	6	A-M6(8+7)	10	50	17	Ethylene glycols	0	0	25	363,5714286	136,4285714	10
26	C2	PEG10000	16	228,5714286	3	AmNO3	0,35	35	13	NaCitrat pH4	0,1	50	6	A-M6(8+7)	10	50	17	Ethylene glycols	0	0	25	363,5714286	136,4285714	10
27	C3	PEG10000	16	228,5714286	3	AmNO3	0,35	35	13	NaCitrat pH4	0,1	50	6	A-M6(8+7)	10	50	17	Ethylene glycols	0	0	25	363,5714286	136,4285714	10
28	C4	PEG10000	16	228,5714286	3	AmNO3	0,35	35	13	NaCitrat pH4	0,1	50	6	A-M6(8+7)	10	50	17	Ethylene glycols	0	0	25	363,5714286	136,4285714	10
29	C5	PEG10000	16	228,5714286	3	AmNO3	0,35	35	13	NaCitrat pH4	0,1	50	6	A-M5(5+10)	10	50	16	Ethylene glycols	0	0	25	363,5714286	136,4285714	10
30	C6	PEG10000	16	228,5714286	3	AmNO3	0,35	35	13	NaCitrat pH4	0,1	50	6	A-M5(5+10)	10	50	16	Ethylene glycols	0	0	25	363,5714286	136,4285714	10
31	C7	PEG10000	16	228,5714286	3	AmNO3	0,35	35	13	NaCitrat pH4	0,1	50	6	A-M5(5+10)	10	50	16	Ethylene glycols	0	0	25	363,5714286	136,4285714	10
32	C8	PEG10000	16	228,5714286	3	AmNO3	0,35	35	13	NaCitrat pH4	0,1	50	6	A-M5(5+10)	10	50	16	Ethylene glycols	0	0	25	363,5714286	136,4285714	10
33	C9	PEG10000	16	228,5714286	3	AmNO3	0,35	35	13	NaCitrat pH4	0,1	50	6	A-M2(6+9)	10	50	8	Ethylene glycols	0	0	25	363,5714286	136,4285714	10
34	C10	PEG10000	16	228,5714286	3	AmNO3	0,35	35	13	NaCitrat pH4	0,1	50	6	A-M2(6+9)	10	50	8	Ethylene glycols	0	0	25	363,5714286	136,4285714	10
35	C11	PEG10000	16	228,5714286	3	AmNO3	0,35	35	13	NaCitrat pH4	0,1	50	6	A-M2(6+9)	10	50	8	Ethylene glycols	0	0	25	363,5714286	136,4285714	10
36	C12	PEG10000	16	228,5714286	3	AmNO3	0,35	35	13	NaCitrat pH4	0,1	50	6	A-M2(6+9)	10	50	8	Ethylene glycols	0	0	25	363,5714286	136,4285714	10
37	D1	PEG10000	14	200	3	AmNO3	0,4	40	13	NaCitrat pH4	0,1	50	6	A-M6(8+7)	10	50	17	Ethylene glycols	0	0	25	340	160	10
38	D2	PEG10000	14	200	3	AmNO3	0,4	40	13	NaCitrat pH4	0,1	50	6	A-M6(8+7)	10	50	17	Ethylene glycols	0	0	25	340	160	10
39	D3	PEG10000	14	200	3	AmNO3	0,4	40	13	NaCitrat pH4	0,1	50	6	A-M6(8+7)	10	50	17	Ethylene glycols	0	0	25	340	160	10
40	D4	PEG10000	14	200	3	AmNO3	0,4	40	13	NaCitrat pH4	0,1	50	6	A-M6(8+7)	10	50	17	Ethylene glycols	0	0	25	340	160	10
41	D5	PEG10000	14	200	3	AmNO3	0,4	40	13	NaCitrat pH4	0,1	50	6	A-M5(5+10)	10	50	16	Ethylene glycols	0	0	25	340	160	10
42	D6	PEG10000	14	200	3	AmNO3	0,4	40	13	NaCitrat pH4	0,1	50	6	A-M5(5+10)	10	50	16	Ethylene glycols	0	0	25	340	160	10
43	D7	PEG10000	14	200	3	AmNO3	0,4	40	13	NaCitrat pH4	0,1	50	6	A-M5(5+10)	10	50	16	Ethylene glycols	0	0	25	340	160	10
44	D8	PEG10000	14	200	3	AmNO3	0,4	40	13	NaCitrat pH4	0,1	50	6	A-M5(5+10)	10	50	16	Ethylene glycols	0	0	25	340	160	10
45	D9	PEG10000	14	200	3	AmNO3	0,4	40	13	NaCitrat pH4	0,1	50	6	A-M2(6+9)	10	50	8	Ethylene glycols	0	0	25	340	160	10
46	D10	PEG10000	14	200	3	AmNO3	0,4	40	13	NaCitrat pH4	0,1	50	6	A-M2(6+9)	10	50	8	Ethylene glycols	0	0	25	340	160	10
47	D11	PEG10000	14	200	3	AmNO3	0,4	40	13	NaCitrat pH4	0,1	50	6	A-M2(6+9)	10	50	8	Ethylene glycols	0	0	25	340	160	10
48	D12	PEG10000	14	200	3	AmNO3	0,4	40	13	NaCitrat pH4	0,1	50	6	A-M2(6+9)	10	50	8	Ethylene glycols	0	0	25	340	160	10

Liu3_Ethylene Glycols Screen Conditions 49-96

Source	1	2	3, 24	4	5, 12	6	7	8	9	10	11	13	14	15	16	17	18	19	20	21	22	23	25	
Stock	PEG3350	PEG8000	PEG10000	AS	NaOAc pH4.75	NaCitrat pH4	Anion-Mix1	A-M2(6+9)	Anion-Mix3	Water	Water2	$AmNO_3$	NaI	NaBr	A-M5(5+10)	A-M6(8+7)	AmCl	AmBr	AmI	AmAc	AmFor	AmTar	Ethylene glycols	
Cstock	50	35	35	3	0,25	1	100	100	100			5	1	1	100	100	1	1	1	1	2	1	0,3	
Vges	500																							
														A-M=Anion-Mix				Ethylene glycols=ethylene glycol, triethylene glycols, tetraethylene glycols						
Number	Well	Prec	Cprec	Vprec	Source	Salt	Csalt	Vsalt	Source	Buffer	Cbuffer	Vbuffer	Source	Additive	Cadditive	Vadditive		Cryo	Ccryo	Vcryo	Source	Vsum	Vwater	Source
49	E1	PEG10000	15	214,2857143	24	$AmNO_3$	0,35	35	13	NaCitrat pH4	0,1	50	6	A-M6(8+7)	10	50	17	Ethylene glycols	0,03	50	25	399,2857143	100,7142857	10
50	E2	PEG10000	15	214,2857143	24	$AmNO_3$	0,35	35	13	NaCitrat pH4	0,1	50	6	A-M6(8+7)	10	50	17	Ethylene glycols	0,03	50	25	399,2857143	100,7142857	10
51	E3	PEG10000	15	214,2857143	24	$AmNO_3$	0,35	35	13	NaCitrat pH4	0,1	50	6	A-M6(8+7)	10	50	17	Ethylene glycols	0,03	50	25	399,2857143	100,7142857	10
52	E4	PEG10000	15	214,2857143	24	$AmNO_3$	0,35	35	13	NaCitrat pH4	0,1	50	6	A-M6(8+7)	10	50	17	Ethylene glycols	0,03	50	25	399,2857143	100,7142857	10
53	E5	PEG10000	15	214,2857143	24	$AmNO_3$	0,35	35	13	NaCitrat pH4	0,1	50	6	A-M5(5+10)	10	50	16	Ethylene glycols	0,03	50	25	399,2857143	100,7142857	10
54	E6	PEG10000	15	214,2857143	24	$AmNO_3$	0,35	35	13	NaCitrat pH4	0,1	50	6	A-M5(5+10)	10	50	16	Ethylene glycols	0,03	50	25	399,2857143	100,7142857	10
55	E7	PEG10000	15	214,2857143	24	$AmNO_3$	0,35	35	13	NaCitrat pH4	0,1	50	6	A-M5(5+10)	10	50	16	Ethylene glycols	0,03	50	25	399,2857143	100,7142857	10
56	E8	PEG10000	15	214,2857143	24	$AmNO_3$	0,35	35	13	NaCitrat pH4	0,1	50	6	A-M5(5+10)	10	50	16	Ethylene glycols	0,03	50	25	399,2857143	100,7142857	10
57	E9	PEG10000	15	214,2857143	24	$AmNO_3$	0,35	35	13	NaCitrat pH4	0,1	50	6	A-M2(6+9)	10	50	8	Ethylene glycols	0,03	50	25	399,2857143	100,7142857	10
58	E10	PEG10000	15	214,2857143	24	$AmNO_3$	0,35	35	13	NaCitrat pH4	0,1	50	6	A-M2(6+9)	10	50	8	Ethylene glycols	0,03	50	25	399,2857143	100,7142857	10
59	E11	PEG10000	15	214,2857143	24	$AmNO_3$	0,35	35	13	NaCitrat pH4	0,1	50	6	A-M2(6+9)	10	50	8	Ethylene glycols	0,03	50	25	399,2857143	100,7142857	10
60	E12	PEG10000	15	214,2857143	24	$AmNO_3$	0,35	35	13	NaCitrat pH4	0,1	50	6	A-M2(6+9)	10	50	8	Ethylene glycols	0,03	50	25	399,2857143	100,7142857	10
61	F1	PEG10000	15	214,2857143	24	$AmNO_3$	0,4	40	13	NaCitrat pH4	0,1	50	6	A-M6(8+7)	10	50	17	Ethylene glycols	0,03	50	25	404,2857143	95,71428571	10
62	F2	PEG10000	15	214,2857143	24	$AmNO_3$	0,4	40	13	NaCitrat pH4	0,1	50	6	A-M6(8+7)	10	50	17	Ethylene glycols	0,03	50	25	404,2857143	95,71428571	10
63	F3	PEG10000	15	214,2857143	24	$AmNO_3$	0,4	40	13	NaCitrat pH4	0,1	50	6	A-M6(8+7)	10	50	17	Ethylene glycols	0,03	50	25	404,2857143	95,71428571	10
64	F4	PEG10000	15	214,2857143	24	$AmNO_3$	0,4	40	13	NaCitrat pH4	0,1	50	6	A-M6(8+7)	10	50	17	Ethylene glycols	0,03	50	25	404,2857143	95,71428571	10
65	F5	PEG10000	15	214,2857143	24	$AmNO_3$	0,4	40	13	NaCitrat pH4	0,1	50	6	A-M5(5+10)	10	50	16	Ethylene glycols	0,03	50	25	404,2857143	95,71428571	10
66	F6	PEG10000	15	214,2857143	24	$AmNO_3$	0,4	40	13	NaCitrat pH4	0,1	50	6	A-M5(5+10)	10	50	16	Ethylene glycols	0,03	50	25	404,2857143	95,71428571	10
67	F7	PEG10000	15	214,2857143	24	$AmNO_3$	0,4	40	13	NaCitrat pH4	0,1	50	6	A-M5(5+10)	10	50	16	Ethylene glycols	0,03	50	25	404,2857143	95,71428571	10
68	F8	PEG10000	15	214,2857143	24	$AmNO_3$	0,4	40	13	NaCitrat pH4	0,1	50	6	A-M5(5+10)	10	50	16	Ethylene glycols	0,03	50	25	404,2857143	95,71428571	10
69	F9	PEG10000	15	214,2857143	24	$AmNO_3$	0,4	40	13	NaCitrat pH4	0,1	50	6	A-M2(6+9)	10	50	8	Ethylene glycols	0,03	50	25	404,2857143	95,71428571	10
70	F10	PEG10000	15	214,2857143	24	$AmNO_3$	0,4	40	13	NaCitrat pH4	0,1	50	6	A-M2(6+9)	10	50	8	Ethylene glycols	0,03	50	25	404,2857143	95,71428571	10
71	F11	PEG10000	15	214,2857143	24	$AmNO_3$	0,4	40	13	NaCitrat pH4	0,1	50	6	A-M2(6+9)	10	50	8	Ethylene glycols	0,03	50	25	404,2857143	95,71428571	10
72	F12	PEG10000	15	214,2857143	24	$AmNO_3$	0,4	40	13	NaCitrat pH4	0,1	50	6	A-M2(6+9)	10	50	8	Ethylene glycols	0,03	50	25	404,2857143	95,71428571	10
73	G1	PEG10000	16	228,5714286	24	$AmNO_3$	0,35	35	13	NaCitrat pH4	0,1	50	6	A-M6(8+7)	10	50	17	Ethylene glycols	0,03	50	25	413,5714286	86,42857143	10
74	G2	PEG10000	16	228,5714286	24	$AmNO_3$	0,35	35	13	NaCitrat pH4	0,1	50	6	A-M6(8+7)	10	50	17	Ethylene glycols	0,03	50	25	413,5714286	86,42857143	10
75	G3	PEG10000	16	228,5714286	24	$AmNO_3$	0,35	35	13	NaCitrat pH4	0,1	50	6	A-M6(8+7)	10	50	17	Ethylene glycols	0,03	50	25	413,5714286	86,42857143	10
76	G4	PEG10000	16	228,5714286	24	$AmNO_3$	0,35	35	13	NaCitrat pH4	0,1	50	6	A-M6(8+7)	10	50	17	Ethylene glycols	0,03	50	25	413,5714286	86,42857143	10
77	G5	PEG10000	16	228,5714286	24	$AmNO_3$	0,35	35	13	NaCitrat pH4	0,1	50	6	A-M5(5+10)	10	50	16	Ethylene glycols	0,03	50	25	413,5714286	86,42857143	10
78	G6	PEG10000	16	228,5714286	24	$AmNO_3$	0,35	35	13	NaCitrat pH4	0,1	50	6	A-M5(5+10)	10	50	16	Ethylene glycols	0,03	50	25	413,5714286	86,42857143	10
79	G7	PEG10000	16	228,5714286	24	$AmNO_3$	0,35	35	13	NaCitrat pH4	0,1	50	6	A-M5(5+10)	10	50	16	Ethylene glycols	0,03	50	25	413,5714286	86,42857143	10
80	G8	PEG10000	16	228,5714286	24	$AmNO_3$	0,35	35	13	NaCitrat pH4	0,1	50	6	A-M5(5+10)	10	50	16	Ethylene glycols	0,03	50	25	413,5714286	86,42857143	10
81	G9	PEG10000	16	228,5714286	24	$AmNO_3$	0,35	35	13	NaCitrat pH4	0,1	50	6	A-M2(6+9)	10	50	8	Ethylene glycols	0,03	50	25	413,5714286	86,42857143	10
82	G10	PEG10000	16	228,5714286	24	$AmNO_3$	0,35	35	13	NaCitrat pH4	0,1	50	6	A-M2(6+9)	10	50	8	Ethylene glycols	0,03	50	25	413,5714286	86,42857143	10
83	G11	PEG10000	16	228,5714286	24	$AmNO_3$	0,35	35	13	NaCitrat pH4	0,1	50	6	A-M2(6+9)	10	50	8	Ethylene glycols	0,03	50	25	413,5714286	86,42857143	10
84	G12	PEG10000	16	228,5714286	24	$AmNO_3$	0,35	35	13	NaCitrat pH4	0,1	50	6	A-M2(6+9)	10	50	8	Ethylene glycols	0,03	50	25	413,5714286	86,42857143	10
85	H1	PEG10000	14	200	24	$AmNO_3$	0,4	40	13	NaCitrat pH4	0,1	50	6	A-M6(8+7)	10	50	17	Ethylene glycols	0,03	50	25	390	110	10
86	H2	PEG10000	14	200	24	$AmNO_3$	0,4	40	13	NaCitrat pH4	0,1	50	6	A-M6(8+7)	10	50	17	Ethylene glycols	0,03	50	25	390	110	10
87	H3	PEG10000	14	200	24	$AmNO_3$	0,4	40	13	NaCitrat pH4	0,1	50	6	A-M6(8+7)	10	50	17	Ethylene glycols	0,03	50	25	390	110	10
88	H4	PEG10000	14	200	24	$AmNO_3$	0,4	40	13	NaCitrat pH4	0,1	50	6	A-M6(8+7)	10	50	17	Ethylene glycols	0,03	50	25	390	110	10
89	H5	PEG10000	14	200	24	$AmNO_3$	0,4	40	13	NaCitrat pH4	0,1	50	6	A-M5(5+10)	10	50	16	Ethylene glycols	0,03	50	25	390	110	10
90	H6	PEG10000	14	200	24	$AmNO_3$	0,4	40	13	NaCitrat pH4	0,1	50	6	A-M5(5+10)	10	50	16	Ethylene glycols	0,03	50	25	390	110	10
91	H7	PEG10000	14	200	24	$AmNO_3$	0,4	40	13	NaCitrat pH4	0,1	50	6	A-M5(5+10)	10	50	16	Ethylene glycols	0,03	50	25	390	110	10
92	H8	PEG10000	14	200	24	$AmNO_3$	0,4	40	13	NaCitrat pH4	0,1	50	6	A-M5(5+10)	10	50	16	Ethylene glycols	0,03	50	25	390	110	10
93	H9	PEG10000	14	200	24	$AmNO_3$	0,4	40	13	NaCitrat pH4	0,1	50	6	A-M2(6+9)	10	50	8	Ethylene glycols	0,03	50	25	390	110	10
94	H10	PEG10000	14	200	24	$AmNO_3$	0,4	40	13	NaCitrat pH4	0,1	50	6	A-M2(6+9)	10	50	8	Ethylene glycols	0,03	50	25	390	110	10
95	H11	PEG10000	14	200	24	$AmNO_3$	0,4	40	13	NaCitrat pH4	0,1	50	6	A-M2(6+9)	10	50	8	Ethylene glycols	0,03	50	25	390	110	10
96	H12	PEG10000	14	200	24	$AmNO_3$	0,4	40	13	NaCitrat pH4	0,1	50	6	A-M2(6+9)	10	50	8	Ethylene glycols	0,03	50	25	390	110	10
				10285,71429				1800				2400				2400				2400		19285,71429	4714,285714	

PACT Premier ^{TM}_E7 Screen Conditions 1-48

Source	1,2,3,4	5	6	7	8	9	10	11,12,13,14	15
Stock	PEG3350	MPD	Bis Tris Propane pH 6.5	Bis Tris Propane pH 7.5	Bis Tris Propane pH 8.5	KNaTartrate	NaOAC	H2O	KCl
Cstock	50	50	0,5	0,5	0,5	2	2		2
Vges	1000								

Number (Destiny)	Well	Prec1	Cprec1	Vprec1	Source	Prec2	Cprec2	Vprec2	Source	Salt1	Csalt1	Vsalt1	Source	Buffer	Cbuffer	Vbuffer	Source	Additive1	Cadditive1	Vadditive1	Source	Additive2	Cadditive2	Vadditive2	Source	Vsum	Vwater	Source
1	A1	PEG3350	25	500	1	MPD	0	0	5	NaOAC	0,2	100	10	Bis Tris Propane pH 6.5	0	0	6	KNaTartrate	0	0	9	KCl	0	0	15	600	400	11
2	A2	PEG3350	25	500	1	MPD	0	0	5	NaOAC	0,2	100	10	Bis Tris Propane pH 6.5	0	0	6	KNaTartrate	0	0	9	KCl	0	0	15	600	400	11
3	A3	PEG3350	22	440	1	MPD	0	0	5	NaOAC	0,2	100	10	Bis Tris Propane pH 6.5	0	0	6	KNaTartrate	0	0	9	KCl	0	0	15	540	460	11
4	A4	PEG3350	22	440	1	MPD	0	0	5	NaOAC	0,2	100	10	Bis Tris Propane pH 6.5	0	0	6	KNaTartrate	0	0	9	KCl	0	0	15	540	460	11
5	A5	PEG3350	20	400	1	MPD	0	0	5	NaOAC	0,2	100	10	Bis Tris Propane pH 6.5	0	0	6	KNaTartrate	0	0	9	KCl	0	0	15	500	500	11
6	A6	PEG3350	20	400	1	MPD	0	0	5	NaOAC	0,2	100	10	Bis Tris Propane pH 6.5	0	0	6	KNaTartrate	0	0	9	KCl	0	0	15	500	500	11
7	A7	PEG3350	18	360	1	MPD	0	0	5	NaOAC	0,2	100	10	Bis Tris Propane pH 6.5	0	0	6	KNaTartrate	0	0	9	KCl	0	0	15	460	540	11
8	A8	PEG3350	18	360	1	MPD	0	0	5	NaOAC	0,2	100	10	Bis Tris Propane pH 6.5	0	0	6	KNaTartrate	0	0	9	KCl	0	0	15	460	540	11
9	A9	PEG3350	16	320	1	MPD	0	0	5	NaOAC	0,2	100	10	Bis Tris Propane pH 6.5	0	0	6	KNaTartrate	0	0	9	KCl	0	0	15	420	580	11
10	A10	PEG3350	16	320	1	MPD	0	0	5	NaOAC	0,2	100	10	Bis Tris Propane pH 6.5	0	0	6	KNaTartrate	0	0	9	KCl	0	0	15	420	580	11
11	A11	PEG3350	14	280	1	MPD	0	0	5	NaOAC	0,2	100	10	Bis Tris Propane pH 6.5	0	0	6	KNaTartrate	0	0	9	KCl	0	0	15	380	620	11
12	A12	PEG3350	14	280	1	MPD	0	0	5	NaOAC	0,2	100	10	Bis Tris Propane pH 6.5	0	0	6	KNaTartrate	0	0	9	KCl	0	0	15	380	620	11
13	B1	PEG3350	10	200	1	MPD	0	0	5	NaOAC	0,1	50	10	Bis Tris Propane pH 6.5	0	0	6	KNaTartrate	0	0	9	KCl	0	0	15	250	750	11
14	B2	PEG3350	10	200	1	MPD	0	0	5	NaOAC	0,1	50	10	Bis Tris Propane pH 6.5	0	0	6	KNaTartrate	0	0	9	KCl	0	0	15	250	750	11
15	B3	PEG3350	10	200	1	MPD	0	0	5	NaOAC	0,12	60	10	Bis Tris Propane pH 6.5	0	0	6	KNaTartrate	0	0	9	KCl	0	0	15	260	740	11
16	B4	PEG3350	10	200	1	MPD	0	0	5	NaOAC	0,12	60	10	Bis Tris Propane pH 6.5	0	0	6	KNaTartrate	0	0	9	KCl	0	0	15	260	740	11
17	B5	PEG3350	10	200	1	MPD	0	0	5	NaOAC	0,14	70	10	Bis Tris Propane pH 6.5	0	0	6	KNaTartrate	0	0	9	KCl	0	0	15	270	730	11
18	B6	PEG3350	10	200	1	MPD	0	0	5	NaOAC	0,14	70	10	Bis Tris Propane pH 6.5	0	0	6	KNaTartrate	0	0	9	KCl	0	0	15	270	730	11
19	B7	PEG3350	10	200	1	MPD	0	0	5	NaOAC	0,16	80	10	Bis Tris Propane pH 6.5	0	0	6	KNaTartrate	0	0	9	KCl	0	0	15	280	720	11
20	B8	PEG3350	10	200	1	MPD	0	0	5	NaOAC	0,16	80	10	Bis Tris Propane pH 6.5	0	0	6	KNaTartrate	0	0	9	KCl	0	0	15	280	720	11
21	B9	PEG3350	10	200	1	MPD	0	0	5	NaOAC	0,18	90	10	Bis Tris Propane pH 6.5	0	0	6	KNaTartrate	0	0	9	KCl	0	0	15	290	710	11
22	B10	PEG3350	10	200	1	MPD	0	0	5	NaOAC	0,18	90	10	Bis Tris Propane pH 6.5	0	0	6	KNaTartrate	0	0	9	KCl	0	0	15	290	710	11
23	B11	PEG3350	10	200	1	MPD	0	0	5	NaOAC	0,25	125	10	Bis Tris Propane pH 6.5	0	0	6	KNaTartrate	0	0	9	KCl	0	0	15	325	675	11
24	B12	PEG3350	10	200	1	MPD	0	0	5	NaOAC	0,25	125	10	Bis Tris Propane pH 6.5	0	0	6	KNaTartrate	0	0	9	KCl	0	0	15	325	675	11
25	C1	PEG3350	12	240	2	MPD	0	0	5	NaOAC	0,1	50	10	Bis Tris Propane pH 6.5	0	0	6	KNaTartrate	0	0	9	KCl	0	0	15	290	710	12
26	C2	PEG3350	12	240	2	MPD	0	0	5	NaOAC	0,1	50	10	Bis Tris Propane pH 6.5	0	0	6	KNaTartrate	0	0	9	KCl	0	0	15	290	710	12
27	C3	PEG3350	12	240	2	MPD	0	0	5	NaOAC	0,12	60	10	Bis Tris Propane pH 6.5	0	0	6	KNaTartrate	0	0	9	KCl	0	0	15	300	700	12
28	C4	PEG3350	12	240	2	MPD	0	0	5	NaOAC	0,12	60	10	Bis Tris Propane pH 6.5	0	0	6	KNaTartrate	0	0	9	KCl	0	0	15	300	700	12
29	C5	PEG3350	12	240	2	MPD	0	0	5	NaOAC	0,14	70	10	Bis Tris Propane pH 6.5	0	0	6	KNaTartrate	0	0	9	KCl	0	0	15	310	690	12
30	C6	PEG3350	12	240	2	MPD	0	0	5	NaOAC	0,14	70	10	Bis Tris Propane pH 6.5	0	0	6	KNaTartrate	0	0	9	KCl	0	0	15	310	690	12
31	C7	PEG3350	12	240	2	MPD	0	0	5	NaOAC	0,16	80	10	Bis Tris Propane pH 6.5	0	0	6	KNaTartrate	0	0	9	KCl	0	0	15	320	680	12
32	C8	PEG3350	12	240	2	MPD	0	0	5	NaOAC	0,16	80	10	Bis Tris Propane pH 6.5	0	0	6	KNaTartrate	0	0	9	KCl	0	0	15	320	680	12
33	C9	PEG3350	12	240	2	MPD	0	0	5	NaOAC	0,18	90	10	Bis Tris Propane pH 6.5	0	0	6	KNaTartrate	0	0	9	KCl	0	0	15	330	670	12
34	C10	PEG3350	12	240	2	MPD	0	0	5	NaOAC	0,18	90	10	Bis Tris Propane pH 6.5	0	0	6	KNaTartrate	0	0	9	KCl	0	0	15	330	670	12
35	C11	PEG3350	12	240	2	MPD	0	0	5	NaOAC	0,25	125	10	Bis Tris Propane pH 6.5	0	0	6	KNaTartrate	0	0	9	KCl	0	0	15	365	635	12
36	C12	PEG3350	12	240	2	MPD	0	0	5	NaOAC	0,25	125	10	Bis Tris Propane pH 6.5	0	0	6	KNaTartrate	0	0	9	KCl	0	0	15	365	635	12
37	D1	PEG3350	14	280	2	MPD	0	0	5	NaOAC	0,1	50	10	Bis Tris Propane pH 6.5	0	0	6	KNaTartrate	0	0	9	KCl	0	0	15	330	670	12
38	D2	PEG3350	14	280	2	MPD	0	0	5	NaOAC	0,1	50	10	Bis Tris Propane pH 6.5	0	0	6	KNaTartrate	0	0	9	KCl	0	0	15	330	670	12
39	D3	PEG3350	14	280	2	MPD	0	0	5	NaOAC	0,12	60	10	Bis Tris Propane pH 6.5	0	0	6	KNaTartrate	0	0	9	KCl	0	0	15	340	660	12
40	D4	PEG3350	14	280	2	MPD	0	0	5	NaOAC	0,12	60	10	Bis Tris Propane pH 6.5	0	0	6	KNaTartrate	0	0	9	KCl	0	0	15	340	660	12
41	D5	PEG3350	14	280	2	MPD	0	0	5	NaOAC	0,14	70	10	Bis Tris Propane pH 6.5	0	0	6	KNaTartrate	0	0	9	KCl	0	0	15	350	650	12
42	D6	PEG3350	14	280	2	MPD	0	0	5	NaOAC	0,14	70	10	Bis Tris Propane pH 6.5	0	0	6	KNaTartrate	0	0	9	KCl	0	0	15	350	650	12
43	D7	PEG3350	14	280	2	MPD	0	0	5	NaOAC	0,16	80	10	Bis Tris Propane pH 6.5	0	0	6	KNaTartrate	0	0	9	KCl	0	0	15	360	640	12
44	D8	PEG3350	14	280	2	MPD	0	0	5	NaOAC	0,16	80	10	Bis Tris Propane pH 6.5	0	0	6	KNaTartrate	0	0	9	KCl	0	0	15	360	640	12
45	D9	PEG3350	14	280	2	MPD	0	0	5	NaOAC	0,18	90	10	Bis Tris Propane pH 6.5	0	0	6	KNaTartrate	0	0	9	KCl	0	0	15	370	630	12
46	D10	PEG3350	14	280	2	MPD	0	0	5	NaOAC	0,18	90	10	Bis Tris Propane pH 6.5	0	0	6	KNaTartrate	0	0	9	KCl	0	0	15	370	630	12
47	D11	PEG3350	14	280	2	MPD	0	0	5	NaOAC	0,25	125	10	Bis Tris Propane pH 6.5	0	0	6	KNaTartrate	0	0	9	KCl	0	0	15	405	595	12
48	D12	PEG3350	14	280	2	MPD	0	0	5	NaOAC	0,25	125	10	Bis Tris Propane pH 6.5	0	0	6	KNaTartrate	0	0	9	KCl	0	0	15	405	595	12

PACT Premier ^{TM}_E7 Screen Conditions 49-96

Source	1,2,3,4	5	6	7	8	9	10	11,12,13,14	15
Stock	PEG3350	MPD	Bis Tris Propane pH 6.5	Bis Tris Propane pH 7.5	Bis Tris Propane pH 8.5	KNaTartrate	NaOAC	H2O	KCl
Cstock	50	50	0,5	0,5	0,5	2	2		2
Vges	1000								

Number (Destiny)	Well	Prec1	Cprec1	Vprec1	Source	Prec2	Cprec2	Vprec2	Source	Salt1	Csalt1	Vsalt1	Source	Buffer	Cbuffer	Vbuffer	Source	Additive1	Cadditive1	Vadditive1	Source	Additive2	Cadditive2	Vadditive2	Source	Vsum	Vwater	Source
49	E1	PEG3350	16	320	3	MPD	0	0	5	NaOAC	0,1	50	10	Bis Tris Propane pH 6.5	0	0	6	KNaTartrate	0	0	9	KCl	0	0	15	370	630	13
50	E2	PEG3350	16	320	3	MPD	0	0	5	NaOAC	0,1	50	10	Bis Tris Propane pH 6.5	0	0	6	KNaTartrate	0	0	9	KCl	0	0	15	370	630	13
51	E3	PEG3350	16	320	3	MPD	0	0	5	NaOAC	0,12	60	10	Bis Tris Propane pH 6.5	0	0	6	KNaTartrate	0	0	9	KCl	0	0	15	380	620	13
52	E4	PEG3350	16	320	3	MPD	0	0	5	NaOAC	0,12	60	10	Bis Tris Propane pH 6.5	0	0	6	KNaTartrate	0	0	9	KCl	0	0	15	380	620	13
53	E5	PEG3350	16	320	3	MPD	0	0	5	NaOAC	0,14	70	10	Bis Tris Propane pH 6.5	0	0	6	KNaTartrate	0	0	9	KCl	0	0	15	390	610	13
54	E6	PEG3350	16	320	3	MPD	0	0	5	NaOAC	0,14	70	10	Bis Tris Propane pH 6.5	0	0	6	KNaTartrate	0	0	9	KCl	0	0	15	390	610	13
55	E7	PEG3350	16	320	3	MPD	0	0	5	NaOAC	0,16	80	10	Bis Tris Propane pH 6.5	0	0	6	KNaTartrate	0	0	9	KCl	0	0	15	400	600	13
56	E8	PEG3350	16	320	3	MPD	0	0	5	NaOAC	0,16	80	10	Bis Tris Propane pH 6.5	0	0	6	KNaTartrate	0	0	9	KCl	0	0	15	400	600	13
57	E9	PEG3350	16	320	3	MPD	0	0	5	NaOAC	0,18	90	10	Bis Tris Propane pH 6.5	0	0	6	KNaTartrate	0	0	9	KCl	0	0	15	410	590	13
58	E10	PEG3350	16	320	3	MPD	0	0	5	NaOAC	0,18	90	10	Bis Tris Propane pH 6.5	0	0	6	KNaTartrate	0	0	9	KCl	0	0	15	410	590	13
59	E11	PEG3350	16	320	3	MPD	0	0	5	NaOAC	0,25	125	10	Bis Tris Propane pH 6.5	0	0	6	KNaTartrate	0	0	9	KCl	0	0	15	445	555	13
60	E12	PEG3350	16	320	3	MPD	0	0	5	NaOAC	0,25	125	10	Bis Tris Propane pH 6.5	0	0	6	KNaTartrate	0	0	9	KCl	0	0	15	445	555	13
61	F1	PEG3350	18	360	3	MPD	0	0	5	NaOAC	0,1	50	10	Bis Tris Propane pH 6.5	0	0	6	KNaTartrate	0	0	9	KCl	0	0	15	410	590	13
62	F2	PEG3350	18	360	3	MPD	0	0	5	NaOAC	0,1	50	10	Bis Tris Propane pH 6.5	0	0	6	KNaTartrate	0	0	9	KCl	0	0	15	410	590	13
63	F3	PEG3350	18	360	3	MPD	0	0	5	NaOAC	0,12	60	10	Bis Tris Propane pH 6.5	0	0	6	KNaTartrate	0	0	9	KCl	0	0	15	420	580	13
64	F4	PEG3350	18	360	3	MPD	0	0	5	NaOAC	0,12	60	10	Bis Tris Propane pH 6.5	0	0	6	KNaTartrate	0	0	9	KCl	0	0	15	420	580	13
65	F5	PEG3350	18	360	3	MPD	0	0	5	NaOAC	0,14	70	10	Bis Tris Propane pH 6.5	0	0	6	KNaTartrate	0	0	9	KCl	0	0	15	430	570	13
66	F6	PEG3350	18	360	3	MPD	0	0	5	NaOAC	0,14	70	10	Bis Tris Propane pH 6.5	0	0	6	KNaTartrate	0	0	9	KCl	0	0	15	430	570	13
67	F7	PEG3350	18	360	3	MPD	0	0	5	NaOAC	0,16	80	10	Bis Tris Propane pH 6.5	0	0	6	KNaTartrate	0	0	9	KCl	0	0	15	440	560	13
68	F8	PEG3350	18	360	3	MPD	0	0	5	NaOAC	0,16	80	10	Bis Tris Propane pH 6.5	0	0	6	KNaTartrate	0	0	9	KCl	0	0	15	440	560	13
69	F9	PEG3350	18	360	3	MPD	0	0	5	NaOAC	0,18	90	10	Bis Tris Propane pH 6.5	0	0	6	KNaTartrate	0	0	9	KCl	0	0	15	450	550	13
70	F10	PEG3350	18	360	3	MPD	0	0	5	NaOAC	0,18	90	10	Bis Tris Propane pH 6.5	0	0	6	KNaTartrate	0	0	9	KCl	0	0	15	450	550	13
71	F11	PEG3350	18	360	3	MPD	0	0	5	NaOAC	0,25	125	10	Bis Tris Propane pH 6.5	0	0	6	KNaTartrate	0	0	9	KCl	0	0	15	485	515	13
72	F12	PEG3350	18	360	3	MPD	0	0	5	NaOAC	0,25	125	10	Bis Tris Propane pH 6.5	0	0	6	KNaTartrate	0	0	9	KCl	0	0	15	485	515	13
73	G1	PEG3350	20	400	4	MPD	0	0	5	NaOAC	0,1	50	10	Bis Tris Propane pH 6.5	0	0	6	KNaTartrate	0	0	9	KCl	0	0	15	450	550	14
74	G2	PEG3350	20	400	4	MPD	0	0	5	NaOAC	0,1	50	10	Bis Tris Propane pH 6.5	0	0	6	KNaTartrate	0	0	9	KCl	0	0	15	450	550	14
75	G3	PEG3350	20	400	4	MPD	0	0	5	NaOAC	0,12	60	10	Bis Tris Propane pH 6.5	0	0	6	KNaTartrate	0	0	9	KCl	0	0	15	460	540	14
76	G4	PEG3350	20	400	4	MPD	0	0	5	NaOAC	0,12	60	10	Bis Tris Propane pH 6.5	0	0	6	KNaTartrate	0	0	9	KCl	0	0	15	460	540	14
77	G5	PEG3350	20	400	4	MPD	0	0	5	NaOAC	0,14	70	10	Bis Tris Propane pH 6.5	0	0	6	KNaTartrate	0	0	9	KCl	0	0	15	470	530	14
78	G6	PEG3350	20	400	4	MPD	0	0	5	NaOAC	0,14	70	10	Bis Tris Propane pH 6.5	0	0	6	KNaTartrate	0	0	9	KCl	0	0	15	470	530	14
79	G7	PEG3350	20	400	4	MPD	0	0	5	NaOAC	0,16	80	10	Bis Tris Propane pH 6.5	0	0	6	KNaTartrate	0	0	9	KCl	0	0	15	480	520	14
80	G8	PEG3350	20	400	4	MPD	0	0	5	NaOAC	0,16	80	10	Bis Tris Propane pH 6.5	0	0	6	KNaTartrate	0	0	9	KCl	0	0	15	480	520	14
81	G9	PEG3350	20	400	4	MPD	0	0	5	NaOAC	0,18	90	10	Bis Tris Propane pH 6.5	0	0	6	KNaTartrate	0	0	9	KCl	0	0	15	490	510	14
82	G10	PEG3350	20	400	4	MPD	0	0	5	NaOAC	0,18	90	10	Bis Tris Propane pH 6.5	0	0	6	KNaTartrate	0	0	9	KCl	0	0	15	490	510	14
83	G11	PEG3350	20	400	4	MPD	0	0	5	NaOAC	0,25	125	10	Bis Tris Propane pH 6.5	0	0	6	KNaTartrate	0	0	9	KCl	0	0	15	525	475	14
84	G12	PEG3350	20	400	4	MPD	0	0	5	NaOAC	0,25	125	10	Bis Tris Propane pH 6.5	0	0	6	KNaTartrate	0	0	9	KCl	0	0	15	525	475	14
85	H1	PEG3350	24	480	4	MPD	0	0	5	NaOAC	0,1	50	10	Bis Tris Propane pH 6.5	0	0	6	KNaTartrate	0	0	9	KCl	0	0	15	530	470	14
86	H2	PEG3350	24	480	4	MPD	0	0	5	NaOAC	0,1	50	10	Bis Tris Propane pH 6.5	0	0	6	KNaTartrate	0	0	9	KCl	0	0	15	530	470	14
87	H3	PEG3350	24	480	4	MPD	0	0	5	NaOAC	0,12	60	10	Bis Tris Propane pH 6.5	0	0	6	KNaTartrate	0	0	9	KCl	0	0	15	540	460	14
88	H4	PEG3350	24	480	4	MPD	0	0	5	NaOAC	0,12	60	10	Bis Tris Propane pH 6.5	0	0	6	KNaTartrate	0	0	9	KCl	0	0	15	540	460	14
89	H5	PEG3350	24	480	4	MPD	0	0	5	NaOAC	0,14	70	10	Bis Tris Propane pH 6.5	0	0	6	KNaTartrate	0	0	9	KCl	0	0	15	550	450	14
90	H6	PEG3350	24	480	4	MPD	0	0	5	NaOAC	0,14	70	10	Bis Tris Propane pH 6.5	0	0	6	KNaTartrate	0	0	9	KCl	0	0	15	550	450	14
91	H7	PEG3350	24	480	4	MPD	0	0	5	NaOAC	0,16	80	10	Bis Tris Propane pH 6.5	0	0	6	KNaTartrate	0	0	9	KCl	0	0	15	560	440	14
92	H8	PEG3350	24	480	4	MPD	0	0	5	NaOAC	0,16	80	10	Bis Tris Propane pH 6.5	0	0	6	KNaTartrate	0	0	9	KCl	0	0	15	560	440	14
93	H9	PEG3350	24	480	4	MPD	0	0	5	NaOAC	0,18	90	10	Bis Tris Propane pH 6.5	0	0	6	KNaTartrate	0	0	9	KCl	0	0	15	570	430	14
94	H10	PEG3350	24	480	4	MPD	0	0	5	NaOAC	0,18	90	10	Bis Tris Propane pH 6.5	0	0	6	KNaTartrate	0	0	9	KCl	0	0	15	570	430	14
95	H11	PEG3350	24	480	4	MPD	0	0	5	NaOAC	0,25	125	10	Bis Tris Propane pH 6.5	0	0	6	KNaTartrate	0	0	9	KCl	0	0	15	605	395	14
96	H12	PEG3350	24	480	4	MPD	0	0	5	NaOAC	0,25	125	10	Bis Tris Propane pH 6.5	0	0	6	KNaTartrate	0	0	9	KCl	0	0	15	605	395	14
				18720				0				3800				0				0				0		22520	25480	

PACT Premier™_H9 Screen Conditions 1-48

Source	1,2,3,4	5	6	7	8	9	10	11,12,13,14	15
Stock	PEG3350	MPD	Bis Tris Propane pH 6.5	Bis Tris Propane pH 7.5	Bis Tris Propane pH 8.5	KNaTartrate	NaOAC	H2O	KCl
Cstock	50	50	0,5	0,5	0,5	2	2		2
Vges	1000								

Number (Destiny)	Well	Prec1	Cprec1	Vprec1	Source	Prec2	Cprec2	Vprec2	Source	Salt1	Csalt1	Vsalt1	Source	Buffer	Cbuffer	Vbuffer	Source	Additive1	Cadditive1	Vadditive1	Source	Additive2	Cadditive2	Vadditive2	Source	Vsum	Vwater	Source
1	A1	PEG3350	20	400	1	MPD	0	0	5	NaOAC	0	0	10	Bis Tris Propane pH 6.5	0,1	200	6	KNaTartrate	0,2	100	9	KCl	0	0	15	700	300	11
2	A2	PEG3350	20	400	1	MPD	0	0	5	NaOAC	0	0	10	Bis Tris Propane pH 6.5	0,1	200	6	KNaTartrate	0,2	100	9	KCl	0	0	15	700	300	11
3	A3	PEG3350	18	360	1	MPD	0	0	5	NaOAC	0	0	10	Bis Tris Propane pH 6.5	0,1	200	6	KNaTartrate	0,2	100	9	KCl	0	0	15	660	340	11
4	A4	PEG3350	18	360	1	MPD	0	0	5	NaOAC	0	0	10	Bis Tris Propane pH 6.5	0,1	200	6	KNaTartrate	0,2	100	9	KCl	0	0	15	660	340	11
5	A5	PEG3350	16	320	1	MPD	0	0	5	NaOAC	0	0	10	Bis Tris Propane pH 6.5	0,1	200	6	KNaTartrate	0,2	100	9	KCl	0	0	15	620	380	11
6	A6	PEG3350	16	320	1	MPD	0	0	5	NaOAC	0	0	10	Bis Tris Propane pH 6.5	0,1	200	6	KNaTartrate	0,2	100	9	KCl	0	0	15	620	380	11
7	A7	PEG3350	14	280	1	MPD	0	0	5	NaOAC	0	0	10	Bis Tris Propane pH 6.5	0,1	200	6	KNaTartrate	0,2	100	9	KCl	0	0	15	580	420	11
8	A8	PEG3350	14	280	1	MPD	0	0	5	NaOAC	0	0	10	Bis Tris Propane pH 6.5	0,1	200	6	KNaTartrate	0,2	100	9	KCl	0	0	15	580	420	11
9	A9	PEG3350	12	240	1	MPD	0	0	5	NaOAC	0	0	10	Bis Tris Propane pH 6.5	0,1	200	6	KNaTartrate	0,2	100	9	KCl	0	0	15	540	460	11
10	A10	PEG3350	12	240	1	MPD	0	0	5	NaOAC	0	0	10	Bis Tris Propane pH 6.5	0,1	200	6	KNaTartrate	0,2	100	9	KCl	0	0	15	540	460	11
11	A11	PEG3350	10	200	1	MPD	0	0	5	NaOAC	0	0	10	Bis Tris Propane pH 6.5	0,1	200	6	KNaTartrate	0,2	100	9	KCl	0	0	15	500	500	11
12	A12	PEG3350	10	200	1	MPD	0	0	5	NaOAC	0	0	10	Bis Tris Propane pH 6.5	0,1	200	6	KNaTartrate	0,2	100	9	KCl	0	0	15	500	500	11
13	B1	PEG3350	14	280	1	MPD	0	0	5	NaOAC	0	0	10	Bis Tris Propane pH 6.5	0,1	200	6	KNaTartrate	0,12	60	9	KCl	0	0	15	540	460	11
14	B2	PEG3350	14	280	1	MPD	0	0	5	NaOAC	0	0	10	Bis Tris Propane pH 6.5	0,1	200	6	KNaTartrate	0,12	60	9	KCl	0	0	15	540	460	11
15	B3	PEG3350	14	280	1	MPD	0	0	5	NaOAC	0	0	10	Bis Tris Propane pH 6.5	0,1	200	6	KNaTartrate	0,14	70	9	KCl	0	0	15	550	450	11
16	B4	PEG3350	14	280	1	MPD	0	0	5	NaOAC	0	0	10	Bis Tris Propane pH 6.5	0,1	200	6	KNaTartrate	0,14	70	9	KCl	0	0	15	550	450	11
17	B5	PEG3350	14	280	1	MPD	0	0	5	NaOAC	0	0	10	Bis Tris Propane pH 6.5	0,1	200	6	KNaTartrate	0,16	80	9	KCl	0	0	15	560	440	11
18	B6	PEG3350	14	280	1	MPD	0	0	5	NaOAC	0	0	10	Bis Tris Propane pH 6.5	0,1	200	6	KNaTartrate	0,16	80	9	KCl	0	0	15	560	440	11
19	B7	PEG3350	14	280	1	MPD	0	0	5	NaOAC	0	0	10	Bis Tris Propane pH 6.5	0,1	200	6	KNaTartrate	0,18	90	9	KCl	0	0	15	570	430	11
20	B8	PEG3350	14	280	1	MPD	0	0	5	NaOAC	0	0	10	Bis Tris Propane pH 6.5	0,1	200	6	KNaTartrate	0,18	90	9	KCl	0	0	15	570	430	11
21	B9	PEG3350	14	280	1	MPD	0	0	5	NaOAC	0	0	10	Bis Tris Propane pH 6.5	0,1	200	6	KNaTartrate	0,22	110	9	KCl	0	0	15	590	410	11
22	B10	PEG3350	14	280	1	MPD	0	0	5	NaOAC	0	0	10	Bis Tris Propane pH 6.5	0,1	200	6	KNaTartrate	0,22	110	9	KCl	0	0	15	590	410	11
23	B11	PEG3350	14	280	1	MPD	0	0	5	NaOAC	0	0	10	Bis Tris Propane pH 6.5	0,1	200	6	KNaTartrate	0,24	120	9	KCl	0	0	15	600	400	11
24	B12	PEG3350	14	280	1	MPD	0	0	5	NaOAC	0	0	10	Bis Tris Propane pH 6.5	0,1	200	6	KNaTartrate	0,24	120	9	KCl	0	0	15	600	400	11
25	C1	PEG3350	16	320	2	MPD	0	0	5	NaOAC	0	0	10	Bis Tris Propane pH 6.5	0,1	200	6	KNaTartrate	0,12	60	9	KCl	0	0	15	580	420	12
26	C2	PEG3350	16	320	2	MPD	0	0	5	NaOAC	0	0	10	Bis Tris Propane pH 6.5	0,1	200	6	KNaTartrate	0,12	60	9	KCl	0	0	15	580	420	12
27	C3	PEG3350	16	320	2	MPD	0	0	5	NaOAC	0	0	10	Bis Tris Propane pH 6.5	0,1	200	6	KNaTartrate	0,14	70	9	KCl	0	0	15	590	410	12
28	C4	PEG3350	16	320	2	MPD	0	0	5	NaOAC	0	0	10	Bis Tris Propane pH 6.5	0,1	200	6	KNaTartrate	0,14	70	9	KCl	0	0	15	590	410	12
29	C5	PEG3350	16	320	2	MPD	0	0	5	NaOAC	0	0	10	Bis Tris Propane pH 6.5	0,1	200	6	KNaTartrate	0,16	80	9	KCl	0	0	15	600	400	12
30	C6	PEG3350	16	320	2	MPD	0	0	5	NaOAC	0	0	10	Bis Tris Propane pH 6.5	0,1	200	6	KNaTartrate	0,16	80	9	KCl	0	0	15	600	400	12
31	C7	PEG3350	16	320	2	MPD	0	0	5	NaOAC	0	0	10	Bis Tris Propane pH 6.5	0,1	200	6	KNaTartrate	0,18	90	9	KCl	0	0	15	610	390	12
32	C8	PEG3350	16	320	2	MPD	0	0	5	NaOAC	0	0	10	Bis Tris Propane pH 6.5	0,1	200	6	KNaTartrate	0,18	90	9	KCl	0	0	15	610	390	12
33	C9	PEG3350	16	320	2	MPD	0	0	5	NaOAC	0	0	10	Bis Tris Propane pH 6.5	0,1	200	6	KNaTartrate	0,22	110	9	KCl	0	0	15	630	370	12
34	C10	PEG3350	16	320	2	MPD	0	0	5	NaOAC	0	0	10	Bis Tris Propane pH 6.5	0,1	200	6	KNaTartrate	0,22	110	9	KCl	0	0	15	630	370	12
35	C11	PEG3350	16	320	2	MPD	0	0	5	NaOAC	0	0	10	Bis Tris Propane pH 6.5	0,1	200	6	KNaTartrate	0,24	120	9	KCl	0	0	15	640	360	12
36	C12	PEG3350	16	320	2	MPD	0	0	5	NaOAC	0	0	10	Bis Tris Propane pH 6.5	0,1	200	6	KNaTartrate	0,24	120	9	KCl	0	0	15	640	360	12
37	D1	PEG3350	18	360	2	MPD	0	0	5	NaOAC	0	0	10	Bis Tris Propane pH 6.5	0,1	200	6	KNaTartrate	0,12	60	9	KCl	0	0	15	620	380	12
38	D2	PEG3350	18	360	2	MPD	0	0	5	NaOAC	0	0	10	Bis Tris Propane pH 6.5	0,1	200	6	KNaTartrate	0,12	60	9	KCl	0	0	15	620	380	12
39	D3	PEG3350	18	360	2	MPD	0	0	5	NaOAC	0	0	10	Bis Tris Propane pH 6.5	0,1	200	6	KNaTartrate	0,14	70	9	KCl	0	0	15	630	370	12
40	D4	PEG3350	18	360	2	MPD	0	0	5	NaOAC	0	0	10	Bis Tris Propane pH 6.5	0,1	200	6	KNaTartrate	0,14	70	9	KCl	0	0	15	630	370	12
41	D5	PEG3350	18	360	2	MPD	0	0	5	NaOAC	0	0	10	Bis Tris Propane pH 6.5	0,1	200	6	KNaTartrate	0,16	80	9	KCl	0	0	15	640	360	12
42	D6	PEG3350	18	360	2	MPD	0	0	5	NaOAC	0	0	10	Bis Tris Propane pH 6.5	0,1	200	6	KNaTartrate	0,16	80	9	KCl	0	0	15	640	360	12
43	D7	PEG3350	18	360	2	MPD	0	0	5	NaOAC	0	0	10	Bis Tris Propane pH 6.5	0,1	200	6	KNaTartrate	0,18	90	9	KCl	0	0	15	650	350	12
44	D8	PEG3350	18	360	2	MPD	0	0	5	NaOAC	0	0	10	Bis Tris Propane pH 6.5	0,1	200	6	KNaTartrate	0,18	90	9	KCl	0	0	15	650	350	12
45	D9	PEG3350	18	360	2	MPD	0	0	5	NaOAC	0	0	10	Bis Tris Propane pH 6.5	0,1	200	6	KNaTartrate	0,22	110	9	KCl	0	0	15	670	330	12
46	D10	PEG3350	18	360	2	MPD	0	0	5	NaOAC	0	0	10	Bis Tris Propane pH 6.5	0,1	200	6	KNaTartrate	0,22	110	9	KCl	0	0	15	670	330	12
47	D11	PEG3350	18	360	2	MPD	0	0	5	NaOAC	0	0	10	Bis Tris Propane pH 6.5	0,1	200	6	KNaTartrate	0,24	120	9	KCl	0	0	15	680	320	12
48	D12	PEG3350	18	360	2	MPD	0	0	5	NaOAC	0	0	10	Bis Tris Propane pH 6.5	0,1	200	6	KNaTartrate	0,24	120	9	KCl	0	0	15	680	320	12

PACT Premier ^{TM}_H9 Screen Conditions 49-96

Source	1,2,3,4	5	6	7	8	9	10	11,12,13,14	15
Stock	PEG3350	MPD	Bis Tris Propane pH 6.5	Bis Tris Propane pH 7.5	Bis Tris Propane pH 8.5	KNaTartrate	NaOAC	H2O	KCl
Cstock	50	50	0,5	0,5	0,5	2	2		2
Vges	1000								

Number (Destiny)	Well	Prec1	Cprec1	Vprec1	Source	Prec2	Cprec2	Vprec2	Source	Salt1	Csalt1	Vsalt1	Source	Buffer	Cbuffer	Vbuffer	Source	Additive1	Cadditive1	Vadditive1	Source	Additive2	Cadditive2	Vadditive2	Source	Vsum	Vwater	Source
49	E1	PEG3350	20	400	3	MPD	0	0	5	NaOAC	0	0	10	Bis Tris Propane pH 8.5	0,1	200	8	KNaTartrate	0,2	100	9	KCl	0	0	15	700	300	13
50	E2	PEG3350	20	400	3	MPD	0	0	5	NaOAC	0	0	10	Bis Tris Propane pH 8.5	0,1	200	8	KNaTartrate	0,2	100	9	KCl	0	0	15	700	300	13
51	E3	PEG3350	18	360	3	MPD	0	0	5	NaOAC	0	0	10	Bis Tris Propane pH 8.5	0,1	200	8	KNaTartrate	0,2	100	9	KCl	0	0	15	660	340	13
52	E4	PEG3350	18	360	3	MPD	0	0	5	NaOAC	0	0	10	Bis Tris Propane pH 8.5	0,1	200	8	KNaTartrate	0,2	100	9	KCl	0	0	15	660	340	13
53	E5	PEG3350	16	320	3	MPD	0	0	5	NaOAC	0	0	10	Bis Tris Propane pH 8.5	0,1	200	8	KNaTartrate	0,2	100	9	KCl	0	0	15	620	380	13
54	E6	PEG3350	16	320	3	MPD	0	0	5	NaOAC	0	0	10	Bis Tris Propane pH 8.5	0,1	200	8	KNaTartrate	0,2	100	9	KCl	0	0	15	620	380	13
55	E7	PEG3350	14	280	3	MPD	0	0	5	NaOAC	0	0	10	Bis Tris Propane pH 8.5	0,1	200	8	KNaTartrate	0,2	100	9	KCl	0	0	15	580	420	13
56	E8	PEG3350	14	280	3	MPD	0	0	5	NaOAC	0	0	10	Bis Tris Propane pH 8.5	0,1	200	8	KNaTartrate	0,2	100	9	KCl	0	0	15	580	420	13
57	E9	PEG3350	12	240	3	MPD	0	0	5	NaOAC	0	0	10	Bis Tris Propane pH 8.5	0,1	200	8	KNaTartrate	0,2	100	9	KCl	0	0	15	540	460	13
58	E10	PEG3350	12	240	3	MPD	0	0	5	NaOAC	0	0	10	Bis Tris Propane pH 8.5	0,1	200	8	KNaTartrate	0,2	100	9	KCl	0	0	15	540	460	13
59	E11	PEG3350	10	200	3	MPD	0	0	5	NaOAC	0	0	10	Bis Tris Propane pH 8.5	0,1	200	8	KNaTartrate	0,2	100	9	KCl	0	0	15	500	500	13
60	E12	PEG3350	10	200	3	MPD	0	0	5	NaOAC	0	0	10	Bis Tris Propane pH 8.5	0,1	200	8	KNaTartrate	0,2	100	9	KCl	0	0	15	500	500	13
61	F1	PEG3350	14	280	3	MPD	0	0	5	NaOAC	0	0	10	Bis Tris Propane pH 8.5	0,1	200	8	KNaTartrate	0,12	60	9	KCl	0	0	15	540	460	13
62	F2	PEG3350	14	280	3	MPD	0	0	5	NaOAC	0	0	10	Bis Tris Propane pH 8.5	0,1	200	8	KNaTartrate	0,12	60	9	KCl	0	0	15	540	460	13
63	F3	PEG3350	14	280	3	MPD	0	0	5	NaOAC	0	0	10	Bis Tris Propane pH 8.5	0,1	200	8	KNaTartrate	0,14	70	9	KCl	0	0	15	550	450	13
64	F4	PEG3350	14	280	3	MPD	0	0	5	NaOAC	0	0	10	Bis Tris Propane pH 8.5	0,1	200	8	KNaTartrate	0,14	70	9	KCl	0	0	15	550	450	13
65	F5	PEG3350	14	280	3	MPD	0	0	5	NaOAC	0	0	10	Bis Tris Propane pH 8.5	0,1	200	8	KNaTartrate	0,16	80	9	KCl	0	0	15	560	440	13
66	F6	PEG3350	14	280	3	MPD	0	0	5	NaOAC	0	0	10	Bis Tris Propane pH 8.5	0,1	200	8	KNaTartrate	0,16	80	9	KCl	0	0	15	560	440	13
67	F7	PEG3350	14	280	3	MPD	0	0	5	NaOAC	0	0	10	Bis Tris Propane pH 8.5	0,1	200	8	KNaTartrate	0,18	90	9	KCl	0	0	15	570	430	13
68	F8	PEG3350	14	280	3	MPD	0	0	5	NaOAC	0	0	10	Bis Tris Propane pH 8.5	0,1	200	8	KNaTartrate	0,18	90	9	KCl	0	0	15	570	430	13
69	F9	PEG3350	14	280	3	MPD	0	0	5	NaOAC	0	0	10	Bis Tris Propane pH 8.5	0,1	200	8	KNaTartrate	0,22	110	9	KCl	0	0	15	590	410	13
70	F10	PEG3350	14	280	3	MPD	0	0	5	NaOAC	0	0	10	Bis Tris Propane pH 8.5	0,1	200	8	KNaTartrate	0,22	110	9	KCl	0	0	15	590	410	13
71	F11	PEG3350	14	280	3	MPD	0	0	5	NaOAC	0	0	10	Bis Tris Propane pH 8.5	0,1	200	8	KNaTartrate	0,24	120	9	KCl	0	0	15	600	400	13
72	F12	PEG3350	14	280	3	MPD	0	0	5	NaOAC	0	0	10	Bis Tris Propane pH 8.5	0,1	200	8	KNaTartrate	0,24	120	9	KCl	0	0	15	600	400	13
73	G1	PEG3350	16	320	4	MPD	0	0	5	NaOAC	0	0	10	Bis Tris Propane pH 8.5	0,1	200	8	KNaTartrate	0,12	60	9	KCl	0	0	15	580	420	14
74	G2	PEG3350	16	320	4	MPD	0	0	5	NaOAC	0	0	10	Bis Tris Propane pH 8.5	0,1	200	8	KNaTartrate	0,12	60	9	KCl	0	0	15	580	420	14
75	G3	PEG3350	16	320	4	MPD	0	0	5	NaOAC	0	0	10	Bis Tris Propane pH 8.5	0,1	200	8	KNaTartrate	0,14	70	9	KCl	0	0	15	590	410	14
76	G4	PEG3350	16	320	4	MPD	0	0	5	NaOAC	0	0	10	Bis Tris Propane pH 8.5	0,1	200	8	KNaTartrate	0,14	70	9	KCl	0	0	15	590	410	14
77	G5	PEG3350	16	320	4	MPD	0	0	5	NaOAC	0	0	10	Bis Tris Propane pH 8.5	0,1	200	8	KNaTartrate	0,16	80	9	KCl	0	0	15	600	400	14
78	G6	PEG3350	16	320	4	MPD	0	0	5	NaOAC	0	0	10	Bis Tris Propane pH 8.5	0,1	200	8	KNaTartrate	0,16	80	9	KCl	0	0	15	600	400	14
79	G7	PEG3350	16	320	4	MPD	0	0	5	NaOAC	0	0	10	Bis Tris Propane pH 8.5	0,1	200	8	KNaTartrate	0,18	90	9	KCl	0	0	15	610	390	14
80	G8	PEG3350	16	320	4	MPD	0	0	5	NaOAC	0	0	10	Bis Tris Propane pH 8.5	0,1	200	8	KNaTartrate	0,18	90	9	KCl	0	0	15	610	390	14
81	G9	PEG3350	16	320	4	MPD	0	0	5	NaOAC	0	0	10	Bis Tris Propane pH 8.5	0,1	200	8	KNaTartrate	0,22	110	9	KCl	0	0	15	630	370	14
82	G10	PEG3350	16	320	4	MPD	0	0	5	NaOAC	0	0	10	Bis Tris Propane pH 8.5	0,1	200	8	KNaTartrate	0,22	110	9	KCl	0	0	15	630	370	14
83	G11	PEG3350	16	320	4	MPD	0	0	5	NaOAC	0	0	10	Bis Tris Propane pH 8.5	0,1	200	8	KNaTartrate	0,24	120	9	KCl	0	0	15	640	360	14
84	G12	PEG3350	16	320	4	MPD	0	0	5	NaOAC	0	0	10	Bis Tris Propane pH 8.5	0,1	200	8	KNaTartrate	0,24	120	9	KCl	0	0	15	640	360	14
85	H1	PEG3350	18	360	4	MPD	0	0	5	NaOAC	0	0	10	Bis Tris Propane pH 8.5	0,1	200	8	KNaTartrate	0,12	60	9	KCl	0	0	15	620	380	14
86	H2	PEG3350	18	360	4	MPD	0	0	5	NaOAC	0	0	10	Bis Tris Propane pH 8.5	0,1	200	8	KNaTartrate	0,12	60	9	KCl	0	0	15	620	380	14
87	H3	PEG3350	18	360	4	MPD	0	0	5	NaOAC	0	0	10	Bis Tris Propane pH 8.5	0,1	200	8	KNaTartrate	0,14	70	9	KCl	0	0	15	630	370	14
88	H4	PEG3350	18	360	4	MPD	0	0	5	NaOAC	0	0	10	Bis Tris Propane pH 8.5	0,1	200	8	KNaTartrate	0,14	70	9	KCl	0	0	15	630	370	14
89	H5	PEG3350	18	360	4	MPD	0	0	5	NaOAC	0	0	10	Bis Tris Propane pH 8.5	0,1	200	8	KNaTartrate	0,16	80	9	KCl	0	0	15	640	360	14
90	H6	PEG3350	18	360	4	MPD	0	0	5	NaOAC	0	0	10	Bis Tris Propane pH 8.5	0,1	200	8	KNaTartrate	0,16	80	9	KCl	0	0	15	640	360	14
91	H7	PEG3350	18	360	4	MPD	0	0	5	NaOAC	0	0	10	Bis Tris Propane pH 8.5	0,1	200	8	KNaTartrate	0,18	90	9	KCl	0	0	15	650	350	14
92	H8	PEG3350	18	360	4	MPD	0	0	5	NaOAC	0	0	10	Bis Tris Propane pH 8.5	0,1	200	8	KNaTartrate	0,18	90	9	KCl	0	0	15	650	350	14
93	H9	PEG3350	18	360	4	MPD	0	0	5	NaOAC	0	0	10	Bis Tris Propane pH 8.5	0,1	200	8	KNaTartrate	0,22	110	9	KCl	0	0	15	670	330	14
94	H10	PEG3350	18	360	4	MPD	0	0	5	NaOAC	0	0	10	Bis Tris Propane pH 8.5	0,1	200	8	KNaTartrate	0,22	110	9	KCl	0	0	15	670	330	14
95	H11	PEG3350	18	360	4	MPD	0	0	5	NaOAC	0	0	10	Bis Tris Propane pH 8.5	0,1	200	8	KNaTartrate	0,24	120	9	KCl	0	0	15	680	320	14
96	H12	PEG3350	18	360	4	MPD	0	0	5	NaOAC	0	0	10	Bis Tris Propane pH 8.5	0,1	200	8	KNaTartrate	0,24	120	9	KCl	0	0	15	680	320	14
				15120				0				0				9600				4380				0		29100	18900	

9 Instrumentation and Chemicals

9.1 Instrumentation

Agarose Gels	Horizon 11.14 (Biometra, Germany) PowerPac Basic (Bio Rad, USA)
AFM system	a) MFP-3D-Bio (Asylum Research, Santa Barbara, CA) b) Optical microscopy (Olympus BX 51, Japan) c) BioLever mini (BL-AC40TS, Olympus, Japan)
Beamlines	a) **X13**, consortiums beamline, HASYLAB, DESY, Hamburg: • Synchrotron source Bending magnet • Wavelength 0.81 Å • Focal spot 2 mm x 0.4 mm • Detector MARCCD 165 mm
	b) **X33**, SAXS beamline, EMBL, HASYLAB, DESY, Hamburg • Synchrotron source DORIS bending magnet Wavelength 1.5 Å • Focal spot 2 mm x 0.6 mm • Large automated sample changer • Detectors Photon counting Pilatus 1M-W pixel detector; Photon counting Pilatus 300K-W pixel detector; Mar345 image plate (345 mm^2)
Centrifuges	a) Centrifuge 5804R (Eppendorf, Germany) b) Centrifuge 5415R (Eppendorf, Germany) c) Centrikon T-1065 (Kontron, Germany)
CD Spectrometer	Jasco 815 (JASCO, UK) • Buffer concentration as low as possible while maintaining protein stability (5 mM in this work) • Stabilizers concentration (metal ions, *etc.*): calculated minimum (50 mM Mg^{2+}, 5 mM Ca^{2+} in present work) • Cell path length: 2 mm
Crystallization robots	Honeybee 961 (Genomic Solutions, USA)
Crystal plate incubator	RUMED 3001 (Rubarth, Germany) incubators
DLS instrumentation	a) *Spectro*SIZE 300 (Nabitec, Germany) b) *Spectro*LIGHT 500 (Nabitec, Germany)
FPLC machine	ÄKTA Purifier P-901 (GE Healthcare, UK)
Imaging system	a) CrystalScore (Diversified Scientific, USA) b) Microscope SZX12 with camera DP10 (both Olympus, Japan)
Microbalance	Sartorius CP224S-OCE (Sartorius, Germany)
pH Meter	Five Easy FE20 (Mettler-Toledo, Switzerland
Photospectrometry	Nanodrop 2000c (ThermoScientific, Peqlab, Germany)
Pipetting robots	Lissy (Zinsser, Germany)
SDS-PAGE	Power Supply EV265 (Consort, Belgium)

	Small II SE 250 electrophoresis chamber (Hoefer, USA)
Thermoblock	Thermostat 3401 (Eppendorf, Germany)
Tube Rotators	Roller mixer SRT6D (Stuart, UK) Rotator SB3 (Stuart, UK)
UV-light source	*Crystal*LIGHT 100 (Nabitec, Germany)
UV Transilluminator	Phero-lum 285 (Biotech Fischer, Germany)

9.2 Formulations and Chemicals

9.2.1 Formulations

9.2.1.1 Commercial Protein Screens and Kits and Hazard symbols and Information about Risk- and Safety-statements

Name	Supplier	Risk label	Risk phrases	Safety phrases
PCT	Hampton	-	-	-
pH Screen	Hampton	Xn	R38, R20/21/22	S26, S46, S24/25
Morpheus	Molecular Dimensions	T, N	R10, R45, R46, R60, R61, R63, R23/25, R36/37/38, R48/20/22, R51/53	S20, S26, S45, S53, S61, S36/37/3
PACT premier	Molecular Dimensions	T	R23/25, R52/53	S20, S36, S45, S61
Macrosol & Stura / Footprint*	Molecular Dimensions	T, N	R10, R45, R46, R60, R61, R25, R36/37/38, R48/20/22, R51/53	S20, S26, S45, S53, S61, S36/37/39
AmSO$_4$ Suite	Qiagen	T$^+$, N	R10, R25, R26, R45, R46, R60, R61, R48/23/25, R51/53	S45, S53, S61, S36/37.
Anions Suite	Qiagen	Xn, O	R8, R22, R36	S15, S16, S26, S36/37/39
Classic Suite	Qiagen	T, N	R10, R45, R46, R60, R61, R23/25, R36/37/38, R48/20/22, R51/53	S20, S26, S45, S53, S36/37/39.
ComPAS Suite	Qiagen	T	R10, R45, R23/24/25, R36/38, R39/23/24/25, R51/53	S13, S26, S45, S53, S61, S36/37/39.
Cryos Suite	Qiagen	T, N	R10, R45, R46, R60, R61, R23/25, R36/37/38, R48/20/22, R51/53	S20, S26, S45, S53, S61, S36/37/39.
JCSG$^+$ Suite	Qiagen	T, N	R10, R21, R41, R45, R23/25, R37/38, R51/53	S13, S20, S26, S45, S53, S36/37/39
MPD Suite	Qiagen	T, N	R10, R22, R23, R43, R45, R46, R60, R61, R36/38, R48/20/22, R51/53	S26, S45, S53, S61, S36/37
pH Clear Suite	Qiagen	Xi	R10, R36	S26
JBS Screen Mixed	Jena Bio	C, Xn, Xi	R35, R41, R42, R36/37/38	S22, S26, S45,

	Science			S24/25, S36/37/39
JBScreen classic1-10	Jena Bio Science	C, Xn, Xi	R35, R41, R42, R36/37/38	S22, S26, S45, S24/25, S36/37/39

Figure 9.2.1.1 Hazard symbols for formulations and respective risk labels (Source: http://de.wikipedia.org/wiki/Gefahrensymbol).

Risk Statements	
R8	Contact with combustible material
R10	May cause fire
R20	Flammable
R21	Harmful by inhalation
R22	Harmful in contact with skin
R25	Harmful if swallowed
R35	Toxic if swallowed
R36	Causes severe burns
R38	Irritating to eyes or skin
R41	Risk of serious damage to eyes
R42	May cause sensitisation by inhalation
R43	May cause sensitisation by skin contact
R45	May cause cancer
R46	May cause heritable genetic damage
R60	May impair fertility
R61	May cause harm to the unborn child
R39/23/24/25	Toxic: danger of very serious irreversible effects through inhalation, in contact with skin and if swallowed
R36/37/38	Irritating to eyes, respiratory system and skin
R23/24/25	Toxic by inhalation, in contact with skin and if swallowed
R20/21/22	Harmful by inhalation, in contact with skin and if swallowed
R48/20/22	Harmful: danger of serious damage to health by prolonged exposure through inhalation and if swallowed
R23/25	Toxic by inhalation and if swallowed
R36/38	Irritating to eyes and skin
R51/53	Toxic to aquatic organisms, may cause long-term adverse effects in the aquatic environment
R37/38	Irritating to respiratory system and skin

Safety Statements	
S13	Keep away from food, drink and animal foodstuffs
S15	Keep away from heat
S16	Keep away from sources of ignition - No smoking
S20	When using do not eat or drink. Do not breathe dust
S22	In case of contact with eyes, rinse immediately with plenty of water and seek medical advice
S26	In case of accident or if you feel unwell seek medical advice immediately (show the label where possible).
S45	If swallowed, seek medical advice immediately and show this container or label
S46	Avoid exposure - obtain special instructions before use
S53	Avoid release to the environment
S61	Refer to special instructions/safety data sheet
S24/25	Avoid contact with skin and eyes
S36/37	Wear suitable protective clothing and gloves
S36/37/39	Wear suitable protective clothing, gloves and eye/face protection
S26	In case of accident or if you feel unwell seek medical advice immediately (show the label where possible).

9.2.1.2 Formation, Buffer and SDS-PAGE

Concentrations of solutions are always in relation to the final volume, e.g. for a 50 % (w/v) solution of PEG, 50 g of the respective PEG were dissolved in water and then the water was added to a total volume of 100 mL.

If not stated differently, the buffer pH was adjusted by titration against 1 M NaOH or 1 M HCl solutions. For NaOAc/HOAc-buffer the pH was adjusted by addition of acetic acid to avoid contamination with Cl-. For 100 mL of 250 mM buffer, 56.5 mL NaOAc solution (250 mM) was mixed with 10.9 mL acetic acid (1 M) and water was added to 100 mL.

A 10% SDS-PAGE was prepared by mixing (in that particular order) 2.1 mL water, 1.3 mL buffer (1.5 M Tris, pH 8.8), 50 µL SDS solution (10 % (w/v) in water), 1.7 mL acrylamide (30 % solution), 3 µL TEMED and 25 µL APS (15 % (w/v) solution in water). The stacking gel (4%) was prepared by mixing 6.1 mL water, 2.5 mL buffer (0.5 M Tris, pH 6.8), 100 µL SDS solution (10 % (w/v) in water), 1.3 mL acrylamide (30 % solution), 10 µL TEMED and 50 µL APS (15 % (w/v) solution in water). Protein bands were stained with Coomassie blue solution (250 mL isopropanol, 100 mL acetic acid, 1 g Coomassie blue, 1000 mL water) and destained in 16.7 % (v/v) acetic acid. For the estimation of molecular mass, protein weight marker PageRuler

Unstained Protein Ladder 26614 (Thermo Scientific, USA) was used.

9.2.2 Chemicals

9.2.2.1 Chemicals Used (GHS Classification)

Compound	CAS-No.	Supplier	GHS hazard	Hazard Statements	Precautionary Statements
$(NH4)_2SO_4$	7283-20-2	Carl Roth	-	-	-
1,3-Propanediol	504-63-2	Merck	-	-	-
1,6-Hexanediol	629-11-8	Merck	-	-	-
1-Propanol	71-23-8	Carl Roth	GHS02 GHS05 GHS07	H225, H318, H336	P210, P233, P305+351+338
Acetic acid	64-19-7	Chem-solute	GHS02 GHS05	H226, H314	P280, P305+351+338, P310
Acrylamide 30%	79-06-1	Carl Roth	GHS06 GHS08	H301, H312, H316, H317, H319, H332, H340, H350, H361f, H372	P201, P280, P301+310, P305+351+338, P308+313
APS	7727-54-0	Carl Roth	GHS03 GHS07 GHS08	H272, H302, H315, H317, H319, H334; H335	P280, P305+351+338, P302+352, P304+341, P342+311
Arginine	74-79-3	Fluka	-	-	-
$BaCl_2$	10361-37-2	Merck	GHS06	H301, H332	P301+310
Bromphenol blue	115-39-9	Applichem	-	-	-
$CaCl_2$	10043-52-4	Merck	GHS07	H319	P305+351+338
CaOAc	5743-26-0	Merck	GHS07	H315, H319, H335	P261, P305+351+338
CHEMS	102601-49-0	Anatrace	-	-	-
Citric acid	77-92-9	Sigma	GHS05	H318	P305+351+338, P311
$CuSO_4$	7758-98-7	Merck	GHS07GHS09	H302, H315, H319, H410	P273, P305+351+338, P302+352
DDM	69227-93-6	Sigma	-	-	-
D-mannose	3458-28-4	Carl Roth	-	-	-
DTT	3483-12-3	Applichem	GHS07	H302, H315, H319, H335	P302+352, P305+351+338
EDTA	60-00-4	Sigma	GHS07	H319	P305+351+338
Ethanol	64-17-5	Carl Roth	GHS02	H225	P210
Ethylene glycol	107-21-1	Merck	GHS07	H302	-

Compound	CAS-No.	Supplier	GHS hazard	Hazard Statements	Precautionary Statements
Galactose	59-23-4	Sigma	-	-	-
Glutathione	70-18-8	Carl Roth	-	-	-
Glycerol	56-81-5	Sigma	-	-	-
Glycine	56-40-6	Applichem	-	-	-
Hepes	7365-45-9	Sigma Aldrich	-	-	-
Galactose	59-23-4	Sigma	-	-	-
Histidine	71-00-1	Sigma	-	-	-
Hydrochloric acid >25 %	7647-01-0	Merck	GHS05 GHS07	H314, H335	P261, P280, P310, P305+351+338
Isopropanol	67-63-0	Carl Roth	GHS02GHS07	H225, H319, H336	P210, P233, P305+351+338
KCl	7447-40-7	Carl Roth	-	-	-
Li_2SO_4	10102-25-7	Merck	GHS07	H302	-
LiCl	7447-41-8	Merck	GHS07	H302; H315, H319, H335	P302+352, P305+351+338
$Mg(HCOO)_2$	6150-82-9	Fluka	-	-	-
$MgCl_2$	7786-30-3	Carl Roth	-	-	-
MgOAc	16674-78-5	Merck	-	-	-
$MgSO_4$	7487-88-9	Merck	-	-	-
MO	111-03-5	Sigma	-	-	-
Mops	1132-61-2	Serva	GHS07	H315, H319, H335	P261, P305+351+338
MPD	107-41-5	Carl Roth	GHS07	H315, H319	-
NaBr	7647-15-6	Merck	-	-	-
NaCl	7647-14-5	Carl Roth	-	-	-
NaF	7681-49-4	Merck	GHS06	EUH032, H301, H315, H319	P264, P280, P301+310
NaI	7681-82-5	Applichem	GHS07	H315, H318	P264, P280, P302+P352, P305+351+338, P321, P332+P313, P362
$NaNO_3$	7631-99-4	Merck	GHS03GHS07	H302, H315, H319, H335	P220, P261, P305+351+338
NaOAc	127-09-3	Applichem	-	-	-
NaOH	1310-73-2	Merck	GHS05	H314	P280, P310, P305+351+338
NH_4Br	12124-97-9	Applichem	-	-	-
NH_4I	12027-06-4	Sigma	GHS07	H315, H319, H335	P261, P305+351+338
NH_4NO_3	6484-52-2	Applichem	GHS03GHS07	H315, H319, H335	P220, P261, P305+351+338

Compound	CAS-No.	Supplier	GHS hazard	Hazard Statements	Precautionary Statements
NH_4OAc	631-61-8	Applichem	-	-	-
$NiSO_4$	10101-98-1	Sigma	GHS07GHS08 GHS09	H302 + H332-H315-H317-H334-H341-H350i-H360D-H372-H410	P201-P261-P273-P280-P308 + P313-P501
Paraffin	8002-74-2	Applichem	-	-	-
PEG 10000	25322-68-3	Merck	-	-	-
PEG 1500	25322-68-3	Fluka	-	-	-
PEG 2000 MME	25322-68-3	Fluka	-	-	-
PEG 300	25322-68-3	Applichem	-	-	-
PEG 3350	25322-68-3	Sigma	-	-	-
PEG 400	25322-68-3	Sigma			
PEG 4000	25322-68-3	Merck	-	-	-
PEG 8000	25322-68-3	Sigma	-	-	-
Proline	147-85-3	Sigma	-	-	-
SDS	151-21-3	Sigma	GHS02 GHS06	H228, H302, H311, H315, H319, H335	P210, P261, P280, P312, P305+351+338
Sodium citrate	6132-05-4	Sigma	-	-	-
Sodium malonate	141-95-7	Sigma	-	-	-
Sodium tartrate	868-18-8	Applichem	-	-	-
$SrCl_2$	10476-85-4	Merck	GHS05GHS07	H315, H318, H335	P261, P280, P305+351+338
TEMED	110-18-9	Merck	GHS02 GHS05 GHS07	H225, H302, H314, H332	P261, P280, P305+351+338
tert-Butanol	75-65-0	AppliChem	GHS02GHS07	H225, H319, H332, H335	P210, P305+351+338, P403+233
Tris	1185-53-1	Fluka	GHS07	H315, H319, H335	P261 P305+351+338
$ZnSO_4$	7446-20-0	Aldrich	GHS05 GHS07GHS09	H302, H318, H410	P273, P280, P501 P305+351+338
β-OG	29836-26-8	Carl Roth	-	-	-

9.2.2.2 GHS and risk symbols and information about hazard-, risk-, safety- and precaution-statements

Figure 9.2.2.1 GHS pictograms (source: http://www.unece.org/trans/danger/publi/ghs/pictograms.html).

GHS Hazard Statements	
EUH032	Contact with acids liberates very toxic gas
H 225	Highly flammable liquid and vapor
H 226	Flammable liquid and vapor
H 228	Flammable solid
H 272	May intensify fire; oxidizer
H 301	Toxic if swallowed
H 302	Harmful if swallowed
H 311	Toxic in contact with skin
H 312	Harmful in contact with skin
H 314	Causes severe skin burns and eye damage
H 315	Causes skin irritation
H 316	Causes mild skin irritation
H 317	May cause an allergic skin reaction
H 318	Causes serious eye damage
H 319	Causes serious eye irritation
H 330	Fatal if inhaled
H 332	Harmful if inhaled
H 334	May cause allergy or asthma symptoms or breathing difficulties if inhaled
H 335	May cause respiratory irritation
H 336	May cause drowsiness or dizziness
H 340	May cause genetic defects
H 350	May cause cancer
H 360	May damage fertility or the unborn child
H 361	Suspected of damaging fertility or the unborn child
H 372	Causes damage to organs through prolonged or repeated exposure
H 410	Very toxic to aquatic life with long lasting effects

GHS Precautionary Statements	
P201	Obtain special instructions before use
P210	Keep away from heat/sparks/open flames/hot surfaces – No smoking
P233	Keep container tightly closed
P260	Do not breathe dust/fume/gas/mist/vapors/spray
P261	Avoid breathing dust/fume/gas/mist/vapors/spray
P264	Wash … thoroughly after handling
P273	Avoid release to the environment
P280	Wear protective gloves/protective clothing/eye protection/face protection
P284	Wear respiratory protection
P310	Immediately call a POISON CENTER or doctor/physician
P311	Call a POISON CENTER or doctor/physician
P321	Specific treatment (see respective MSDS)
P362	Take off contaminated clothing and wash before reuse
P301+310	IF SWALLOWED: Immediately call a POISON CENTER or doctor/physician
P308+313	IF exposed or concerned: Get medical advice/attention
P403+233	Store in a well-ventilated place. Keep container tightly closed
P304+341	IF INHALED: If breathing is difficult, remove victim to fresh air and keep at rest in a position comfortable for breathing
P332+313	If skin irritation occurs: Get medical advice/attention
P342+311	Call a POISON CENTER or doctor/physician
P302+352	IF ON SKIN: Wash with soap and water
P305+351+338	IF IN EYES: Rinse cautiously with water for several minutes. Remove contact lenses if present and easy to do continue rinsing

10 Acknowledgements

I am thankful to Prof. Dr. Dachuan Yin who has given me the strength and ambition to acquire knowledge and complete this auspicious task.

I am grateful to my parents, my wife Yan Luo, my daughter Sibei Liu, my nephew Qingran Yao and niece Lingjia Zhao for their love, care and pray for me and for their continuous encouragement and support to achieve this milestone. Thanks to my sister Xiaorong Liu and brother in law Mingxi Zhao for their support throughout my work.

I feel honored to express my sincere appreciation and gratitude to my respected supervisor Prof. Dr. Ch. Betzel for his continuous pursuance, consistent encouragement, keen interest, kind and motivating attitude and his most valuable guidance and support to complete this task. I am grateful to him for providing me all the facilities and opportunities for a successful completion of this work.

I am deeply indebted to Dr. Dominik Oberthür for his helpful discussions, nice suggestions, technical advice, moral support, correcting of my manuscript. It was nice to work with him in the lab as he makes science easier by creating a friendly and relaxed environment. His support was absolutely indispensable.

I endow special thanks to Dr. Johannes Raff, for providing S-layer protein samples, his helpful discussions and interest in my results, the preparation and discussion of the manuscript, his kind and welcoming temperament.

I am very much grateful to my friends Dr. Ge Yang, Dr. Zhiguo He, Miss Kun Yu, and Mr. Zhenye Zhong for their helping me whenever needed.

Special thanks to Dr. Sven Falke for his help in the discussion of the manuscript and Mr. Robin Schubert for his help in the English - German translation of this thesis.

My sincere appreciation and thanks to my colleagues, especially PD Dr. Perbandt, Dr. Redecke, and Dr. Rehders for their extended cooperation, timely and precious advice towards successful completion of this work.

I shall always cherish the knowledge I gained from all these experienced people during my

stay at Germany.

At the end I would like to thank the Northwestern Polytechnical University, Xi'an, China, for sending me abroad, and CSC, China Scholarship Council for funding my stay here.

--Jun Liu

11 Curriculum Vitae

JUN LIU

Sex: Male

Nationality: Chinese

Birthday: 21.05.1978

E-mail: jun@chemie.uni-hamburg.de

Address: Notkestr. 85, 22607 Hamburg, Germany

Education and Work Experience

01/2011-present University of Hamburg **Ph.D** Student at the Department of Chemistry

- **Research subject**: Structural Biology

  Topic: Structure and Dynamics of Bacterial S-Layer Proteins

01/2009-10/2010 Northwestern Polytechnical University **Guest Scientist** in School of Life Science

- **Research subject**: Structural Biology

  Topic: Utilization High Field Magnets in Materials Processing including Protein Crystallization Project

10/2005-06/2008 Shihezi University **M Sci.** in Preventive Veterinary Science **Rank: 5/51**

- **Research subject**: Molecular Biology

  Title: Research on Preventive Polyvalent Recombinant Vector Vaccine and its Immunogenic of Dairy Cattle Mastitis (03/2006-02/2008)

- Expression and purification of clumping factor A from *Staphylococcus aureus*, and supervising bachelor thesis

09/2002-09/2005 Bio-pharmaceutical Co., Ltd. of Xiangxin Group **Sales Manager**

09/1998-07/2002 Shihezi University **Bachelor** in Veterinary Science **Rank: 1/27**

- **Research subject**: Study on the Hemostasis Methods of Cutting Sika for Deer Antler

- **Excellent intern** in Black Bear Station of Sichuan P.R China (09/2001-03/2002)

Study the methods of anesthesia and hemostasis

Publications:

1. **Jun Liu**, Da-Chuan Yin*, Yun-Zhu Guo, Xi-Kai Wang, Si-Xiao Xie, Qin-Qin Lu, Yong-Ming Liu. (2011) Selecting Temperature for Protein Crystallization Screens Using the Temperature Dependence of the Second Virial Coefficient. ***PLoS ONE.*** **6:e17950**

2. Xian-Fang Zhang, **Jun Liu**, Yun-Zhu Guo, Xiao-Liang Ma, and Da-Chuan Yin *. (2011) Progresses on Developing Screening Kits for Protein Crystallization. ***Progresses in Biochemistry & Biophysics*****. 38:280-287**

3. Yun-Zhu Guo, Da-Chuan Yin*, Qin-Qin Lu, Xi-Kai Wang, and **Jun Liu.** (2010) Enhancement of nucleation during hanging drop protein crystallization using HF Treatment of cover glasses. ***Cryst. Res. Technol.*** **45 :158–166**

Workshop:

1. **Jun Liu**, Dominik Oberthür, and Christian Betzel. (2012) Structure and Dynamics of Bacterial Surface Layer Proteins. ***FEBS Advanced methods in macromolecular crystallization.*** **June 22-29**

Awards & Honors

- **Enterprise scholarship** 1999 and 2007 awarded to top 3% students
- **University scholarship** 1999, 2000, 2001, 2006 and 2007 awarded to top 10% students
- **Outstanding undergraduate** Shihezi University(09/2001)

12 Eidesstattliche Erklärung

Hiermit erkläre ich an Eides statt, diese Arbeit selbstständig und ohne fremde Hilfe verfasst, sowie keine anderen, als die von mir angegebenen Hilfsmittel verwendet zu haben.

Ferner versichere ich, dass ich noch keine Promotionsversuche an anderen Universitäten unternommen habe.

Hamburg, 12 März 2014

_____

(Jun Liu)